6-18-2021

Polar-Coded OFDM with Index Modulation

Si-yu Zhang
University of Windsor

Polar-Coded OFDM with Index Modulation

by

Si-yu Zhang

A Dissertation

Submitted to the Faculty of Graduate Studies

through Electrical and Computer Engineering

in Partial Fulfilment of the Requirements for

the Degree of Doctor of Philosophy at the

University of Windsor

Windsor, Ontario, Canada

2021

Polar-Coded OFDM with Index Modulation

by

Si-yu Zhang

APPROVED BY:

W. Gross, External Examiner

McGill University

R. Gras

School of Computer Science

A. Ahmadi

Department of Electrical and Computer Engineering

H. Wu

Department of Electrical and Computer Engineering

B. Shahrrava, Advisor

Department of Electrical and Computer Engineering

April 9, 2021

DECLARATION OF CO-AUTHORSHIP/PREVIOUS PUBLICATION

I. Co-Authorship

I hereby declare that this thesis presents the research outcome with the assistance and under the supervision of professor, Dr. Behnam Shahrrava. In all cases, including Chapter.3, Chapter.5 Chapter.6 and Chapter.7, the key ideas, primary contributions, experimental designs, simulation implementation, data analysis and interpretation, were performed by the author, Si-yu Zhang, with the review and revision being provided by Dr. Behnam Shahrrava.

I am aware of the University of Windsor Senate Policy on Authorship and I certify that I have properly acknowledged the contribution of other researchers to my thesis, and have obtained written permission from each of the co-author(s) to include the above material(s) in my thesis.

I certify that, with the above qualification, this thesis, and the research to which it refers, is the product of my own work.

II. Previous Publication

This thesis includes 7 original papers that have been previously published/ submitted for publication in peer reviewed journals/conferences, as follow:

Chapter	Publication title/full citation	Status
3	Zhang, Si-yu, and Behnam Shahrrava. "Stopping Criterion for Belief Propagation Polar Code Decoders based on Bits Difference Ratio." 2019 IEEE 10th Annual Information Technology, Electronics and Mobile Communication Conference (IEMCON) [1]	Published
3	Zhang Si-yu, and Behnam Shahrrava. " A Hybrid SD Scheme for Short Polar Codes using Variable Step Size." Physical Communications	Submitted
3	Zhang Si-yu, and Behnam Shahrrava. "Enhanced BP Decoding Schemes for Polar Codes."IET Communications [2]	Published
5	Zhang Si-yu, and Behnam Shahrrava. "Polar Decoding for Wireless System with Noisy Channel Estimates." Wireless Personal Communications	Submitted
5	Zhang, Si-yu, and Behnam Shahrrava. "Turbo Receiver for Polar-Coded OFDM systems with unknown CSI." 2020 IEEE Canadian Conference on Electrical and Computer Engineering (CCECE) [3]. IEEE.	Published
6	Zhang Si-yu, and Behnam Shahrrava. "A SLM Scheme for PAPR Reduction in Polar-Coded OFDM-IM Systems Without Using Side Information." IEEE Transactions on Broadcasting [4]	Published
7	Zhang Si-yu, and Behnam Shahrrava. "Polar-Coded OFDM with Index Modulation." IEEE ACCESS [5]	Published

I certify that I have obtained a written permission from the copyright owners to include the above published materials in my thesis. I certify that the above material describes work completed during my registration as a graduate student at the University of Windsor.

III. General

I declare that, to the best of my knowledge, my thesis does not infringe upon anyones copyright nor violate any proprietary rights and that any ideas, techniques, quotations, or any other material from the work of other people included in my thesis, published or otherwise, are fully acknowledged in accordance with the standard referencing practices. Furthermore, to the extent that I have included copyrighted material that surpasses the bounds of fair dealing within the meaning of the Canada Copyright Act, I certify that I have obtained a written permission from the copyright owners to include such materials in my thesis.

I declare that this is a true copy of my thesis, including any final revisions, as approved by my thesis committee and the Graduate Studies office, and that this thesis has not been submitted for a higher degree to any other University or Institution.

ABSTRACT

Polar codes, as the first error-correcting codes with an explicit construction to provably achieve the symmetric capacity of memoryless channels, which are constructed based on channel polarization, have recently become a primary contender in communication networks for achieving tighter requirements with relatively low complexity.

As one of the contributions in this thesis, three modified polar decoding schemes are proposed. These schemes include enhanced versions of successive cancellation-flip (SC-F), belief propagation (BP), and sphere decoding (SD). The proposed SC-F utilizes novel potential incorrect bits selection criteria and stack to improve its error correction performance. Next, to make the decoding performance of BP better, permutation and feedback structure are utilized. Then, in order to reduce the complexity without compromising performance, a SD by using novel decoding strategies according to modified path metric (PM) and radius extension is proposed. Additionally, to solve the problem that BP has redundant iterations, a new stopping criterion based on bit different ratio (BDR) is proposed. According to the simulation results and mathematical proof, all proposed schemes can achieve corresponding performance improvement or complexity reduction compared with existing works.

Beside applying polar coding, to achieve a reliable and flexible transmission in a wireless communication system, a modified version of orthogonal frequency division multiplexing (OFDM) modulation based on index modulation, called OFDM-in-phase/quadrature-IM (OFDM-I/Q-IM), is applied. This modulation scheme can simultaneously improve spectral efficiency and bit-error rate (BER) performance with great flexibility in design and implementation. Hence, OFDM-I/Q-IM is considered as a potential candidate in the new generation of cellular networks.

As the main contribution in this work, a polar-coded OFDM-I/Q-IM system is proposed. The general design guidelines for overcoming the difficulties associated

with the application of polar codes in OFDM-I/Q-IM are presented. In the proposed system, at the transmitter, we employ a random frozen bits appending scheme which not only makes the polar code compatible with OFDM-I/Q-IM but also improves the BER performance of the system. Furthermore, at the receiver, it is shown that the *a posteriori* information for each index provided by the index detector is essential for the iterative decoding of polar codes by the BP algorithm. Simulation results show that the proposed polar-coded OFDM-I/Q-IM system outperforms its OFDM counterpart in terms of BER performance.

DEDICATION

I would like to dedicate this thesis to my parents

who provide me with two essential things

Life and Love

ACKNOWLEDGEMENTS

It was a great pleasure to study at the University of Windsor. I have enjoyed my six years spent here, both within and outside my research, for my MASc and Ph.D degrees

I would like to express my sincere gratitude and appreciation to everyone who helped make this thesis possible. First of all, I would appreciate my parents. Their support encouraged me to overcome all difficulties that I met during my study. They supported me to study aboard and gave me financial support, without whom, I could not achieve my study.

Also, I am deeply indebted to my supervisor Dr. Shahrrava, the professor of Electrical and Computer Engineering at University of Windsor, for guiding me throughout the writing of this thesis. As one of the best professors I have ever had, Dr.Shahrrava impressed upon me that a good teacher instructs students in matters far beyond those in textbooks. His broad knowledge and logical way of thinking have been of great value; without his detailed and constructive comments on my research, none of this thesis would be possible.

Moreover, Dr.H.Wu, Dr.A.Ahmadi from the department of ECE, Dr.R.Gras from the School of Computer Science, also gave me a lot of help. They read through my thesis page by page and gave me advice about how to use words in technical writing. I really appreciate it. Also, I would like to acknowledge Dr. Warren J. Gross, from McGill University, for serving as my External Examiner. His professional suggestions really inspired me.

Finally, I wish to extend my gratitude to the faculties of ECE department at University of Windsor for their efforts and help during my study for the Ph.D degree.

TABLE OF CONTENTS

LIST OF TABLES

LIST OF FIGURES

LIST OF ACRONYMS

ADC analog to digital converter

AWGN additive white Gaussian noise

B-DMC binary memoryless channel

BEC binary erasure channel

BER bit error rate

BLER block error rate

BP belief propagation

BPSK binary phase shift keying

CCDF cumulative distributive function

CDMA code-division multiple access

CP cyclic prefix

CRC cyclic redundancy check

CSI channel state information

D2D device to device

DAB digital audio broadcasting

DAB digital audio broadcasting

DAC digital to analog converter

DFT discrete fourier transform

DSC doubly selective channel

DVB digital video broadcasting

EM expectation maximum

FBMC filtered bank multi-carrier

FER frame error rate

FFT fast fourier transform

GA Gaussian approximation

GFDM generalized frequency division multiplexing

HPA high power amplifier

ICI inter-carrier interference

IDFT inverse discrete fourier transform

IFFT inverse fast fourier transform

ISI inter-symbol interference

LDPC low density parity check

LLR log-likekihood ratio

LS least square

LTE long term evolution

M2M machine to machine

MCM multi-carrier modulations

MIMO multiple input multiple outputr

ML maximum likelihood

MU multi user

NR new radio

OFDM orthogonal frequency division multiplexing

OFDM-I/Q-IM OFDM with in-phase/quadrature IM

OFDM-IM OFDM with index modulation

OW optical wireless

P/S parallel to serial

PAPR peak to average power ratio

PDF probability density function

PM path metric

PTS partial transmit sequence

QAM quadrature amplitude modulation

QPSK quadrature phase shift keying

S/P serial to parallel

SAP sub-carrier activation pattern

SC successive cancellation

SD sphere decoding

SED squared Euclidean distance

SI side information

SISO soft input soft output

SLM selected mapping

SM spatial modulation

SE spectral efficiency

SNR signal-to-noise ratio

STBC space-time block code

UFMC universal filtered multi-carrier

UWA under water acoustic

WLAN wireless local area networks

WMAN wireless local and metropolitan area networks

1 INTRODUCTION

1.1 Channel coding and its development

Channel coding technologies have undergone continuous development and progress since 1948 when Claude Shannon established the theory [6]. From the comparatively simple hamming codes to the recent capacity achievable polar codes, performance of channel coding techniques is constantly improving with variant complexity. Different channel coding has different properties and thus is suitable for various applications. According to the development of channel coding and the corresponding theory, channel coding schemes can be categorized into two types:

- Algebraic coding (classical coding)
- Probabilistic coding (modern coding)

1.1.1 Algebraic coding

In the early stage of channel coding, major technological innovations and breakthroughs took place in algebraic coding. The construction of algebraic codes rely on three parameters (N, K, d). In this chapter, the author denote N as the codeword length, K as the length of information bits coming from the message source, and d as the minimum hamming distance, which actually measures the minimum differences between two codewords. Here, the binary domain linear algebra is used, that is, each element of the codeword and message sequence takes values from $\{0, 1\}$, and the corresponding operations are implemented in GF(2). As an instance, a $(7, 4, 2)$ hamming code represents a length-7 code with 4 information bits, and its minimum hamming distance is 2. For a linear algebraic code, the minimum hamming distance is equivalent to the minimum weight of a non-zero codeword, i.e. the number of "1" elements in the non-zero codeword. The main goal of algebraic coding is to select 2^K

linear codes from all 2^N vectors in the codeword space under the given parameters (N, K), and makes the value of d as large as possible. This is equivalent to find a set of linear codes so that the smallest difference between any two codewords is as large as possible. Intuitively, it can be imagined that in a N-dimensional space, each of 2^N codewords is corresponding to a point distributed in this high-dimensional space. When any 2^K points are selected, the distance characteristics between these points must be determined. It is unnecessary to consider the maximum distance between any two points, because although this maximum value is the easiest to distinguish two points, it is impossible to characterize the difficulty of distinguishing two points with smaller distances. But as long as the minimum distance d between any two points is determined, it can be guaranteed that the distance between any two other points is at least as large as d. Therefore, for any decoding scheme that is able to distinguish the two nearest points, it is able to distinguish any other two points. The minimum hamming distance d can be considered to indicate the worst case. Intuitively, by raising the value of d, the worst case can become not so "bad".

For a linear code, hard decoding is usually applied. The received vector is firstly converted to a hard-valued sequence consisting of $\{0, 1\}$, and then various decoding schemes are implemented, which are different from that of the probabilistic coding methods. For a linear code with minimum hamming distance d, all errors caused by no more than $d/2$ channels can be corrected (when d is odd, the result is $(d - 1)/2$), but for more errors, such linear code cannot correct them. Typical linear codes in early era include hamming codes [7], Golay codes [8], Reed-Muller (RM) codes [9], etc. Then, the field of algebraic coding ushered in a relatively prosperous period. At this stage, scholars applied finite field theory to coding research. Such theory provides a very good theoretical basis for the goal that researchers have been working to find the largest possible distance d. Typical codes based on finite field theory include Bose-Chaudhuri-Hocquenghem (BCH) [10] and Reed-Solomon (RS) codes [11]. These codes are able to achieve impressive performance enhancement and have been applied in many practical scenarios. Other coding techniques that are representative include algebraic geometry (AG) codes [12] and so on. However, the performance of these algebraic codes still have a remarkable gap from the Shannon limit, which are caused by several reasons. One of them is that the algebraic codes usually apply hard decoding schemes, thus some information has been lost before being sent to decoders. According to the information theory, this part of the lost information is equivalent to being discarded permanently, so it is inevitable that the partial information extracted from the receiving sequence causes performance loss. In addition, the part of reason why Shannon limit cannot be realized is the design and construction of codes. In the research to prove Shannon limit, random coding is adopted without particularly emphasizing the minimum hamming distance d, which promotes the development of probabilistic coding.

1.1.2 Probabilistic coding

The design of probabilistic coding is more in line with Shannon's theory. This idea is not dedicated to finding a large d, but trying to find a class of codes that have the best average performance and appropriate complexity. In other words, the probabilistic coding is a dynamic approach which usually achieves better performance. The first kind of codes that have a distinctly different design from algebraic coding are convolutional codes [13]. Unlike block coding for linear codes, convolutional codes belong to flow coding. It typically utilizes a shift register and a binary adder to continuously encode the input bits stream. In a convolutional code, there are two types of sequences: one is the observed sequence; the other is the state sequence, which is determined by the states of shift registers. After the occurrence of convolutional codes, several feasible schemes have been proposed for its decoding, such as the sequential search algorithm [14]. Then, Viterbi decoding [15] was developed for the decoding of convolutional codes, and it has been shown to achieve optimal decoding performance [16]. The Viterbi algorithm utilizes the mathematical relationship between the Markov state sequence and observed sequence, and the one-step transfer characteristic of the Markov state sequence to advance from the initial state to final state, reducing the complexity to a degree that can be effectively realized. Actually, the Viterbi decoding can be also regarded as a type of dynamic planing because convolutional codes with Markov state sequences have the optimal substructure that Viterbi algorithm can achieve the optimal decoding performance with low complexity. The advent of convolutional codes have also led to the beginning of soft decoding, rather than hard-decision based decoding. The soft decoding can introduce more information to improve the decoding performance.

Another well-known decoding scheme for convolutional codes is Bahl-Jelinek-Cocke-Raviv (BCJR) algorithm [17]. BCJR scheme utilizes the forward-backward iterative decoding to calculate the corresponding probabilities. BCJR decoding is a soft input soft output (SISO) algorithm, which is a very effective decoding scheme for turbo codes cascaded with symbol detectors. The fundamental idea of BCJR decoding scheme is to use Markov one-step transfer characteristics. By introducing the current state, total probability formula is utilized to add all possible values of the state, and Bayesian formula is used to derive the iterative relationship. In the history of probabilistic coding, there is also a kind of important techniques called concatenated codes [18], which cascade two block codes to improve error correction capability thus better decoding performance can be achieved [18]. In addition to this traditional cascading approach, there is an another kind of codes called generalized concatenated codes [19], which adopt a multi-level structure, and the corresponding coding scheme is appropriately designed for each level. At the receiving side, multistage decoding that is decoded sequentially, and when decoding the i^{th} level, it is necessary to use all decoding results of previous $i-1$ levels until the end of last level.

As one of the most famous coding techniques in development of modern coding, turbo codes [20] achieve very closely performance to Shannon limit, and the invention of turbo codes has caused a huge sensation in the aftermath. Turbo coding is different from conventional algebraic codes. Turbo codes do not intentionally make the minimum hamming distance d as large as possible. In fact, the idea of turbo codes was originally inspired by treating decoders as signal-to-noise ratio (SNR) amplifiers. Therefore, when turbo coding was proposed, it did not use too much mathematics to design a sophisticated code structure, and the idea was to straightforwardly iterate decoders of two convolutional codes in the form of a turbine. That is, the output of a decoder D_1 is fed back to another decoder D_2 to improve the decoding performance of D_2, and the result of D_2 is fed back to D_1 to improve the performance of D_1. Through this continuous iterative feedback, two decoders provide information to each other, ultimately improving the overall decoding performance. A simple but typical turbo decoder is illustrated in Fig.1.1, where Π and Π^{-1} denote an interleaver and deinterleaver, respectively. More details about turbo codes can be found in [21]. The emergence of turbo coding shifts people's concern from the algebraic coding to probabilistic coding. Moreover, scholars have re-explored the low density parity check (LDPC) coding, which is a representative of codes on graphs [22, 23]. Based on this innovation, many new coding schemes that are able to approach the Shannon limit, such as repeat-accumulate (RA) codes [24] and accumulate-repeat-accumulate (ARA) codes [25], are proposed, and efficient graph-based decoding algorithms, such as belief propagation (BP) [26], are also widely studied and applied to various scenarios.

Although the field of coding has evolved over the past few decades, there are still many problems that need to be explored. For example, the trade off between decoding performance and complexity, coding and decoding based on multi-level structure and graph theory. These questions are worth thinking and studying. For the readers who are interested in coding theory, more details can be found in [27].

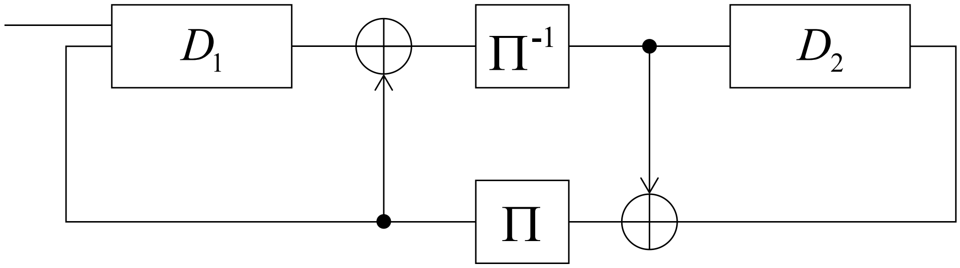

Fig. 1.1: Block diagram of a turbo decoder

1.2 Research status of polar codes

In 2009, the first paper on the theory of polar codes was published [28]. Polar codes have both characteristics of algebraic and probabilistic coding, which are different from most existing coding schemes. First, as long as the code length is given, the corresponding polar coding structure is uniquely determined, and the encoding process can also be completed by a generating matrix, which is consistent with the idea of algebraic coding. Second, polar coding is not designed to minimize the hamming distance. Instead, channel combination and splitting are utilized to determine the specific polar coding structure, and probabilistic decoding algorithms are also applied. This is more in line with the probabilistic coding.

Specifically, polar coding introduces a concept called channel polarization. For a polar code of length $N = 2^n$ (n is any positive integer), it utilizes N independent copies of channel W for channel combination and splitting to obtain new N split channels $\{W_N^{(1)}, W_N^{(2)}, ..., W_N^{(N)}\}$. With the increase of code length N, the channel after split will develop to two extremes, that is, the trend of polarization. Some of the split channels will approach the perfect channels, which are noise-free channels with capacity approaching 1, and the other part of split channels will be completely noisy, which capacity approaches 0. Assuming that the binary input symmetric capacity of the original channel W is denoted as $I(W)$, when the code length N approaches infinity, the ratio of split channel capacity approaching 1 is approximately $K = N \times I(W)$. Correspondingly, the ratio of channel capacity approaching 0 is approximately

$N \times (1 - I(W))$. The behavior of polarization of a length 1024 polar code for a binary erasure channel (BEC) is given in Fig.1.2. For a reliable channel with capacity of 1, message bits can be placed directly without any operation, which is equivalent to an encoding rate of $R = 1$. For an unreliable channel with capacity of 0, frozen bits are placed, which is equivalent to an encoding rate of $R = 0$. These positions of frozen bits are known by both the transmitting and receiving sides in advance. It can be seen that when the code length $N \to \infty$, the reachable coding rate of polar codes is $R = N \times I(W)/N = I(W)$. Hence, polar codes can be theoretically proved to achieve the binary discrete memoryless channel (B-DMC) capacity. The successive cancellation (SC) decoding is a typical method for polar decoding. During the channel splitting, since the obtained i^{th} channel $W_N^{(i)}$ is related to all the previous $i-1$ channels, decoding of the i^{th} channel can be implemented only all $i-1$ split channels are decoded. The SC decoding algorithm proceeds sequentially from $i = 1$ to $i = N$. Unlike LDPC codes, polar codes have a specific code structure, so it is the first known channel coding that can be theoretically proved to achieve the channel capacity, and polar codes have a definite construction method. The decoding structure of polar codes is similar to the butterfly diagram [29]. Due to this regular recursive structure, the en/decoding complexity of polar codes using SC decoding can be generalized to $O(N\log N)$.

To use polar coding for data transmission, it is necessary to distinguish the reliability of N split channels. In other words, which channels are reliable and which are not. Initially, the construction of polar codes utilizes the Bhattacharyya parameter $Z(W)$ [28] as a measure of the reliability of each split channel. The larger $Z(W)$ indicates the lower reliability of the channel. When W is a binary erasure channel (BEC), each $Z(W_N^{(i)})$ can be calculated recursively with complexity of $O(N\log N)$. Nevertheless, for other channels, such as binary input symmetric, or binary input additive white Gaussian noise channels, there is no such a method to calculate $Z(W_N^{(i)})$

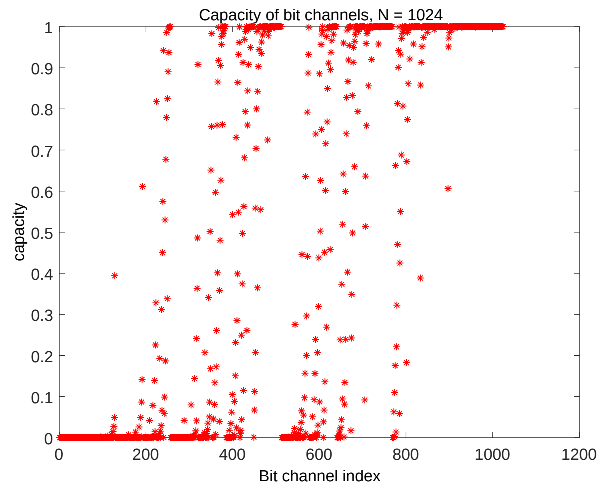

Fig. 1.2: Channel polarization for BEC ε=0.5

accurately. An effective approximation method was developed for channels other than BEC by introducing channel degradation and channel evolution [30]. Moreover, it has been introduced that there are some methods to achieve channel polarization, so as to realize a polar code with an arbitrary codeword length of $N = l^n$, where l is any positive integer. This method was introduced in [31]. Also, the relationship between decoding performance and code length can be found in [32]. These articles further enriched the theoretical basis of polar codes.

The capacity achievement of polar codes is only a theoretical proof due to the inefficient channel polarization caused by limited code length. Therefore, in practice, the performance of polar codes under SC is sub-optimal, especially when the code length is short or moderate. Also, the latency of SC based decoding is high. To improve the throughput of polar decoding, despite some fast SC decoders [33, 34, 35], some scholars applied decoding algorithms adopted by other codes to polar decoding, such as BP that is widely used in LDPC codes [36]. BP decoding for polar codes [37, 38] has some improvement compared with the SC decoding method in terms of latency, but there are a large number of short loops in the decoding factor graph, which increases the correlation of update in decoding process [39]. Therefore, there is still a clear gap between the performance of BP and maximum likelihood (ML). To improve the decoding performance of BP, many articles have been proposed [40, 41, 42]. Instead of solving the problem directly by changing the update strategy or eliminate short loops, most modified BP tried to generate more than one candidates using permutation or scrambling to improve the decoding performance. Also, some works did modifications on the encoding side [43, 44]. Since the capacity achievement of polar codes has been proved by using SC, many improved SC based methods were proposed, such as SC-list (SCL) decoding and its modified versions [45, 46, 47, 48, 49]. For SCL, by maintaining multiple paths in parallel during the decoding process, the probability of correct codeword loss can be reduced, thereby achieving better performance. Moreover, by introducing the cyclic redundancy check (CRC), the error correction capability of SCL can be significantly improved. Using SCL, for some code lengths, the decoding performance of polar codes is better than that of turbo and LDPC codes [47, 50]. Nevertheless, most polar decoding algorithms cannot achieve the ML performance (except for SCL decoding with very large size), especially for short or moderate code length. As an alternative way to achieve ML decoding, sphere decoding (SD) can achieve ML performance with high complexity [51]. Unlike the ML decoder which searches all possible outputs, SD only visits candidates within a sphere with radius r. Although SD significantly reduces the complexity compared with ML decoding scheme, it is still too complicated to be implemented in practice. Therefore, many articles were proposed to decrease the complexity of SD for polar codes [52, 53, 54].

With the continue in-depth study, polar coding has been applied in some practical scenarios. At the 2016 conference in Lisbon, Portugal, participants debated on what channel coding should be used in the 5G enhanced mobile broadband (eMBB) scenario. Finally, both LDPC and polar codes are selected to be adopted to the 5G new radio (NR) interface by the third-generation partnership project (3GPP) [55]. Polar codes would be applied in the signaling channel, and LDPC codes would be applied in the data channel. Therefore, polar codes has won a position in 5G era.

1.3 OFDM based systems

Besides channel coding, as a practical communication system, a reliable transmission scheme is also required. By combining the transmission, channel coding and other necessary techniques (i.e. constellation mapping, resources allocation, channel estimation), a communication network can achieve the performance that meet requirements for practical scenarios. Orthogonal frequency division multiplexing (OFDM) has been applied in 4G wireless networks because of its strong resistance for frequency selective fading. Also, such benefits of OFDM based systems also make them a very strong candidate for next generation wireless communication networks.

OFDM is a special kind of multi-carrier modulation (MCM). OFDM divides a high speed data stream into several low speed data streams and modulate them on sub-carriers that are orthogonal with each other, making the symbol period longer than the delay spread. This property can avoid small scale fading and inter-symbol interference (ISI) [56]. Moreover, OFDM is spectrally efficient since sub-carriers have significant overlap in the frequency domain [57].

The concept of OFDM was proposed in 1965 as a special case of the frequency division multiplexing [58]. Compared with the conventional FDM, OFDM allows the spectrum from different sub-carriers that are orthogonal to be overlapped with each other, which improves the spectral efficiency of the system. In 1971, the discrete Fourier transform (DFT) was utilized into the MCM [59]. In practice, the fast Fourier transform (FFT) implementation of the DFT has made OFDM modulation and demodulation feasible and very successful. In the 1980s, Peled and Ruiz [60] inserted cyclic prefix (CP) to OFDM signals to guarantee the orthogonality among sub-carriers, which dramatically decreased the ISI caused by a multi-path channel.

OFDM has been adopted extensively in 4G long term evolution (LTE), IEEE 802.16 (WiMAX), and IEEE 802.11 (WLAN) standards for its relatively high resistance against frequency selective fading [61]. Compared with single carrier modulations, OFDM has several advantages, which caused OFDM to replace code division multiple access (CDMA) techniques in 4G LTE networks. The main advantages of OFDM are listed as follows [62]:

- Robustness against narrow-band co-channel interference
- Robustness against ISI and fading caused by multipath propagation
- High spectral efficiency
- Simple implementation using FFT/IFFT
- Frequency diversity

However, OFDM also has some obstacles that need to be overcome in the implementation of OFDM systems:

- Sensitivity to carrier offset and drift
- High peak to average power ratio (PAPR)

Moreover, similar to polar codes, OFDM is also a potential candidate as the waveform format of 5G communication networks [63]. Since to the strong performance of OFDM in frequency selective channels, it is worth to investigate the polar-coded OFDM based system. In practice, communication channels are frequency selective instead of pure additive white Gaussian noise (AWGN). However, polar codes are mostly designed for AWGN channels, which may be insufficient when using in frequency selective channels. Although there are some investigations for polar codes construction in fading channels [64, 65, 66], it is more practical and straightforward to combine the standard polar code with some existing techniques to improve its performance. Many related schemes that are helpful to OFDM or polar decoding can be introduced for system performance improvement. Moreover, the introduction of polar code in OFDM based systems can contribute to the solutions of the problems that MCM techniques are currently facing, such as high PAPR.

As an extended version of OFDM, OFDM with index modulation (OFDM-IM) introduces the concept of spatial modulation (SM) to the frequency domain [67]. Compared with the conventional OFDM, OFDM-IM provides an interesting trade-off between energy efficiency and system performance from the adjustment of the number of active sub-carriers in systems [68]. Nevertheless, it was shown that OFDM-IM shows weak performance in low SNR scenarios [69]. Several articles have been proposed to improve the performance of OFDM-IM and are able to achieve effective results. Most of these modified OFDM-IM are generalized in [70]. Thanks to the significant flexibility, OFDM-IM has been currently attracting a number of researches and playing a very strong candidate in the next generation wireless networks. It is very interesting to investigate the performance of polar-coded OFDM-IM systems, especially compared with the conventional polar-coded OFDM system because both OFDM and OFDM-IM are potential candidates for 5G while polar codes have already been accepted by 5G standards. Moreover, all improved techniques for polar en/decoding applied in OFDM systems are expected to be smoothly transfered to OFDM-IM. Unfortunately, based on author's best knowledge, no article investigates such problems. This gives us a chance to develop a polar-coded OFDM-IM based system which is expected to be able to achieve better performance than that of the polar-coded OFDM system.

1.4 Main research contents of the thesis

The main contribution of this thesis is to propose a general design guideline of polar-coded OFDM-IM systems. Nevertheless, before it, there are many related works developed during the author's Ph.D program, including modified polar decoding methods, modified polar-coded OFDM systems, and a low PAPR OFDM-IM system utilizing polar codes.

1.4.1 Modified polar decoding schemes

This thesis starts from proposing several modified polar decoding schemes, which achieve better error performance than their counterparts. These polar decoding methods are based on SC-flip (SC-F), BP and SD, respectively. Then, to reduce the redundant iterations of BP, a stopping criterion is proposed. The research contents of this part are summarized as follows:

- **A novel SC flip stack decoding based on GA for polar codes**:

  In this part, an enhanced SC-F decoding is proposed. As a modified version of SC, SC-F decoding can achieve better error performance than that of SC without increasing significant complexity. In the proposed method, compared with the conventional SC-F, new criteria based on Gaussian approximation (GA) are applied to accurately recognize incorrect bits. Further, to correct more than one errors, a stack based on ML rule is utilized. Based on these two modifications, simulation results show that the proposed method can achieve better performance than that of conventional SC-F and SCL decoding with lower complexity.

- **Novel decoding schemes for polar codes based on BP**:

  In this part, we propose two decoding schemes for polar codes based on the BP algorithm. The basic idea of the proposed schemes, called "interleaved-BP" (I-BP) and "multiple candidates-BP" (M-BP), is to construct multiple candidates with different reliability values from the received signal and to decode each candidate by a BP decoder. Then, the output of the BP decoder that meets the stopping criterion or the maximum likelihood (ML) rule is chosen as the decoded data. Simulation results show that both the proposed polar decoders outperform the one based only on a single conventional BP decoder. In conjunction with each of the proposed schemes, a feedback structure is also proposed to achieve more performance gain. The proposed feedback structure takes as input the output of each BP decoder, and enhances the *a posteriori* information of reliable bits and flips unreliable bits. Then, the processed information is fed back into its corresponding decoder. Simulation results show that the performance gain of the proposed schemes with this feedback, compared to the ones without the feedback, may be as large as 1 dB at a frame-error rate (FER) 10^{-2} on frequency selective channels and 2 dB at a FER of 0.07 on doubly selective channels (DSC).

- **Stopping criterion for BP polar decoder based on bit different ratio**:

  As an iterative decoding method, BP exchanges information between the nodes of decoding factor graph. However, sometimes the information between nodes is not changed but the number of iterations has not reached the preset value. This situation results in iteration redundancy, which decreases decoding efficiency and waste energy. In this thesis, we propose a novel stopping criterion for BP polar decoders. The proposed criterion is based on the bit difference ratio (BDR). The BDR stopping method is implemented by monitoring the fluctuation of BDR along with the number of iterations to decide if the BP decoding process can be terminated. Simulation results indicate that the proposed criterion can provide superiority in iteration reduction compared with the current stopping criteria [71, 72, 73, 74]. Hence, the proposed BDR stopping criterion can effectively reduce the energy waste and decoding latency of decoding procedure. Moreover, by loosing constraints, the proposed stopping criterion can achieve more iteration reduction at the cost of BER degradation.

- **A hybrid SD scheme for short polar codes using variable step size**:

  In this part, we propose a hybrid stack SD scheme for polar codes based on radius extension and a modified optimum PM. The proposed SD scheme utilizes variable step size obtained from the PM and increases the corresponding radius until a valid polar codeword is found. Simulation results show that for short polar codes, compared with existing SD schemes, the proposed scheme achieves more complexity reduction without compromising the ML optimality.

1.4.2 Modified polar-coded OFDM systems

After introducing the polar decoding schemes, improved polar-coded OFDM systems are investigated. These related works are presented in Chapter 5, which contains two modified polar-coded OFDM systems which introduces existing techniques to improve error performance. First, a channel compensator for BP with noisy channel estimate is proposed. Then, a turbo receiver that combines the expectation maximum (EM) soft symbol detector and BP decoder is proposed, which significantly improves the error correction performance of polar-coded OFDM systems. The research contents of this part are summarized as follows:

- **Polar decoding for wireless system with noisy channel estimates**:

  In this section, a channel compensator $\boldsymbol{C}$ to improve conventional BP polar decoding performance with noisy channel estimates is proposed. It is known that in practice, channel estimates for fading channels are usually available. However, inaccurate channel estimates may leads decoding performance degradation. In this section, we prove that utilizes channel compensator can effectively enhance the BER performance of polar codes over fading channels. However, it is proved that the min-sum (MS) based decoding schemes cannot enjoy this benefit brought by channel compensators. By introducing the variance of channel estimate errors σ_m^2, inaccurate initial LLRs can be re-regulated using a channel compensator $\boldsymbol{C}$, which helps enhance BER performance. Simulation results suggest that BP decoders utilizing $\boldsymbol{C}$ can achieve 1.5 dB SNR gain without complexity increment.

- **Turbo receiver of polar-coded OFDM system with unknown CSI**:

  In this section, a turbo receiver for polar-coded OFDM systems in frequency-selective fading channels with unknown channel state information (CSI) is proposed. The receiver iteratively exchanges the soft information between an expectation-maximization (EM) symbol detector and a soft polar decoder that is based on the BP. By utilizing such receiver, the error correction performance of systems can be significantly improved even with unknown CSI. Simulation results show that by using the proposed turbo receiver, around 5 dB coding gain at a BER of 5×10^{-2} can be obtained compared with receivers that detect symbols and implement decoding separately with unknown CSI.

1.4.3 A SLM scheme for PAPR reduction in polar-coded OFDM-IM systems without using side information

In this section, we propose a novel SLM scheme based on a polar coding technique for PAPR reduction in OFDM-IM systems. The proposed scheme by utilizing random frozen bits in polar codes generates different number of candidate sequences. Then the candidate sequence with the smallest PAPR is selected for transmission. The proposed scheme can be considered as one block in an OFDM-IM system that performs both PAPR reduction and error correction. For a fair comparison, the performance of an OFDM-IM system based on the proposed scheme is compared with a system that carries out the same operations with two separate blocks where a polar encoder is cascaded with the one for PAPR reduction (such as conventional SLM or partial transmit sequence (PTS)), and a polar coded OFDM-IM system without any PAPR reduction scheme. Moreover, based on our proposed SLM scheme, a novel receiver without using side information (SI) is proposed. This SI free receiver is based on SCL. Simulation results show that as the polar code can bring both error correction and PAPR reduction capabilities by using our proposed scheme. Also, the proposed SI free receiver can achieve similar BER performance as that of the ideal case in both AWGN and frequency selective channels.

1.4.4 Polar-coded OFDM with index modulation

In this part, we apply polar codes to a modified version of OFDM systems with index modulation which is called OFDM with in-phase/quadrature index modulation (OFDM-I/Q-IM). We provide general design guidelines for the proposed polar-coded OFDM-I/Q-IM systems. In the proposed system, at the transmitter, we employ a random frozen bits appending scheme which not only makes the polar code compatible with OFDM-I/Q-IM but also improves the BER performance of the system. Furthermore, at the receiver, it is shown that the *a posteriori* information for each index provided by the index detector is essential for the iterative decoding of polar codes by the BP algorithm. Simulation results show that the proposed polar-coded OFDM-I/Q-IM system outperforms its OFDM counterpart in terms of BER performance.

1.5 The organization of the thesis

In Chapter 2, preliminary knowledge on polar codes designed for memoryless channels is given. The author starts from the theory of polarization, which is the reason that polar codes can achieve the channel capacity when the code length tends to infinity. Then, practical polar codes constructions, including encoding and decoding methods are reviewed.

In Chapter 3, the author gives several improved polar decoding schemes in terms of error correction performance enhancement or complexity reduction.

After introducing the works related to polar decoding, in Chapter 4, the background of OFDM based systems is reviewed. This chapter starts from the introduction of OFDM, including the principle and transceiver of OFDM. Then, as a modified version of OFDM, the concept of OFDM-IM is introduced. Moreover, the comparison between OFDM-IM and OFDM is also provided in this chapter.

In Chapter 5, enhanced polar-coded OFDM systems are proposed. By introducing some existing techniques, these proposed systems can improve their error performance.

Then, in Chapter 6, to reduce the high PAPR in OFDM-IM systems, the SI free SLM scheme based on polar codes is introduced and the polar-coded OFDM-I/Q-IM system is proposed in Chapter 7.

In Chapter 8, the author conclude the thesis by summarizing the main contributions of each chapter and discussing the potential interesting open questions for future research.

2 THE THEORY OF POLAR CODES

This chapter mainly introduces the basic en/decoding principles of polar codes, and its effective implementation structure. These preliminaries provide the basis for the subsequent research and analysis.

2.1 The theory of polarization

This section gives the preliminaries of the polarization theory. The first part of this section introduces the chain rule of mutual information and the second part of this section gives the definition of channel split and polarization

2.1.1 Chain rule of mutual information

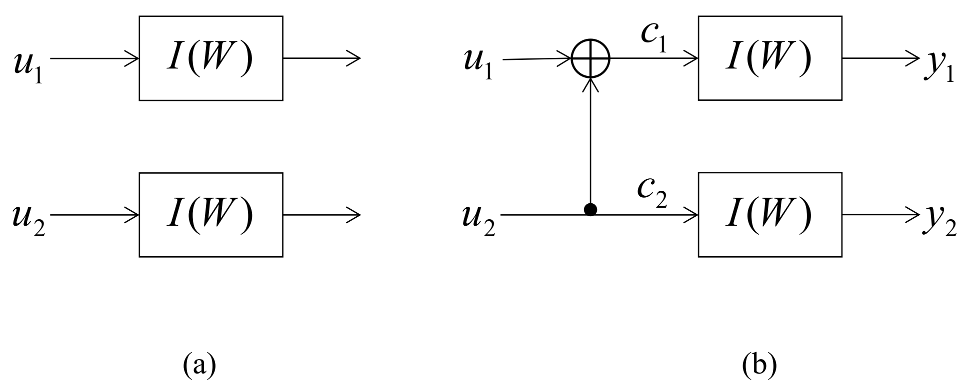

Fig. 2.1: (a). Conventional transmission mechanism (b). Polar coding transmission mechanism

In Fig.2.1.(a), the author uses u_1 and u_2 to represent the source message bits. For simplicity, let $u_1, u_2 \in \{0, 1\}$, and their inter-operations are in binary fields. After they are sent over a symmetric channel with capacity of $I(W)$, y_1 and y_2 are received. Here, the symmetric capacity $I(W)$ refers to the channel capacity when the input distribution is uniform symmetrical. Examining the mutual information obtained by using such channel twice, we can obtain the following result:

$$
\begin{aligned}
I(u_1, u_2; y_1, y_2) &\overset{(1)}{=} I(u_1; y_1, y_2) + I(u_2; y_1, y_2|u_1) \\
&\overset{(2)}{=} I(u_1; y_1) + I(u_2; y_2) \\
&= I(W) + I(W) \\
&= 2I(W)
\end{aligned} \tag{2.1}
$$

where (1) is obtained from the chain rule of mutual information, and (2) is because two channels utilized by u_1 and u_2 are independent. Then, we investigate Fig.2.1.(b), which illustrates the mechanism of a polar code transmission. Unlike the conventional transmission mechanism, before sending u_1 and u_2 to channels, binary operations need to be implemented first to obtain $c_1 = u_1 \oplus u_2$, and $c_2 = u_2$. Now, examining the mutual information obtained by such operations, we can obtain the following result:

$$
\begin{aligned}
I(u_1, u_2; y_1, y_2) &= I(c_1, c_2; y_1, y_2) \\
&= I(u_1; y_1, y_2) + I(u_2; y_1, y_2|u_1) \\
&\overset{(1)}{=} I(W_2^{(1)}) + I(W_2^{(2)}) \\
&\overset{(2)}{=} 2I(W)
\end{aligned} \tag{2.2}
$$

where in (1), the author denotes $I(W_2^{(1)}) = I(u_1; y_1, y_2)$, $I(W_2^{(2)}) = I(u_2; y_1, y_2|u_1)$. (2) is because two channels are still independent of each other. Since u_1 and u_2 are independent, we have:

$$
\begin{aligned}
I(W_2^{(2)}) &= I(u_2; y_1, y_2) \\
&= I(u_2; y_1, y_2, u_1) \\
&= I(u_2; y_2) + I(u_2; y_1, u_1|y_2) \\
&= I(W) + I(u_2; y_1, u_1|y_2) \\
&\geq I(W) \qquad (2.3)
\end{aligned}
$$

Therefore, $I(W_2^{(1)}) \leq I(W) \leq I(W_2^{(2)})$.

Based on above conclusions and Fig.2.1.(b), we have actually defined two split channels:

$$
\begin{aligned}
W_2^{(1)}: &\quad u_1 \to y_1, y_2 \\
W_2^{(2)}: &\quad u_2 \to u_1, y_1, y_2
\end{aligned} \qquad (2.4)
$$

Here, let give an example to illustrate the polarization phenomenon. Assume that channel W is a BEC with erase rate $\varepsilon = 0.4$, which means $I(W) = 1 - \varepsilon = 0.6$. When decoding u_1 in Fig.2.1.(b), we have $u_1 = y_1 \oplus y_2$. It is easy to know that when one of $\{y_1, y_2\}$ is a delete symbol, the value of u_1 cannot be obtained. At this time, the decoding of u_1 fails, which probability can be calculated as: $p_1 = \varepsilon \times (1-\varepsilon) + \varepsilon^2 + (1-\varepsilon) \times \varepsilon = 0.64$. On the other hand, it is known that $u_2 = y_1 \oplus u_1$ or $u_2 = y_2$, thus as long as either of these two results provides a non-deletion symbol, then u_2 will be decoded correctly. That is, when u_1 is correctly decoded, u_2 will fail for decoding only if $\{y_1, y_2\}$ are all incorrect symbols. The corresponding probability can be calculated as: $p_2 = \varepsilon \times \varepsilon = 0.16$. From above calculations, we know that for a BEC with $\varepsilon = 0.4$, the delete probability of u_1 and u_2 are 0.64 and 0.16, respectively, resulting in $0.64 > 0.4 > 0.16$. From the perspective of channel capacity, after simple calculations, we have: $I(W_2^{(1)}) = 1 - 0.64 = 0.36$ and $I(W_2^{(2)}) = 1 - 0.16 = 0.84$, satisfying $I(W_2^{(1)}) + I(W_2^{(2)}) = 2I(W)$ and $I(W_2^{(1)}) \leq I(W) \leq I(W_2^{(2)})$.

2.1.2 Definition of channel split and polarization

From Fig.2.1.(b), we can obtain two split $W_2^{(1)}$ and $W_2^{(2)}$ by independently utilizing channels W. Now using this recursive idea one more time, if we copy the structure in Fig.2.1.(b), we can obtain two independent split channels $W_2^{(1)}$ and $W_2^{(2)}$. Then we apply the same arithmetic structure to $W_2^{(1)}$ and $W_2^{(2)}$, respectively and obtain Fig.2.2.

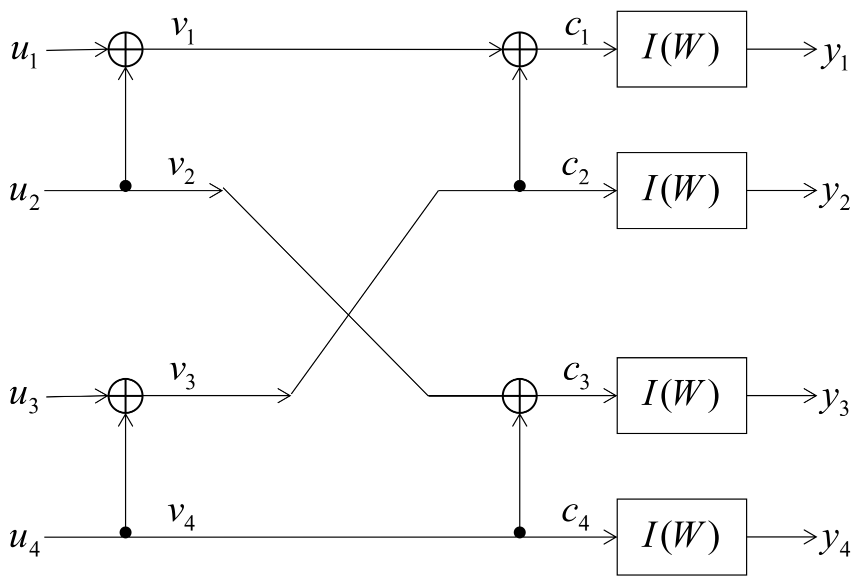

Fig. 2.2: Recursive structure of a polar code construction

The author defines N split channels after recursive structure as:

$$W_N^{(i)} :\ u_i \rightarrow y_1^N \times u_1^{(i-1)} \tag{2.5}$$

where $i = 1, 2, ..., N$, and here, the author denotes u_i^j as vector $[u_i, ..., u_j]$. Then after calculations, the transition probability of the i^{th} split channel can be written as:

$$\begin{aligned} W_N^{(i)}(y_1^N, u_1^{i-1}|u_i) &= \frac{P(y_1^N, u_1^{i-1}, u_i)}{P(u_i)} \\ &= \frac{\sum_{u_{i+1}^N \in \chi^{N-i}} P(y_1^N, u_1^i, u_{i+1}^N)}{1/2} \\ &= \frac{\sum_{u_{i+1}^N \in \chi^{N-i}} (P(u_1^N) \times W_N(y_1^N|u_1^N))}{1/2} \\ &= \frac{1/2^N \sum_{u_{i+1}^N \in \chi^{N-i}} W_N(y_1^N|u_1^N)}{1/2} \\ &= \sum_{u_{i+1}^N \in \chi^{N-i}} \frac{1}{2^{N-1}} W_N(y_1^N|u_1^N) \end{aligned} \tag{2.6}$$

where $\chi \in \{0, 1\}$, and $W_N(y_1^N|u_1^N) = \prod_{i=1}^N W(y_i|c_i)$. Here, considering a specific case for a $N = 8$ polar code in BEC with $\varepsilon = 0.4$. After recursive calculations, we can obtain the capacity of each split channel:

$$\begin{aligned} &I(W_8^{(1)}) = 0.0168 \quad I(W_8^{(2)}) = 0.2424 \quad I(W_8^{(3)}) = 0.3486 \quad I(W_8^{(4)}) = 0.8322 \\ &I(W_8^{(5)}) = 0.4979 \quad I(W_8^{(6)}) = 0.9133 \quad I(W_8^{(7)}) = 0.9495 \quad I(W_8^{(8)}) = 0.9993 \end{aligned} \tag{2.7}$$

Hence, under the construction mechanism of polar codes, each split channel has different capacity. If we have 4 bits to transmit, we should select 4 split channels that have the highest capacities, which are the $4^{th}, 6^{th}, 7^{th}, 8^{th}$ channels. For the rest channels, some pre-known bits should be arranged, such as “0” bits. Thus, the information sequence after zero insertion can be denoted as $u_1^8 = [0, 0, 0, u_4, 0, u_6, u_7, u_8]$, where u_4, u_6, u_7, u_8 are called information or free bits, and u_1, u_2, u_3, u_5 are called frozen bits, which are usually zeros. These bits are known by transmitters and receivers in advance. Further, it has been concluded [28] that:

- When the code length N approaches infinity, the capacity of a split channel obtained through the construction will show a tendency of polarization, that is, it will approach 0 or 1.

- Assume that the symmetry capacity of a channel W is $I(W)$, then, when the code length approaches infinity, there will be about $N \times I(W)$ split channels whose capacity is 1, and about $N \times (1 - I(W))$ split channels with capacity of 0.

- When message bits are placed on split channels with capacity of 1, the achievable rate is $R = N \times I(W)/N = I(W)$. It means that polar codes can reach the symmetrical channel capacity when the code length approaches infinity.

- When the channel input distribution is symmetrical, that is the channel capacity $C = I(W)$, polar codes can reach the channel capacity.

Compared with turbo and LDPC codes, polar codes have a specific coding structure. This explicit structure is sufficient to prove that polar codes can reach the channel capacity, not in an average sense. A simple but direct illustration for the understanding of polar codes is given in Fig.2.3. A message sequence u_1^N is sent to a polarization structure and a codeword c_1^N is obtained. Then, c_1^N is sent to real physical channels, and a signal y_1^N is received. However, since the polarization structure actually constructs a set of split channels, it can be considered that each bit u_i in the message sequence is sent to the corresponding split channel $W_N^{(i)}$ for transmission with received sequence $\{y_1^N, u_1^{i-1}\}$.

2.2 Polar encoding

A polar code $C(N, K)$ is assumed with rate $R = K/N$, where $N = 2^n$ denotes the code length, and K ($K \leq N$) indicates the number of information bits. Given an input sequence u_1^N (after zero insertion) and codeword x_1^N, the encoding process can be expressed as a matrix product. Take a construction of polar code with length N and rate R as an example. In Arikan's original paper [28], before encoding, the input sequence u_1^N is permuted by a permutation matrix $\mathbf{B}_N$. Then, the sequence after

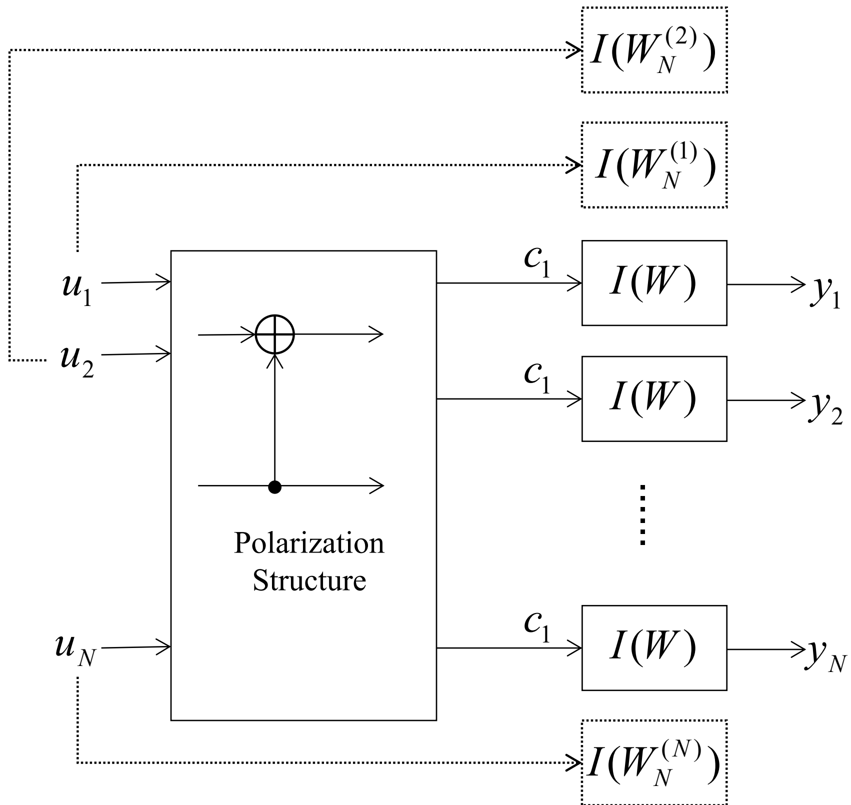

Fig. 2.3: Direct illustration of polar codes

permutation are multiplied by a generation matrix $\mathbf{G}^{\otimes n}$. Here, it yields:

$$x_1^N = u_1^N \mathbf{B}_N \mathbf{G}^{\otimes n} \tag{2.8}$$

where $\mathbf{G}^{\otimes n}$ denotes the n^{th} Kronecker power of $\mathbf{G}$, as written below:

$$\mathbf{G} = \begin{bmatrix} 1 & 0 \\ 1 & 1 \end{bmatrix} \tag{2.9}$$

$\mathbf{B}_N$ is a permutation matrix, which can be defined recursively as: $\mathbf{B}_N = \mathbf{R}_N(\mathbf{I}_2 \otimes \mathbf{B}_{N/2})$, where $\mathbf{I}_2$ is a 2×2 identity matrix. The effect of matrix $\mathbf{R}_N$ is as follows:

$$[u_1, u_2, u_3, u_4, ..., u_N] \times \mathbf{R}_N = [u_1, u_3, u_5, ...u_{N-1}, u_2, u_4, u_6, ..., u_N] \tag{2.10}$$

Since the matrix $\mathbf{B}_N$ only serves as a re-ordering of indices and it does not affect the properties of polar codes, the author omits this permutation for simplicity in the following parts of this thesis.

The polar encoding procedure aims to identify the K most reliable bit-channels using various polar construction methods [28, 30, 75, 76, 77] to carry information bits u_1^N. The indices of the rest $N-K$ frozen bits are recorded in $\mathbb{F}$. For instance, to build a $C(8,4)$ polar code, $\mathbf{G}^{\otimes 3}$ can be expressed as:

$$\mathbf{G}^{\otimes 3} = \begin{bmatrix} 1 & 0 & 0 & 0 & 0 & 0 & 0 & 0 \\ 1 & 1 & 0 & 0 & 0 & 0 & 0 & 0 \\ 1 & 0 & 1 & 0 & 0 & 0 & 0 & 0 \\ 1 & 1 & 1 & 1 & 0 & 0 & 0 & 0 \\ 1 & 0 & 0 & 0 & 1 & 0 & 0 & 0 \\ 1 & 1 & 0 & 0 & 1 & 1 & 0 & 0 \\ 1 & 0 & 1 & 0 & 1 & 0 & 1 & 0 \\ 1 & 1 & 1 & 1 & 1 & 1 & 1 & 1 \end{bmatrix} \tag{2.11}$$

Four rows are taken for information bits. In such example, u_1, u_2, u_3, u_5 are assumed to be picked as frozen bits, and the other four positions u_4, u_6, u_7, u_8 carry the information. An illustration of the encoding process for a BEC with $\varepsilon = 0.5$ is given in Fig.2.4. Accordingly, the $C(8,4)$ code can be built by performing $x_1^N = u_1^N \mathbf{G}^{\otimes 3}$, as expressed below:

$$\begin{bmatrix} x_1 \\ x_2 \\ x_3 \\ x_4 \\ x_5 \\ x_6 \\ x_7 \\ x_8 \end{bmatrix}^T = \begin{bmatrix} 0 \\ 0 \\ 0 \\ u_4 \\ 0 \\ u_6 \\ u_7 \\ u_8 \end{bmatrix}^T \begin{bmatrix} 1 & 0 & 0 & 0 & 0 & 0 & 0 & 0 \\ 1 & 1 & 0 & 0 & 0 & 0 & 0 & 0 \\ 1 & 0 & 1 & 0 & 0 & 0 & 0 & 0 \\ 1 & 1 & 1 & 1 & 0 & 0 & 0 & 0 \\ 1 & 0 & 0 & 0 & 1 & 0 & 0 & 0 \\ 1 & 1 & 0 & 0 & 1 & 1 & 0 & 0 \\ 1 & 0 & 1 & 0 & 1 & 0 & 1 & 0 \\ 1 & 1 & 1 & 1 & 1 & 1 & 1 & 1 \end{bmatrix} \tag{2.12}$$

It is shown that due to the recursive structure of $\mathbf{G}$, the encoding complexity of polar codes can be reduced from $O(N^2)$, which is the complexity of vector-matrix multiplication, to $O(N\log N)$ [78].

2.3 SC based polar decoding

Polar codes decoded by SC can achieve the channel capacity of B-DMCs when the code length is long enough [28]. In this section, SC and SCL [45] decoding are reviewed. The author notes that there are also some other polar decoding schemes, such as SC-F [79], BP [38], SD [51]. These decoding schemes will be reviewed in the next chapter.

2.3.1 SC polar decoding

For SC decoding, hard decision of the i^{th} estimate $\hat{u}_i$ depends on both received vectors y_1^N and the previous estimation $\hat{u}_1^{i-1}$. The corresponding $\hat{u}_i$ is determined according to its LLR, which is denoted as:

$$L(\hat{u}_i) = \ln(\frac{P(u_i = 0|y_1^N, \hat{u}_1^{i-1})}{P(u_i = 1|y_1^N, \hat{u}_1^{i-1})}) \tag{2.13}$$

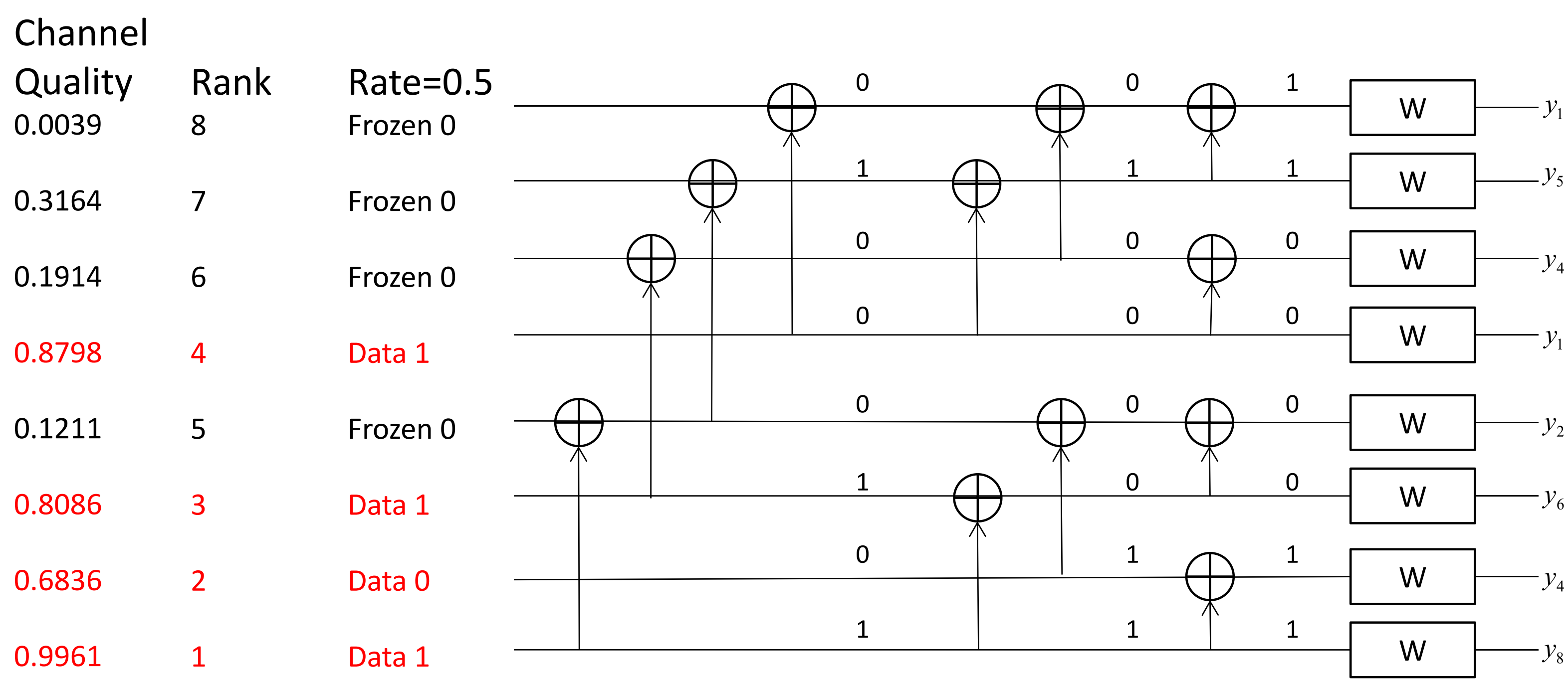

Fig. 2.4: Encoding procedure for a $C(8, 4)$ polar code, BEC with $\varepsilon = 0.5$

Then, the hard decision of $\hat{u}_i$ can be obtained as follows:

$$\hat{u_i} = h(L(\hat{u}_i)) = \begin{cases} u_i, & \text{if } i \in \mathbb{F} \\ \frac{1-\mathrm{sgn}(L(\hat{u}_i))}{2}, & \text{if } i \in \mathbb{F}^c \end{cases} \tag{2.14}$$

where c represent the complementary, and $\mathrm{sgn}(x)$ is the sign function.

It has been reported in [28] that the LLR of $\hat{u}_i$ can be obtained recursively according to the encoding graph of polar coding. Here, the author defines the function $f(a, b, k)$ and $g(a, b, k)$ as follows:

$$f(a, b) = \ln(\frac{1 + e^{a+b}}{e^a + e^b}) \tag{2.15}$$

$$g(a, b, k) = (-1)^k a + b \tag{2.16}$$

where, $a, b \in \mathbb{R}, k \in \{0, 1\}$.

$$L_N^{(2j-1)}(y_1^N, \hat{u}^{2j-2}) = f(L_{N/2}^j(y_1^{N/2}, \hat{u}_{1,o}^{2j-2} \oplus \hat{u}_{1,e}^{2j-2}), L_{N/2}^j(y_{N/2+1}^N, \hat{u}_{1,e}^{2j-2})) \tag{2.17}$$

$$L_N^{(2j)}(y_1^N, \hat{u}^{2j-1}) = g(L_{N/2}^j(y_1^{N/2}, \hat{u}_{1,o}^{2j-2} \oplus \hat{u}_{1,e}^{2j-2})) \tag{2.18}$$

LLR values can be obtained via (2.17) and (2.18) recursively, and in above equations, $1 \leq j \leq N/2$. $\hat{u}_{1,o}^{(2j-2)}$ and $\hat{u}_{1,e}^{(2j-2)}$ denote the odd and even part of $\hat{u}_1^{(2i-2)}$, respectively. The author notes that when $N = 1$, the recursion stops and $L_1^1(y_i)$ should be obtained from the channel input, which equals to $\ln(\frac{P(y_i|x_i=1)}{P(y_i|x_i=0)})$, where $1 \leq i \leq N$. The decoding complexity of SC can be generalized to $O(N\log N)$.

2.3.2 SCL polar decoding

Unlike SC decoding that only keeps one survival path and do hard decision directly, SCL decoding attempts both $\hat{u}_i = 0$ and $\hat{u}_i = 1$ ($i \in \mathbb{F}^c$) by splitting current path into two paths. If the number of decoding paths is larger than a pre-defined list size L, the SCL decoder discards the least probable paths based on the PM, which is given in (2.19), where $l = 1, 2...L$, and keeps the best L paths.

$$PM_l^i = \begin{cases} PM_l^{(i-1)} & \text{if} \quad i \in \mathbb{F} \text{ or } \mathbb{F}^c \text{ and } u_i[l] = h(L_l(u_i)) \\ PM_l^{(i-1)} + |L_l(u_i)| & \text{if} \quad i \in \mathbb{F}^c \text{ or } \mathbb{F} \text{ and } u_i[l] \neq h(L_l(u_i)) \\ +\infty & \text{if} \quad i \in \mathbb{F} \text{ and incorrect value} \end{cases} \tag{2.19}$$

Moreover, by attaching CRC bits behind the original polar codeword, the performance of SCL decoding can be further improved [50]. It has been concluded that due to the large list size, the complexity of SCL decoding, generalized as $O(LN\log N)$, is higher than that of SC decoding. Therefore, to decrease the complexity of SCL, an adaptive-SCL (A-SCL) decoding was proposed [47]. Instead of keeping a fixed list size L, A-SCL doubles the size L only when the estimate $\hat{u}_1^N$ obtained by current size-L SCL cannot pass the CRC. By using such iterative method, unnecessary paths splitting can be avoided while the performance is maintained [80].

2.3.3 Comparison between polar codes and existing coding schemes

Although polar codes have the capacity-achieving construction and provide a new idea for channel coding theory. Compared with other existing codes, polar codes still have many open issues for practical applications. Here, the author summarizes a comparison between these codes in Table.2.1. The author notes that for turbo and LDPC codes, the conclusion is directly quoted from book [81].

The advantages of polar codes can be summarized as follows:

- The design and construction of polar codes are more straightforward and less complex than its competitors.
- Polar codes have been proved to achieve capacity of symmetric B-DMCs because

Table 2.1: Comparison among polar codes, LDPC codes, and turbo codes

<table>
<tr><td rowspan="2"></td><td colspan="2">Encoding</td><td colspan="2">Design and construction</td></tr>
<tr><td>Structure</td><td>Complexity</td><td>Methods</td><td>Complexity</td></tr>
<tr><td rowspan="3">Polar</td><td rowspan="3">Recursive encoder</td><td rowspan="3">$O(N\log N)$ medium</td><td>DE [82]</td><td>High</td></tr>
<tr><td>Tal and Vardy [30]</td><td>Medium</td></tr>
<tr><td>GA [76]</td><td>Low</td></tr>
<tr><td>Turbo</td><td>Convolutional encoder</td><td>$O(mN)$ low</td><td>Interleaver optimization</td><td>High</td></tr>
<tr><td>LDPC</td><td>Matrix multiplication</td><td>$O(N^2)$ high</td><td>Degree distribution optimization</td><td>High</td></tr>
<tr><td colspan="5">Decoding</td></tr>
<tr><td></td><td>Algortithms</td><td>Complexity</td><td colspan="2">Performance</td></tr>
<tr><td rowspan="3">Polar</td><td>SC</td><td>$O(N\log N)$ low</td><td colspan="2">Sub-optimal</td></tr>
<tr><td>SCL</td><td>$O(LN\log N)$ medium</td><td colspan="2">Approach ML</td></tr>
<tr><td>BP</td><td>$O(TN\log N)$ high</td><td colspan="2">Sub-optimal</td></tr>
<tr><td>Turbo</td><td>Iterative BCJR</td><td>$O(T4N2^m)$ high</td><td colspan="2">Approach ML</td></tr>
<tr><td>LDPC</td><td>BP</td><td>$O(T(N\bar{d}_v + M\bar{d}_c))$ high</td><td colspan="2">Approach ML</td></tr>
<tr><td>Notation List</td><td colspan="4">One turbo code has two convolutional component codes
m: memory length of the component codes
T: maximum iterations
N: code length
M: number of check nodes
L: list size
$\bar{d}_v(\bar{d}_c)$: average check degree distribution of the LDPC code</td></tr>
</table>

of their code structures. Therefore, polar codes have a theoretic advantage over the other two codes.

- Polar codes can achieve better performance than that of other codes with some specific decoding schemes (SCL or SCL+CRC) with lower complexity, which is shown in Table.2.1.

Nevertheless, polar codes also have disadvantages compared with its competitors, which are:

- For polar codes construction, the channel reliability should be calculated based on different channel types, which means the code construction is channel dependent though the code structure is universal (The positions of information bits may be different with different channel types.).

- Classical polar decoding methods have obvious disadvantages. SC based schemes are easy to be implemented, but they usually have high latency. BP decoding has high throughput, but its performance is not satisfying compared with turbo and LDPC codes due to the structure of polar codes. SD achieves ML performance, but its complexity is very high, which is almost impractical when the code length is long.

2.4 Summary

In this chapter, the author gave the preliminary knowledge of polar codes, including: the theory of channel polarization, polar encoding and decoding. The author notes that although in this thesis, how to construct polar codes is not the priority, the introduction of polar encoding is necessary and helpful for the development of the following chapters. Further, the author also reviewed SC and SCL decoding algorithms for polar codes, which are usually used as a benchmarks when comparing with polar decoding schemes. Moreover, the comparison of polar codes and other classical channel coding schemes was also provided. According to the comparison, we know that polar coding has its unique advantages, which help it to become a strong candidate for next generation communication networks. Therefore, many works related to polar decoding have been proposed.

In next chapter, the author will introduce several modified polar decoding schemes developed during the author's PhD program. These modified polar decoding schemes can surpass existing methods by improving the error performance or reducing the complexity.

3 MODIFIED POLAR DECODING SCHEMES

In order to design a polar-coded OFDM-IM system, the investigation in polar decoding is inevitable. Therefore, during the author's Ph.D study, most polar decoding schemes are investigated. These schemes own different advantages and the author found most of them can be improved in terms of their error correction performance or complexity reduction. In this chapter, the author introduces three modified polar decoding schemes based on SC, BP and SD, respectively, and they are able to achieve enhanced performance in terms of error correction or complexity reduction. Furthermore, in this chapter, the author also introduces a novel stopping criterion to reduce BP decoding latency.

3.1 A novel SC flip stack decoding based on GA for polar codes

3.1.1 Introduction

Polar coding is regarded as a major breakthrough in information theory. Polar codes achieve channel capacity using SC decoding with long codeword length [28]. Nevertheless, when the code length is moderate or short, the decoding performance of SC is sub-optimal. To improve the performance of SC, SC-F based schemes were proposed by flipping potential incorrect bits [79, 83, 84]. Compared with SC decoding, SC-F achieves lower frame error rate (FER) with similar complexity in moderate to high SNRs. However, the conventional SC-F still has inferior performance than that of SCL [45], which is caused by following reasons: first, SC-F flips one bit in each iteration, leading the case that has more than one errors cannot be corrected. Second, criteria of choosing unreliable bits in SC-F are too naive to make an efficient decoding. Therefore, to solve these drawbacks, in this section, a stack is utilized to correct more error bits, and GA [75] is introduced to effectively recognize incorrect bits. By using these modifications, the proposed SC-F is able to correct more than one errors and achieve lower FER performance than that of the conventional SC-F.

3.1.2 SC decoding in a block by block perspective

We note that SC decoding is usually introduced in a view of bit by bit prospect, as what we have introduced in Chapter.2. However, in this section, we describe SC in a block by block prospective for a better understanding of the proposed SC-F. For simplicity, a $C(2^4, 9)$ polar code is given as an example, where 2^4 is the code length N, "9" is the number of information bits, and the indices of information bits are $[6, 7, 8, 11, 12, 13, 14, 15, 16]$. Fig.3.1.(b) illustrates a decoding tree of SC, where black leaf nodes are information bits, and the white ones are frozen bits. In most articles, these nodes are called: rate-0 (white), rate-r (gray) and rate-1 (black, which are A,B,C,D in Fig.3.1.(b)) based on different kinds of bits (frozen or free) they contain [85]. As shown in Fig.3.1.(a), a decoding node v receives a soft information vector α_v from its parents p_v and is responsible to produce an estimate $\hat{u}_v$. The initialization of root nodes are obtained from the channel output y_1^N with $\alpha_{vroot} = (\lambda_1, \lambda_2, ...\lambda_N)$, where λ_i is the i^{th} received LLR, which is denoted as: $\lambda_i = \ln\frac{P(y_i|x_i=0)}{P(y_i|x_i=0)}$. When a local decoder v is activated, α_{vl} is obtained through:

$$\alpha_{vl}[i] = f(\alpha_v[2i-1], \alpha_v[2i]), \text{ for } i = 1, ..., 2^{n-d_v-1} \tag{3.1}$$

and given to v_l, where n and d_v is equivalent to $\log_2 N$ and the depth of node v, respectively. The operator $f(x)$ is defined as: $2\tanh^{-1}(\tanh(\frac{x}{2})\tanh(\frac{x}{2}))$. After receiving $\hat{u}_{vl}$ from v_l, the local decoder v then activates its right node v_r and α_{vr} can be obtained via:

$$\alpha_{vr}[i] = \alpha_v[2i-1](1 - 2\hat{u}_{vl}[i]) + \alpha_v[2i] \text{ for } i = 1, ..., 2^{n-d_v-1} \tag{3.2}$$

Then, node v receives $\hat{u}_{vr}$ from v_r and calculates $\hat{u}_v$ via:

$$\begin{aligned} \hat{u}_v[2i] &= \hat{u}_{vr}[i] \\ \hat{u}_v[2i-1] &= \hat{u}_{vl}[i] \oplus \hat{u}_{vr}[i], \text{ for } i = 1, ..., 2^{n-d_v-1} \end{aligned} \tag{3.3}$$

Then, node v passes $\hat{u}_v$ to p_v. The local decoder v is finished when node v obtained $\hat{u}_v$. Then, the same operation is operated at the next node. Finally, leaf nodes perform the following hard decision if such leaf nodes are not frozen:

$$\hat{u}_{v,leaf} = \begin{cases} 0, \text{ if } \alpha_{v,leaf} \geq 0 \\ 1, \text{ otherwise} \end{cases}$$

Here, the $\hat{u}_{v,leaf}$ is denoted as the estimated information bits.

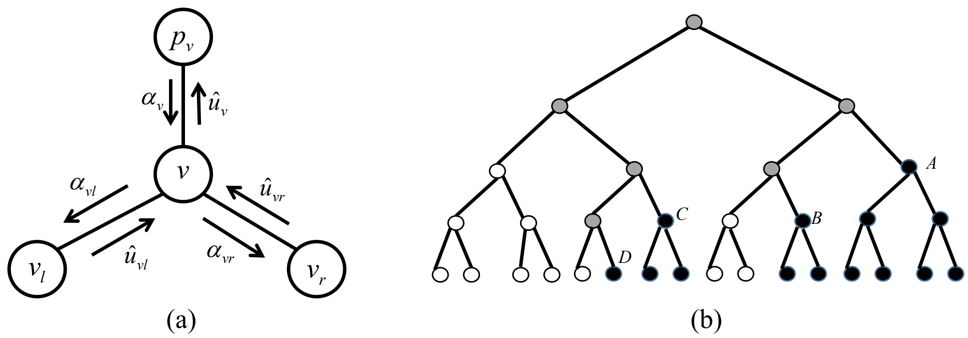

Fig. 3.1: Illustration of (a). local decoder of SC; (b). full binary tree for $N = 2^4$

3.1.3 Criteria for unreliable bit selection

It has been illustrated that in most SC decoding scenarios, there is only one bit error occurred, and this behavior becomes remarkable with the increase of SNR. However, this sole incorrectness may compromise consecutive output LLRs and leads "error propagation". Hence, SC-F aims to correct the first error bit that could cause error propagation. Intuitively, criteria of selecting unreliable bits are critical for SC-F decoding. Here, unlike the conventional SC-F that only relies on LLRs, we propose two criteria based on GA and "critical set" [86], which are helpful to find these unreliable bits.

Criterion.1: Assume a node v with length m, $\alpha_v = [\alpha_1, \alpha_2, ..., \alpha_m]$, and $\mathbf{u}_v = [u_1, u_2, ..., u_m]$. A bit can be regarded as unreliable if $|\alpha_i| < \ln\frac{1-\bar{P}_e(u_i)}{\bar{P}_e(u_i)}$, where $\bar{P}_e(u_i)$ is the average error probability of the i^{th} bit, and $\bar{P}_e(u_i)$ is low. The proof of this criterion is given in the appendix.

Criterion.2: The first incorrect bit is highly possible in set $\mho$, which contains the first unfrozen bits of all rate-1 nodes and may have variant length. The proof of Criterion.2 has been given in [86].

3.1.4 The proposed SC-F scheme

We know that for polar codes, the FER performance of ML decoding is superior than that of the conventional SC-F. The ML result can be obtained by minimizing the squared Euclidean distance (SED) between the estimated $\hat{u}_1^N$ and received sequence y_1^N, which can be described as: $\hat{u}_1^N = \underset{u}{\operatorname{argmin}}(|y_1^N - (\mathbf{1} - 2u_1^N \mathbf{G}^{\otimes n})|^2)$, where $\mathbf{1}$ is an all one vector. However, in the conventional SC-F, estimates may not have the lowest SED among intermediate estimated results obtained during the flipping process. Also, the received sequence may have more than one incorrect bits due to the channel condition. Intuitively, a stack that stores the indices of flipping bits that result in the lowest SED during the iterations can be utilized to correct more than one errors. The usage of stack is illustrated in Fig.3.2. For example, the 4^{th} and 10^{th} bits are incorrectly decoded. In the conventional SC-F, after flipping the 4^{th} bit, the CRC fails and the sequence remains unchanged. However, due to the lower SED after flipping the 4^{th} bit, the proposed method includes this bit to the stack. Compared with the conventional SC-F, the procedure of the proposed method is given as follows.

Step.1: Initialization: set a stack $ID = \varnothing$. Then, do a SC decoding, and obtain LLRs α_i, for $i = 1, 2, ..., N$. If CRC passes, output $\hat{u}_1^N$, otherwise, go to **Step.2**.

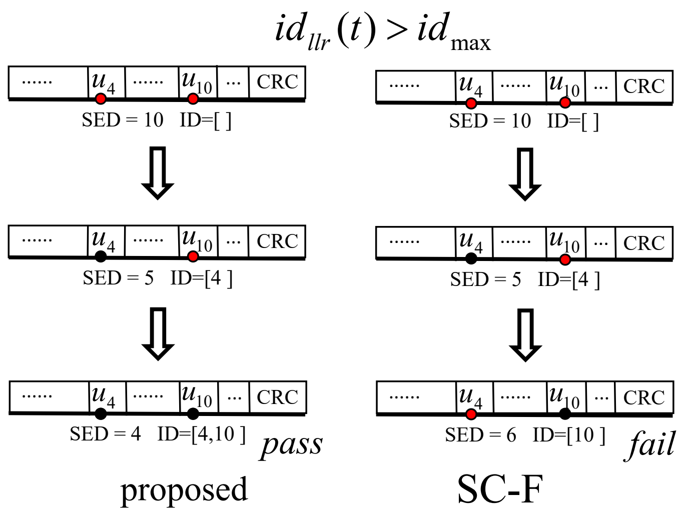

Fig. 3.2: Illustration of decoding procedure between the conventional SC-F and the proposed method

Step.2: Construct a flipping set idbook$_{llr}$: first, construct indices set $\mho$ based on *Criterion.2*. Then, for a node i in set $\mho$ with LLRs α_i, if $|\alpha_i| < k\ln\frac{1-\bar{P}_e(u_i)}{\bar{P}_e(u_i)}$, where k is a constant obtained from experiments, which is great than 1, includes such i into idbook$_{llr}$.

Step.3: Do SC-F and check: set a iteration number T. Then, do SC-F based on idbook$_{llr}$. If CRC passes, output $\hat{u}_1^N$. Otherwise, update the stack based on following rules: after one flipping on bit i in the iteration t, if the corresponding SED is smaller than the previous one in the stack, store such index i in the list of stack ID[ ] and keep the current $\hat{u}_1^N$ for next iteration.

Step.4: Output and check: if CRC passes or $t = T$, output $\hat{u}_1^N$, otherwise, $t = t+1$ and go to the **Step.3**.

We note that when the corresponding SED of $id_{llr}(t)$ is smaller than that of the stored one, if the present flipping bit index $id_{llr}(t)$ at the t^{th} iteration is smaller than the largest index id_{max} saving in the stack, only the indices in stack that are smaller than $id_{llr}(t)$ can be used in the next iteration. Let assume that the 4^{th} bit is the wrong decision. However, since $|\alpha_4| > |\alpha_{10}|$, the 10^{th} bit is flipped first. After, since the SED is lower than that of the previous one, the stack stores index 10. However, when the 4^{th}

bit comes to the stack, the index 10 must be removed from the stack. Otherwise, SC-F decoding can never be successful even reaching the maximum number of iterations.

The value of $\hat{P}_e(\hat{u}_i)$ can be obtained off-line via GA. Also, the set $\mho$ can be obtained off-line based on the structure of polar codes. Therefore, the complexity of the proposed method does not increase compared with the conventional SC-F.

3.1.5 Simulation results

In this section, FER and complexity performances between the proposed SC-F and the conventional SC-F in AWGN channels are compared. In our simulations, code length $N = 1024$ and code rate $R = 0.5$. Moreover, since SCL decoding can achieve an impressive performance among existing polar decoding methods [87], the performance of SCL with $L = 16$ is also included as a reference. We note that the CRC used in this part was 16 bits and the generation polynomial was $x^{16} + x^{15} + x^2 + x^1$)

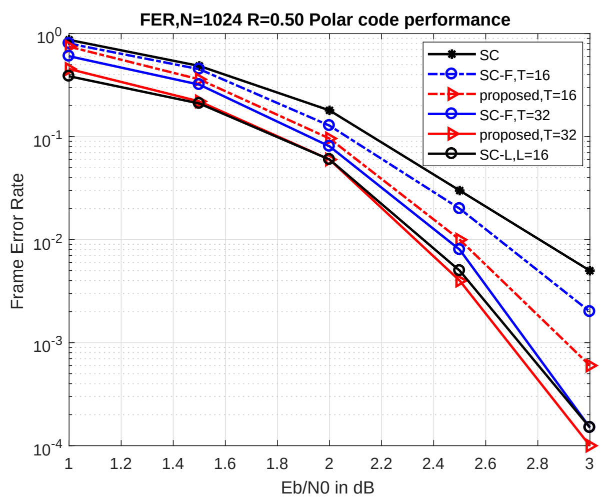

Fig. 3.3: FER performance among the proposed SC-F, conventional SC-F, and SCL decoding methods

Fig.3.3 indicates the FER performance of the proposed SC-F and conventional SC-F in AWGN channels. In the simulation, different iterations T are used. It is shown that the proposed SC-F achieves better FER performance than that of the conventional SC-F with the same number of T. The increase of T is helpful to obtain a better performance. Additionally, it is shown that in low SNR scenarios, the gap between two different methods is small. However, with the increase of SNR, the proposed method is more likely to find incorrect bits. Moreover, compared with SCL decoding, the proposed SC-F with $T = 32$ can achieve a similar decoding performance.

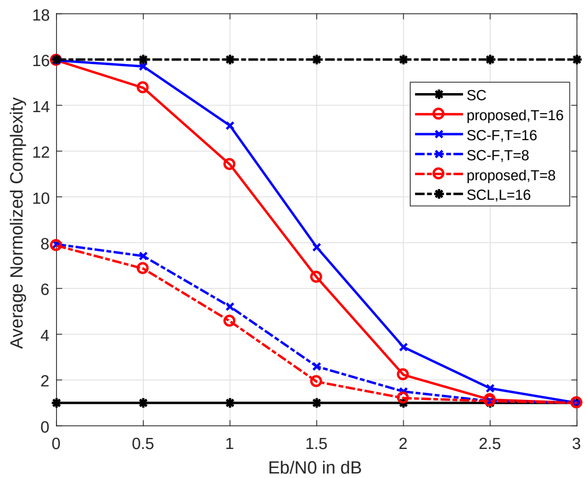

Fig. 3.4: Average normalized computational complexity among the conventional, proposed SC-F and SCL decoding methods

In Fig.3.4, we give the average normalized complexity [79] of the proposed and conventional SC-F when $T = 8$ and $T = 16$. As a reference, the complexities of SC and SCL are also included. It is indicated that the complexity of proposed decoding method is lower than that of the conventional SC-F when Eb/N0 is low. It is because by including more bits into the stack, the proposed method can correct more than one bits, which may lead the decoding process terminate earlier. Additionally, it is illustrated that the complexity of both SC-F converge very quick, and when the Eb/N0 is larger than 2.5 dB, the complexity of both SC-F methods are almost the same as that of SC. Also, compared with SCL decoding, the proposed SC-F can achieve similar FER performance with lower complexity.

3.2 Novel decoding schemes for polar codes based on BP

3.2.1 Introduction

Polar codes have been considered as a type of capacity-achieving codes for B-DMCs [28]. SC [28] and BP [38] are two widely applied decoding algorithms for polar codes. In general, SC is less complex than other types of decoding methods [87] (e.g. BP or SD [51]). However, with the constraint of code length, SC exhibits sub-optimal error correction performance with high latency. Therefore, many researchers have attempted to improve SC by increasing its complexity [50, 88, 89, 90, 45]. Meanwhile, BP is considered as an alternative polar decoding method. Although BP still show sub-optimal performance, it exhibits higher throughput and lower latency due to its parallel structure. Nevertheless, only a few recent works, [41]- [40], have developed modified versions of BP polar decoding to achieve better performance. In [41], to solve three common error patterns present in BP, a post-processing approach was proposed and achieved significant performance gain. In [40], it was prposed a BP-list (BPL) decoding algorithm that outperformed SCL. Furthermore, a noise aided BP (N-BP) proposed in [42] improved decoding performance by adding random noise. Besides these modified BP decoders, some schemes based on outer code concatenation or modified polar coding constructions were also proposed [43, 44]. However, these methods tried to modify the structure of polar codes.

In this section, we first propose two enhanced BP decoders to improve the error correction performance of polar codes. The interleaved-BP (I-BP) consists of a group of distinct interelavers, designed according to decoding factor graphs. The multiple candidates-BP (M-BP) yields several candidates by adding random offsets with different variances. Both I-BP and M-BP can generate several estimated codeword candidates which have different soft values. Then, the candidate that meets stopping criterion [71] and ML rule is selected. In conjunction with the proposed BP decoders, a feedback structure is introduced. This structure enhances reliable bits and flips unreliable bits based on their LLRs. If at the end of a round of decoding neither the stopping criterion nor the ML rule is met, the receiver feeds back the processed (enhanced or flipped) *a posteriori* information of the selected candidate yielded by M-BP or I-BP as the initial messages used for the next iteration. By exchanging these informations iteratively, the error correction performance of the decoder can be improved at the expense of increasing complexity and latency.

3.2.2 Belief propagation decoding

In this section, we consider a $C(N, K)$ polar code of length $N = 2^M$ with K ($K \leq N$) free bits. Here, the index sets of frozen and free bits are denoted as $\mathbb{F}$ and $\mathbb{F}^c$, respectively. The message vector $\mathbf{u}$ and polar codeword $\mathbf{x}$ are denoted as $[u[1], u[2], ..., u[N]]$ and $[x[1], x[2], ..., x[N]]$, respectively.

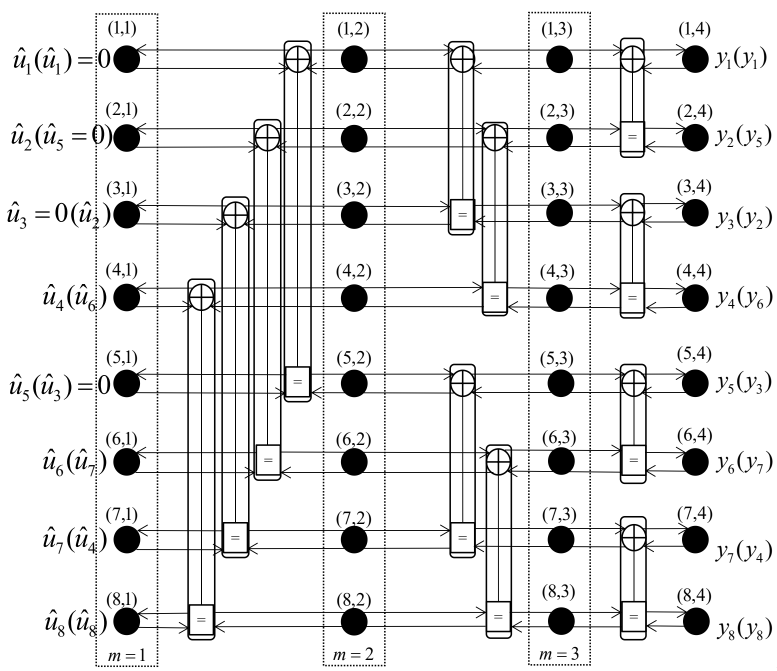

Fig. 3.5: Factor graph of a $C(8, 5)$ polar code

BP polar decoding can be viewed as a message-passing algorithm over the factor graph of polar code. For example, Fig.3.5 illustrates the factor graph for a $C(8, 5)$ polar code, with $u[1], u[3], u[5]$ as frozen bits. A BP decoder consists of $MN/2$ *processing elements* (PE), where $M = \log_2 N$. Fig.3.6 gives a detailed view of the message flow for a single PE. The soft messages from right to left and left to right are denoted by $L^t_{i,m}$ and $R^t_{i,m}$, respectively, where $i = 1, \ldots, N$ is the bit index, $m = 1, \ldots, M$ is the stage index, and t is the iteration number. The leftmost value of $R^t_{i,1}$ is 0 ($i \in \mathbb{F}^c$) for free bits and ∞ for frozen bits ($i \in \mathbb{F}$). The rightmost messages $L^t_{i,M+1}$ is obtained according to $\ln \frac{P(x[i]=0|\mathbf{y})}{P(x[i]=1|\mathbf{y})}$, where $\mathbf{y}$ denotes the received signal. In each iteration, the message-passing algorithm is initiated from $m = M$ (rightmost) and $m = 1$ (leftmost), respectively. The update equations for a PE can be simplified considerably by the following scaled min-sum (SMS) updates, [91]:

$$
\begin{aligned}
L^t_{i,m} &= g(L^{t-1}_{i,m+1}, L^{t-1}_{i+N/2^m,m+1} + R^t_{i+N/2^m,m}) \\
L^t_{i+N/2^m,m} &= L^{t-1}_{i+N/2^m,m+1} + g(L^{t-1}_{i,m+1}, R^t_{i,m}) \\
R^t_{i,m+1} &= g(R^t_{i,m}, L^{t-1}_{i+N/2^m,m+1} + R^t_{i+N/2^m,m}) \\
R^t_{i+N/2^m,m+1} &= R^t_{i+N/2^m,m} + g(L^{t-1}_{i,m+1}, R^t_{i,m})
\end{aligned} \tag{3.4}
$$

where $g(a, b)$ is defined as follows:

$$
g(a, b) = \alpha \ \mathrm{sgn}(a) \ \mathrm{sgn}(b) \ \min(|a|, |b|) \tag{3.5}
$$

and α is a constant scaling factor.

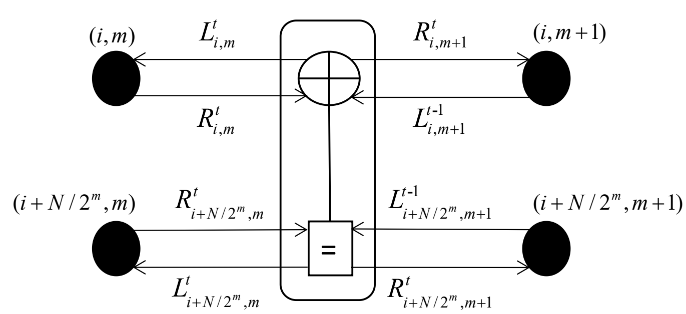

Fig. 3.6: PE for a BP decoder

The BP algorithm is run for a fixed number of iterations T or can be stopped as soon as a codeword is obtained. At the tth iteration, from the *a posteriori* information computed on the left side of the factor graph at node $(i, 1)$, the hard decision of the information bit $u[i]$ denoted by $\hat{u}[i]$ is obtained, as

$$\hat{u}[i] = \text{sgn}(L_{i,1}^t + R_{i,1}^t). \tag{3.6}$$

Similarly, at the same iteration, the hard decision of the code bit $x[i]$ denoted by $\hat{x}[i]$ can be obtained on the right side of the graph at node $(i, M+1)$, as

$$\hat{x}[i] = \text{sgn}(L_{i,1+M}^t + R_{i,1+M}^t). \tag{3.7}$$

A possible stopping rule is the following: if the vectors $\hat{\mathbf{u}} = [\hat{u}[1], \ldots, \hat{u}[N]]$ and $\hat{\mathbf{x}} = [\hat{x}[1], \ldots, \hat{x}[N]]$, consisting of the hard decisions of $x[i]$ and $u[i]$, respectively, can satisfy the following equation, [71, 1]:

$$\hat{\mathbf{x}} = \hat{\mathbf{u}}\mathbf{G}^{\otimes M}.$$

The performance of the BP decoder can be improved by running more iterations [92]. The latency of BP is $O(\text{log}N)$ [38], which is low relative to that of SC, which is $O(N)$.

A typical BP decoding process is given in the Algorithm.3.1.

3.2.3 Novel decoding schemes based on BP for polar codes

In this section, I-BP is first proposed. Then, M-BP is proposed in the second part. Last, in the third part of this section, the proposed feedback structure is introduced.

3.2.3.1 Interleaved-BP decoding scheme :

A BP factor graph is illustrated in Fig.3.5, where a $C(8, 5)$ polar code with $\mathbb{F} = \{1, 3, 5\}$ is processed. Ideally, we assume that $\mathbf{x} = \mathbf{y}$. According to the fac-

Algorithm 3.1 (N, K) BP polar decoding: $(\hat{\mathbf{u}}, \hat{\mathbf{x}}) = \mathbf{BP}(\mathbf{y}, \mathbb{F})$

Initialization :
Initial values for BP using the received vector $\mathbf{y}$: $\lambda[i] = \ln\frac{P(x[i]=0|\mathbf{y})}{P(x[i]=1|\mathbf{y})}$;
The index set of the frozen bits $\mathbb{F}$;
The maximum iterations T and scale factor α
For each node (i, m), initialize messages $L_{i,m}^t$ and $R_{i,m}^t$;
if $(m == 1)$ & $(i \in \mathbb{F})$ **then**
  $R_{i,m}^t \leftarrow \infty$, $t = 0, 1, ...T$;
else if $(m == M)$ **then**
  $L_{i,m}^t \leftarrow \lambda[i]$, $t = 0, 1, ...T$;
else
  $L_{i,m}^0 \leftarrow 0, R_{i,m}^0 \leftarrow 0$;
end if
while $1 < t < T$ **do**
  Update: $L_{i,m}^t$ and $R_{i,m}^t$ according to eq.(3.4);
  Update: $\hat{\mathbf{x}}$ according to (3.7) and $\hat{\mathbf{u}}$ according to (3.6);
  $t \leftarrow t + 1$ & Start the next iteration;
end while
Output: $\hat{\mathbf{u}}$ and $\hat{\mathbf{x}}$

tor graph, the following observations can be obtained: if the input sequence $\mathbf{y}$ is $[y[1], y[2], y[3], y[4], y[5], y[6], y[7], y[8]]$, according to the factor graph, the estimated result can be calculated as:

$$\begin{bmatrix} u[1] \\ u[2] \\ u[3] \\ u[4] \\ u[5] \\ u[6] \\ u[7] \\ u[8] \end{bmatrix}^T = \begin{bmatrix} y[1] \\ y[2] \\ y[3] \\ y[4] \\ y[5] \\ y[6] \\ y[7] \\ y[8] \end{bmatrix}^T \begin{bmatrix} 1 & 0 & 0 & 0 & 0 & 0 & 0 & 0 \\ 1 & 1 & 0 & 0 & 0 & 0 & 0 & 0 \\ 1 & 0 & 1 & 0 & 0 & 0 & 0 & 0 \\ 1 & 1 & 1 & 1 & 0 & 0 & 0 & 0 \\ 1 & 0 & 0 & 0 & 1 & 0 & 0 & 0 \\ 1 & 1 & 0 & 0 & 1 & 1 & 0 & 0 \\ 1 & 0 & 1 & 0 & 1 & 0 & 1 & 0 \\ 1 & 1 & 1 & 1 & 1 & 1 & 1 & 1 \end{bmatrix} \tag{3.8}$$

thus $\hat{\mathbf{u}}$ in order $[1, 2, 3, 4, 5, 6, 7, 8]$ can be obtained. Likewise, if $\mathbf{y}$ in order $[1, 5, 2, 6, 3, 7, 4, 8]$ is sent to the decoder (indicated in the brackets of Fig.3.5), the corresponding output is calculated as:

$$\begin{bmatrix} u[1] \\ u[5] \\ u[2] \\ u[6] \\ u[3] \\ u[7] \\ u[4] \\ u[8] \end{bmatrix}^T = \begin{bmatrix} y[1] \\ y[5] \\ y[2] \\ y[6] \\ y[3] \\ y[7] \\ y[4] \\ y[8] \end{bmatrix}^T \begin{bmatrix} 1 & 0 & 0 & 0 & 0 & 0 & 0 & 0 \\ 1 & 1 & 0 & 0 & 0 & 0 & 0 & 0 \\ 1 & 0 & 1 & 0 & 0 & 0 & 0 & 0 \\ 1 & 1 & 1 & 1 & 0 & 0 & 0 & 0 \\ 1 & 0 & 0 & 0 & 1 & 0 & 0 & 0 \\ 1 & 1 & 0 & 0 & 1 & 1 & 0 & 0 \\ 1 & 0 & 1 & 0 & 1 & 0 & 1 & 0 \\ 1 & 1 & 1 & 1 & 1 & 1 & 1 & 1 \end{bmatrix} \tag{3.9}$$

which is $\hat{\mathbf{u}}$ in the same order $[1, 5, 2, 6, 3, 7, 4, 8]$.

From the above observations, we can see that when $\mathbf{y}$ with a specific order is input, output $\hat{\mathbf{u}}$ with the same order can be calculated according to the factor graph. This specific input order of $\mathbf{y}$ can be achieved by a group of interleavers. A block diagram of the proposed I-BP is given in Fig.3.7. The received sequence $\mathbf{y}$ is firstly interleaved by a group of interleavers before sending to a set of BP decoders. An interleaver is a device that operates on a block of N symbols to reorder or permute them, without repeating or omitting any of the symbols in the block [93]. From a mathematical point of view, an interleaver can be considered as a bijective map that maps every vector to a permuted version of itself. Here, we define a set of J distinct interleavers $\{\Pi_j\}$ with the following mapping functions:

$$\pi_j(i) = \begin{cases} \left\lfloor \frac{(i-1)}{2^j} \right\rfloor 2^j + \Phi_j[\frac{(i+1)}{2}] & i \text{ is odd} \\ \left\lfloor \frac{(i-2)}{2^j} \right\rfloor 2^j + \Phi_j[\frac{i}{2}] + 2^{j-1} & i \text{ is even} \end{cases} \tag{3.10}$$

where $1 \leq j \leq J$, $1 \leq i \leq N$, $\lfloor \cdot \rfloor$ means the integer value of the argument. Φ_j is a length $N/2$ sequence, which is defined as:

$$\Phi_j = \underbrace{[1, ..., 2^{j-1}, 1, ..., 2^{j-1}, ..., 1, ..., 2^{j-1}]}_{\frac{N}{2}} \tag{3.11}$$

For example, if $N = 8$, $j = 2$, Φ_2 is written as: $[1, 2, 1, 2]$. Then, the interleaver Π_2 is expressed as: $\Pi_2 : [1, 3, 2, 4, 5, 7, 6, 8]$. Based on the factor graph and above observations, interleavers $\{\Pi_j\}$ with $j = 1, 2, 3$ for a length-8 polar code is given in Table.3.1.

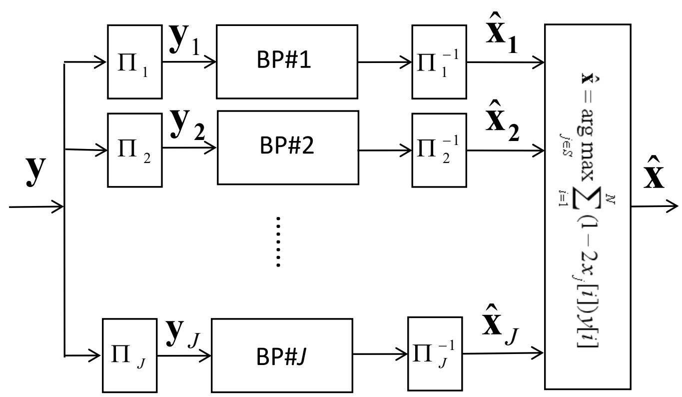

Fig. 3.7: Block diagram of the proposed I-BP decoder

Table 3.1: Available Interleavers for a $N = 8$ Polar Code

Π_j	[$\pi_j(1)$,$\pi_j(2)$,$\pi_j(3)$,...,$\pi_j(8)$]
Π_1	[1, 2, 3, 4, 5, 6, 7, 8]
Π_2	[1, 3, 2, 4, 5, 7, 6, 8]
Π_3	[1, 5, 2, 6, 3, 7, 4, 8]

The interleavers $\{\Pi_j\}$ can generate J different vectors $\mathbf{y}_j$,

$$\mathbf{y}_j = [y_j[1], y_j[2], ..., y_j[N]], \tag{3.12}$$

by permuting symbols in the input sequence $\mathbf{y}$, as:

$$\begin{aligned}\mathbf{y}_j &= \Pi_j(\mathbf{y}) \\ &= [y[\pi_j(1)], y[\pi_j(2)], ..., y[\pi_j(N)]]\end{aligned} \tag{3.13}$$

As a result, the components of the new vectors $\mathbf{y}_j$ are obtained from the components of $\mathbf{y}$ as follows:

$$y_j[i] = y[\pi_j(i)] \tag{3.14}$$

for $j = 1, 2, ..., J$ and $i = 1, 2, ..., N$.

According to (3.10), we know that as long as j is defined, the interleaver Π_j is solely determined. Essentially, the mapping of these interleavers are defined based on the relationship of nodes connected by "$\oplus$" according to the factor graph on each stage m. Therefor, the number of available interleavers is limited to M, thus $J \leq M$. We note that if random interleavers are applied, transmitted bits may cannot be recovered by utilizing the BP polar decoding graph. For instance, if $\mathbf{y}$ with a random order $[2, 1, 8, 7, 4, 3, 6, 5]$ is sent to a BP decoder, the output sequence using the decoding graph will be:

$$\begin{bmatrix} y[1] \oplus y[1] \oplus y[2] \oplus y[3] \oplus y[4] \oplus y[5] \oplus y[6] \oplus y[7] \oplus y[8] \\ y[1] \oplus y[3] \oplus y[5] \oplus y[7] \\ y[5] \oplus y[6] \oplus y[7] \oplus y[8] \\ y[5] \oplus y[7] \\ y[3] \oplus y[4] \oplus y[5] \oplus y[6] \\ y[3] \oplus y[5] \\ y[5] \oplus y[6] \\ y[5] \end{bmatrix} \tag{3.15}$$

which is not a valid codeword. Therefore, I-BP implements at most M distinct interleaving operations using Π_j based on (3.10). Then, a parallel BP decoding are implemented continuously until stopping criteria are met or $t = T$. Subsequently, de-interleavers Π_j^{-1} are required to obtain $\hat{\mathbf{x}}_j$ in the correct order. After finishing decoding and de-interleaving operations, J candidates can be obtained. Denote S as the indices set of J candidates. The following rule is employed to choose a candidate as the final output:

$$\hat{\mathbf{x}} = \underset{j \in S}{\operatorname{argmax}} \sum_{i=1}^{N} (1 - 2x_j[i])y[i], \;\; j = 1, 2, ...J \tag{3.16}$$

which is virtually the ML rule for BPSK modulation.

In practice, the interleavers of I-BP can be obtained in advance since the decoding factor graph is pre-determined. We note that by applying the proposed interleavers, indices of frozen bits, as well as the structures of BP decoders, are not changed. However, by utilizing different interlavers, final LLRs of $\hat{\mathbf{u}}$ or $\hat{\mathbf{x}}$ may be changed because of different intermediate computations in the factor graph. These different soft values may generate variant estimated $\hat{\mathbf{x}}$, which give us more chance to choose the correct estimate.

3.2.3.2 Multiple candidates-BP decoding scheme :

It is known that the initial LLRs which are depended on the received vector $\mathbf{y}$ are critical to BP decoding. The proposed M-BP yields a group of different initial values by adding a set of random vectors $\mathbf{d}_j = [d_j[1], d_j[2], ..., d_j[N]]$ with $1 \le j \le J$, where J denotes the maximum number of candidates. By utilizing these different initial $\mathbf{y}_j$, where $\mathbf{y}_j = [y_j[1], y_j[2], ..., y_j[N]]$, J different estimated codewords $\hat{\mathbf{x}}_j = [x_j[1], x_j[2]..., x_j[N]]$ or information bits $\hat{\mathbf{u}}_j = [u_j[1], u_j[2]..., u_j[N]]$ can be obtained.

After generating J candidates, M-BP also follows (3.16) to select the final output.

An initial vector $\mathbf{y}_j$ for M-BP decoding can be expressed in the following way:

$$y_j[i] = y[i] + d_j[i], \quad i = 1, 2, ...N \tag{3.17}$$

where $d_j[i]$ denotes a Gaussian variable with zero mean and variance σ_0^2. Here, we also denote the set of candidates $\hat{\mathbf{x}}_j$ as S

A very practical problem is how to choose the optimal σ_0^2, which is utilized to generate a random vector $d_j[i]$. Parameter optimization with careful mathematical proof remains an open question. In [42], it was shown that using noise generated by random variance can improve the decoding performance of BP. In this part, instead of using random variance σ_0^2 [42], a fix value of σ_0^2 is obtained from experiments. Fig.3.8 shows that the value of σ_0 is associated with the value of SNR. It is indicated that the impact of σ_0^2 is small at low SNRs. Hence, in the simulation, we choose $\sigma_0^2 = 0.2$ based on the result when SNR is 2.5 dB.

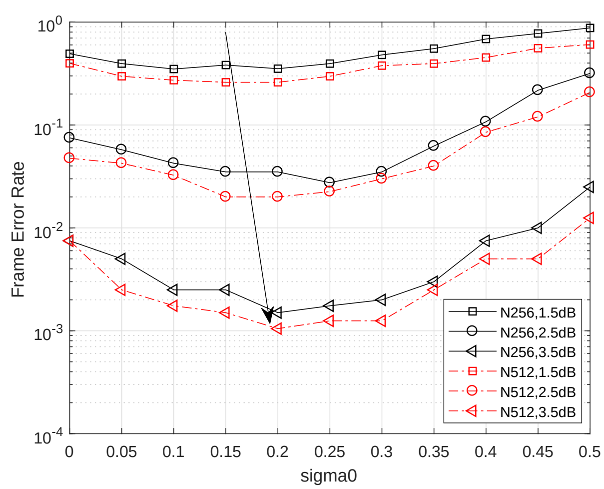

Fig. 3.8: Impact of σ_0 in M-BP on FER with 1/2 code rate, variable code length and SNR

The block diagram indicating the proposed M-BP is given in Fig.3.9. According to the block diagram, the received signal $\mathbf{y}$ is first scrambled by a random vector $\mathbf{d}_j$. Then, J parallel BP decoding are implemented. Then, M-BP selects candidates that satisfies stopping criteria and output the most probable one based on (3.16). We note that unlike I-BP, the available number of candidates for M-BP is not limited by M, which provides flexibility. Nevertheless, simulation results show that I-BP can obtain better performance than that of I-BP with the same number of candidates.

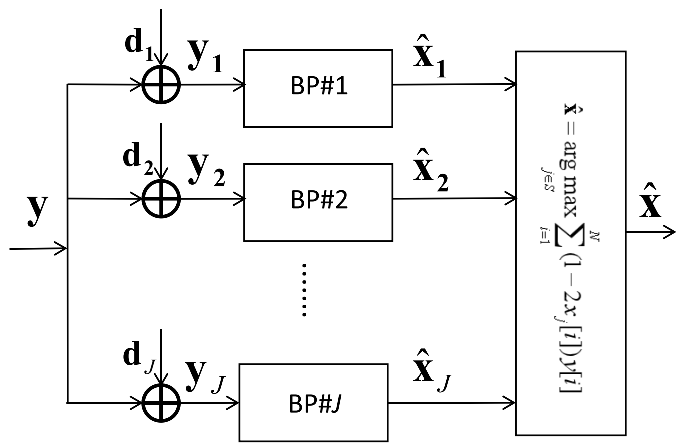

Fig. 3.9: Block diagram of the proposed M-BP decoder

3.2.3.3 M-BP and I-BP with the feedback structure :

From the previous section, we know that the proposed BP schemes generate multiple candidates, which have different LLRs. In these decoding procedures, some decoded bits are unchanged even they are affected by different permutations or offsets, revealing that these bits are reliable. In contrast, some decoded bits have low reliability (measured by LLRs) or oscillate easily during the decoding procedure, suggesting that these bits are unreliable and may be potentially incorrect. Inspired by these behaviors, in this section, a feedback structure is proposed, which can be cascaded to the proposed BP schemes. The feedback structure freezes reliable bits and flips unreliable bits. Subsequently, these processed bits are fed back to decoders as the leftmost priori information $\mathbf{R}$ and the *a posterirori* information $\mathbf{L}$ on the rightmost side, to enhance the decoding performance. These information are exchanged iteratively until the output sequence meets stopping criteria or the iteration of the feedback structure *iter* reaches its maximum I.

Fig.3.10 shows a proposed BP (M-BP or I-BP) decoder cascaded with the feedback structure. For all J candidates obtained from the 1^{st} trial, the i^{th} bit is considered as reliable if all $|LLR_i^{out}|$ of J candidates are larger than a threshold β, where β denotes a constant larger than 0. The calculation of $|LLR_i^{out}|$ is given by:

$$|LLR_i^{out}| = |L_{i,1}^T + R_{i,1}^T|, \quad i = 1, 2, ...N \tag{3.18}$$

Then, the candidate $\mathbf{x}_{\tilde{j}}$ and the corresponding $\mathbf{y}_{\tilde{j}}$ are picked by candidate selector according to:

$$\tilde{j} = \underset{j \in S}{\operatorname{argmax}} \sum_{i=1}^{N} (1 - 2x_j[i]) y[i] \tag{3.19}$$

The indices of unreliable bits are stored in a set id based on their $|LLR_i^{out}|$. We note that for the proposed feedback structure, after the 1^{st} failed trail, instead of using all J initial $\mathbf{y}_j$ from candidate generator as the inputs of next trails, $\mathbf{y}_{\tilde{j}}$ at current iteration $iter$ is used as the inputs to all J BP decoders. Then, like what has been done to $|LLR_i^{out}|$, similar calculations are also conducted on the information of the input sequence $\mathbf{y}_{\tilde{j}}$, which is written as $|LLR_i^{in}|$ and calculated by:

$$|LLR_i^{in}| = |L_{i,1+M}^T + R_{i,1+M}^T|, \quad i = 1, 2, ...N \tag{3.20}$$

If the $|LLR_i^{in}|$ is larger than a threshold β, this bit is trustworthy, and the corresponding $|LLR_i^{in}|$ should be enhanced in the next iteration.

After finding reliable and unreliable bits that need to be processed, $\mathbf{R}$ are updated based on set id and threshold β. If the corresponding bits are reliable, they are considered as pre-known. However, if these bits belong to set id, the corresponding messages are flipped by freezing them to opposite values. We note that in order to take advantages of J parallel BP decoders, each decoder flips one distinct bit in set id and enhance all bits that are considered as reliable. The update of message $R_{i,1}^t$ is written as:

$$
R_{i,1}^{t} = \begin{cases} \operatorname{sgn}(LLR_i^{out})LLR_{\max} & \text{for } LLR_i^{out} > \beta \\ +\infty & \text{if } i \in \mathbb{F} \\ -\operatorname{sgn}(LLR_i^{out})LLR_{\max} & \text{if } \ i \in id \\ 0 & \text{else} \end{cases} \tag{3.21}
$$

where $LLR_{\max}$ denotes the maximum positive value we can define in a decoding procedure, which effectively biases $\hat{u}[i]$ to 0 or 1.

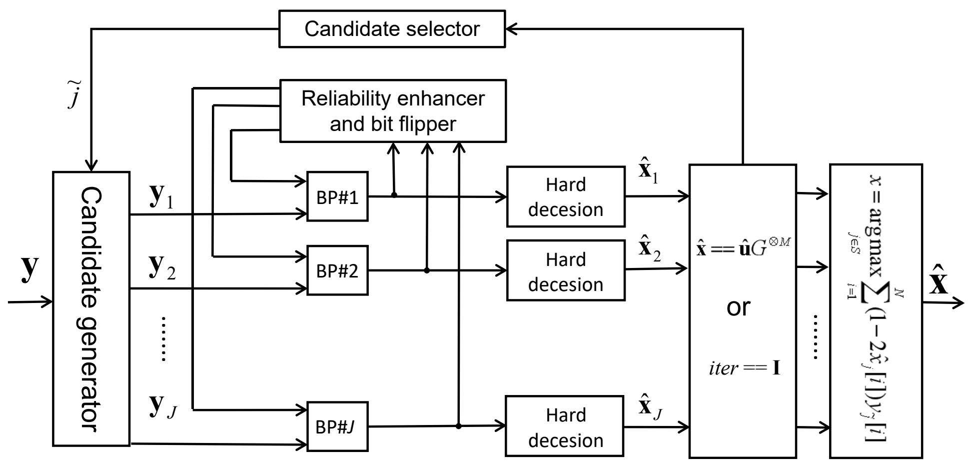

Fig. 3.10: Block diagram of the proposed BP cascaded with the feedback structure

Then, the message $L_{i,M+1}^{t}$ in J BP decoders are also required to be updated based on the value of $|LLR_i^{in}|$. LLRs of reliable bits can be considered as pre-known and then updated by:

$$
L_{i,M+1}^{t} = \begin{cases} \operatorname{sgn}(LLR_i^{in})LLR_{\max} & \text{for } \ LLR_i^{in} > \beta \\ \text{unchanged} & \text{otherwise} \end{cases} \tag{3.22}
$$

This feedback structure aims to choose the $\hat{\mathbf{x}}$ that meets stopping criteria and (3.16). Here, we define the distance between the received $\mathbf{y}$ and the estimated vector $\hat{\mathbf{x}}_j$ at iteration $iter$ as:

$$\mathrm{D}(\hat{\mathbf{x}}_j, iter) = \sum_{i=1}^{N} ||(1-2x_j[i])y_j[i]||^2, \quad j = 1, 2, ...J \tag{3.23}$$

We know that the $\hat{\mathbf{x}}$ obtained in current iteration $iter$ may have larger distance than that in the previous iteration. Therefore, if the current $\mathrm{D}(\hat{\mathbf{x}}_{j,iter})$ is larger than $\mathrm{D}(\hat{\mathbf{x}}_{j,iter-1})$, all updated information need to be dropped, and the former information in iteration $iter-1$ should be used in the decoding trial in $iter+1$. Otherwise, the updated LLRs obtained in iteration $iter$ must be used. In such ways, more than one incorrect bits may be corrected by the feedback decoding structure. Finally, if the estimated codeword $\hat{\mathbf{x}}$ meets stopping criteria or the iteration $iter$ meets its maximum I, the decoding should stop and the estimated codeword must be output. The decoding process of the proposed feedback structure with M-BP is given in Algorithm.3.2.

The proposed feedback structure can be regarded as an extended SCF decoding [79] in BP field. However, unlike SCF that only flips unreliable bits, our proposed feedback structure also enhance reliable bits. Then, since BP is an iterative decoding, the proposed scheme not only updates the initial LLRs on the rightmost side, but also the information on the leftmost side. In addition, unlike SCF that locates unreliable bits based on the result in only one decoding trial, the proposed method selects potential reliable and unreliable bits according to the results given by J parallel BP decoders. Moreover, the proposed feedback structure implements J distinct bits flip simultaneously, which achieves lower latency.

3.2.4 Advantages and benefits

Similar to the conventional BP, the first benefit of I-BP and M-BP is their lower latency compared with SC based polar decoders. It has been suggested that the BP

Algorithm 3.2 Decoding process utilizing the proposed feedback structure:

Initialization: $\mathbf{x}_{tep} = 0$, set $I = \varnothing$;
while $iter = 1 : I$ **do**
  if $iter == 1$ **then**
    Obtain $\hat{\mathbf{x}}_j$, $\hat{\mathbf{u}}_j$, $\mathbf{L}$, and $\mathbf{R}$ from a M-BP decoder using $\mathbf{y}_j$;
    Calculate LLR_i^{out} according to eq.(3.18) and LLR_i^{in} according to eq.(3.20);
    Sort LLR_i^{in} in descending order to build a set id;
    Find $\tilde{j}$ according to eq.(3.19);
  else
    Obtain $\hat{\mathbf{x}}_j$, $\hat{\mathbf{u}}_j$ from a M-BP decoder using $\mathbf{y}_{\tilde{j}}$, update $\mathbf{R}$ according to eq.(3.21), and $\mathbf{L}$ according to eq.(3.22);
    Find $\tilde{j}$ according to eq.(3.19);
  end if
  if $\hat{\mathbf{x}}_j == \hat{\mathbf{u}}_j \mathbf{G}^{\otimes M}$ or $iter == I$ **then**
    Decoding finish, and output the $\hat{\mathbf{x}}$ that meets eq.(3.16);
  else
    $\mathbf{L}_{tep} \leftarrow \mathbf{L}$; $\mathbf{R}_{tep} \leftarrow \mathbf{R}$;
    Update $\mathbf{R}$ according to eq.(3.21), and $\mathbf{L}$ according to eq.(3.22);
  end if
  if $D(\mathbf{x}_{tep}) \leq D(\mathbf{x}_{\tilde{j}})$ **then**
    $\mathbf{R} \leftarrow \mathbf{R}_{tep}$, $\mathbf{L} \leftarrow \mathbf{L}_{tep}$
  else
    $\mathbf{x}_{tep} = \mathbf{x}_{\tilde{j}}$;
  end if
end while

based decoding enjoys advantages of high throughput and low latency for its parallel hardware implementations [94]. The latency of I-BP and M-BP decoding methods is $O(log_2 N)$. In contrast, SC based decoding requires higher latency, which can be scaled with $O(N)$. The second benefit of the proposed schemes refer to their simplicity. I-BP and M-BP decoders do not require any modification on BP decoder itself, which is different from some other modified BP decoders [40]. The only additional step takes place on the input sequence, which can be permuted in advance. The third benefit of the proposed methods refers to their flexibility. On the one hand, to save hardware resources, M-BP or I-BP can be implemented serially using unchanged decoding structures. On the other hand, to improve the efficiency, the proposed methods can be employed in a parallel way. According to the simulation result, although the proposed BP still has performance gap to Fast-SCL [95], the parallel nature of BP decoding makes this decoder interesting for applications with stringent latency requirements, which is about 1/6 of Fast-SCL [96]. Furthermore, BP based decoders yield soft outputs, which can be applied in joint detection and decoding that cannot be achieved by hard decision based decoders. We note that the proposed decoding schemes also pay the cost like high hardware complexity due to the parallel structure, whereas this issue can be solved by changing the proposed schemes to sequential structures. Also, the feedback structure increases latency. Nevertheless, simulation results suggest that compared with the gain from adding feedback structures, the latency increase is tolerable, especially in moderate and high SNR scenarios.

3.2.5 Simulation results

In this section, some simulation results are presented and evaluated. The proposed BP decoding schemes are compared from several aspects. First, the FER performance between the two proposed BP and the conventional BP are compared. Then, the FER performance of the proposed BP cascading the feedback structure (denoted as "F-BP") are provided and compared with the proposed BP without such structure. Also, to show the advantage of the feedback structure, F-BP schemes are performed and evaluated in different channels (e.g. fading and AWGN channels). Last, the proposed BP schemes are compared with existing modified BP decoders, including BP-List [40] (denoted as "BPL"), noise aided BP [42] ("N-BP"), and SCL [97]. In our simulations, coding rate R is 0.5. Perfect synchronization is assumed, and the maximum iteration (T) is 50 for $N = 512$ polar codes and 40 for $N = 256$ polar codes. Moreover, in the proposed methods, fixed threshold $\beta = 5$ and $\beta = 3$ are used in AWGN and selective channels, respectively.

Fig.3.11 and Fig.3.12 show the FER performance among I-BP, M-BP and the conventional BP with $N = 256$ and $N = 512$, respectively. According to the simulation results, we know that although all proposed decoders can improve the FER performance compared with the conventional BP, I-BP exhibits better FER performance than that of M-BP with identical number of candidates. Additionally, increasing the amount of interleavers or random vectors **d** can benefit the FER performance. Further, compared with the conventional BP, performance gains become more remarkable at high SNRs. Note that the number of interleavers in I-BP is limited to M, which may not be sufficient for the requirement of some cases. Nevertheless, by combing with M-BP, more candidates can be generated. Such hybrid BP decoding scheme is open for future investigation. Moreover, we include the performance of PBP proposed in [96] because of their similarities and following differences: The proposed I-BP does not introduce any CRC, all termination process are based on stopping criteria. The proposed I-BP can only cover M candidates by utilizing, which are less than that of PBP decoding. The proposed I-BP is based on a groups of interleavers and the PBP decoding is based on bits shifting. The proposed I-BP can achieve sightly better performance when the number of candidates is the same, which is shown in Fig.3.12.

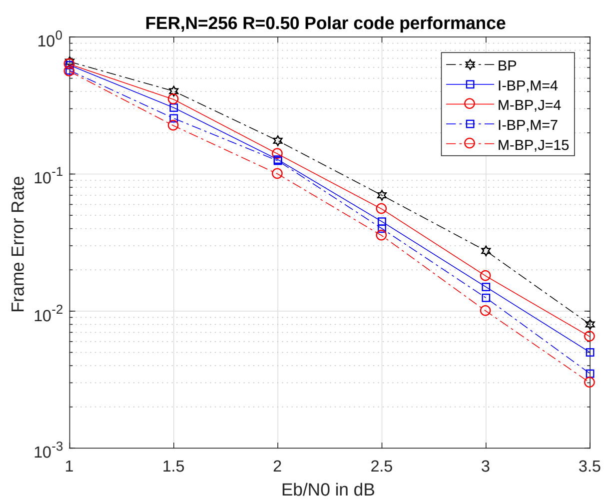

Fig. 3.11: FER performance among different BP decoders with $N = 256$

Then, in Fig.3.13,we investigate the FER performance between the proposed BP schemes with and without the feedback structure in AWGN channels. It is illustrated

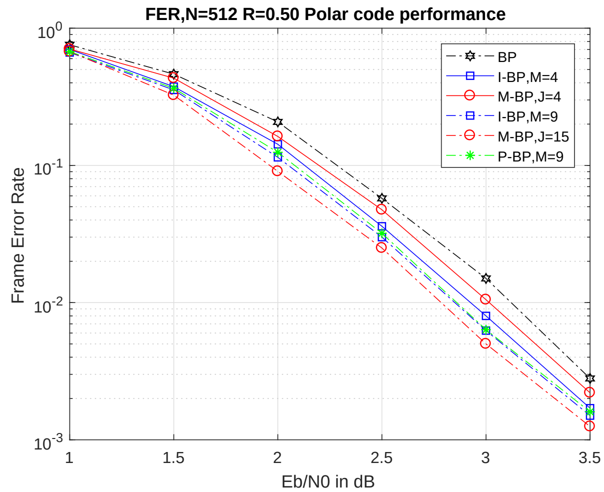

Fig. 3.12: FER performance among different BP decoders with $N = 512$

Table 3.2: Relative Frequency of Iteration Numbers for variant Eb/N0

Iteration numbers	1	2	3	4	5	6	7
Eb/N0=1.5dB	540	151	54	15	7	7	226
Eb/N0=2.0dB	747	130	43	12	6	2	60
Eb/N0=2.5dB	893	102	1	0	0	0	4

that the feedback structure is capable to further improve the FER performance. By increasing the maximum iteration I, the performance can be enhanced at the cost of increasing latency. Moreover, the enhancement with I becomes remarkable in moderate or high SNR scenarios. Conclusively, the feedback structure helps the proposed BP schemes improve their decoding performance at the cost of increasing latency. Nevertheless, Fig.3.14 suggests that in moderate and high SNR scenarios, BP with the feedback structure exhibit a comparable latency to conventional BP. Further, Fig.3.15 and Table.3.2 reveal that when I is 7, in most cases, BP with the proposed structure can obtain $\hat{\mathbf{x}}$ correctly within 3 iterations. For example, when $Eb/N0$ is 1.5 dB, more than 70% decoding procedures can be successfully finished within 3 iterations. This behavior becomes more remarkable when SNRs are high.

To comprehensively investigate the proposed BP schemes, the FER performance of the feedback structures cascading I-BP and M-BP (denoted as "F-IBP" and "F-

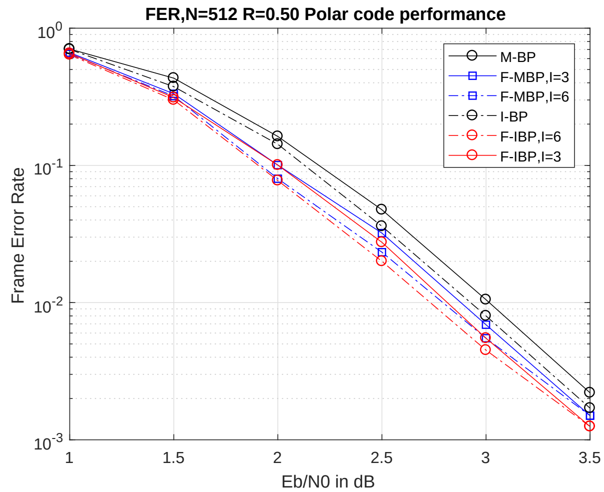

Fig. 3.13: FER performance between BP decoders with and without the feedback structure

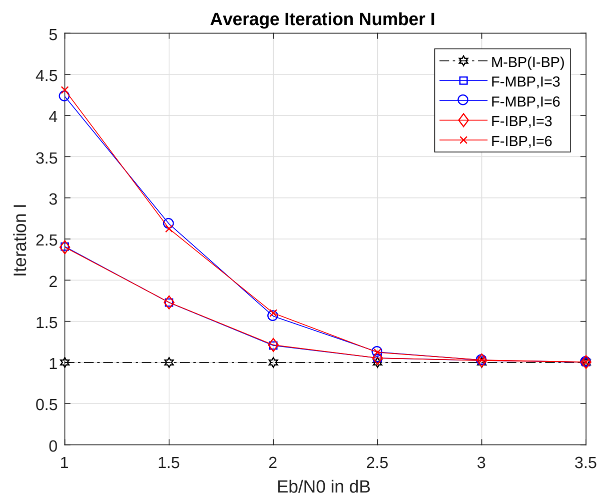

Fig. 3.14: Average iterations *iter* among different BP decoders with the feedback structure

MBP") are compared in Fig.3.16, using $J = 4$ in frequency selective channels combing with OFDM. Fig.3.16 suggests that like what happened in AWGN channels, the proposed BP with feedback structure also exhibits better FER performance than that of the BP without such structure. Besides, compared with M-BP, F-MBP obtains nearly 1 dB gains at probability 1×10^{-2}. Hence, the feedback structure exhibits stronger error correction ability in frequency selective channels. Intuitively, we can also expect that increasing I can improve the FER performance though this benefit

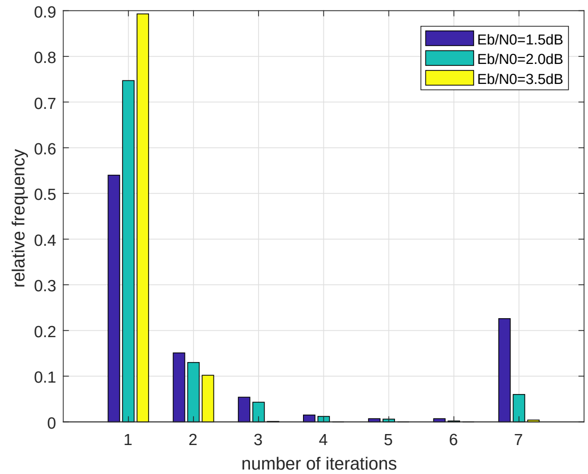

Fig. 3.15: Relative frequency of iterations for F-MBP decoders with different $Eb/N0$

will vanish gradually with the increment of I.

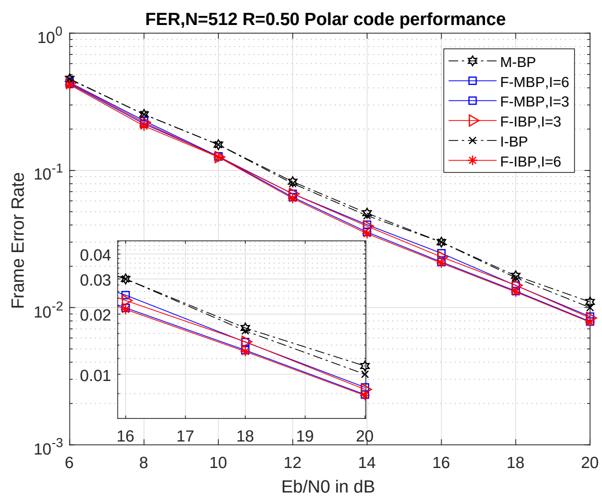

Fig. 3.16: FER performance among BP decoders with and without the proposed feedback structure in frequency selective channels

Furthermore, in Fig.3.17, FER performance of the proposed BP decoding schemes combined with OFDM systems are compared in doubly selective channels (DSC) [98]. We note that a least square (LS) channel estimator was employed for simplicity [99]. It is therefore speculated though all BP decoding schemes undergo performance degradation in DSCs, those using the feedback receiving structure are capable of achieving better FER performance than other modified BP decoders. The feedback receiver can obtain nearly 2 dB gains at the probability 0.07, a data noticeable than that in frequency selective channels.

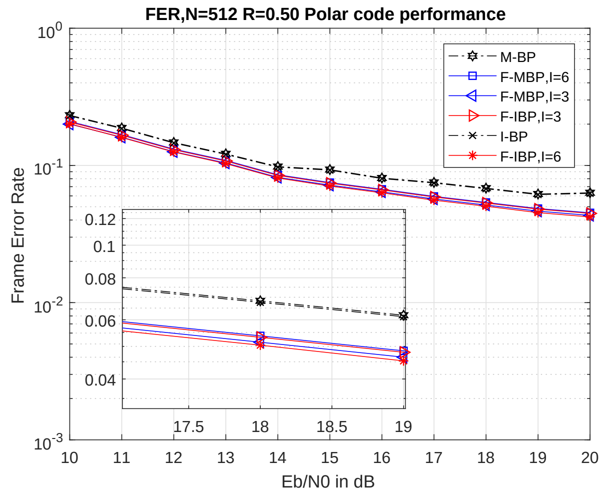

Fig. 3.17: FER performance among BP decoders with and without the feedback structure in DSCs

Last, the proposed BP decoders as well as their feedback cascaded versions are compared with some existing polar decoding schemes in AWGN channels. Fig.3.18 suggests that with the same number of candidates, the proposed BP decoding schemes exhibit superior FER performance than that of existing modified BP decoding schemes. For instance, when $Eb/N0$=3.0 dB, F-BP can achieve almost 0.4 dB gain than that of the conventional BP. Then, compared with N-BP which uses random noise with variance σ_0, the proposed M-BP can still achieve better performance. Moreover, as a reference, the FER of a SCL decoder with list size 4 is also provided. It is illustrated that the proposed BP schemes achieve better performance than that of the SCL decoding except that in the case with $Eb/N0$=3.5 dB.

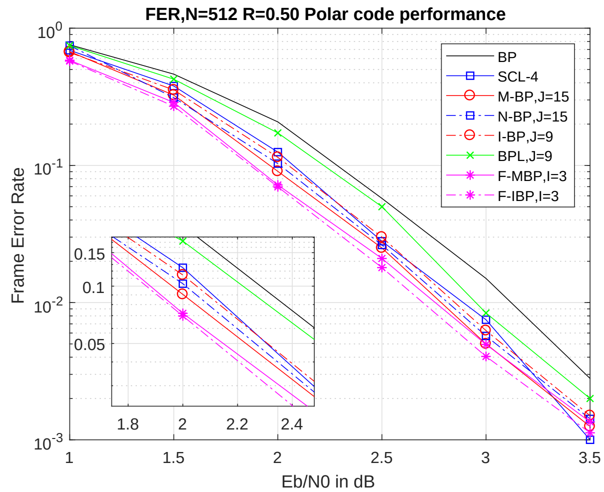

Fig. 3.18: FER performance among the proposed BP and other polar decoding schemes.

3.3 Stopping criterion for BP polar code decoders based on bits difference ratio

3.3.1 Introduction

It has been concluded that because of the inherently parallel architecture, BP decoding schemes have much lower latency than SC based schemes. The low-latency merit renders BP more suitable to 5G applications, particularly for those which have low time-delay requirements. However, a BP decoder may achieve decoding process before reaching its pre-set maximum iterations, which results in redundant implementations and energy waste. Hence, setting an inappropriate iteration will lead the decoding process lose efficiency. Additionally, unnecessary iterations may compromise the low-latency advantage of BP, which is unacceptable in many applications with low latency requirements.

To construct a low-latency BP decoder, an effective stopping criterion is required. Some investigations have been done in several articles [71, 72, 73, 74]. In [71], generation matrix $\mathbf{G}^{\otimes n}$ is used to reduce unnecessary iterations. If the estimated information bits $\hat{u}_1^N \mathbf{G}^{\otimes n}$ equals to the estimated codewords $\hat{x}_1^N$, the decoding procedure can stop successfully. Moreover, two similar methods, proposed in [72] and [73], are based on errors of the worst protected information bits (WIB) and the best protected frozen bits (FBER), respectively. It have been concluded that these two proposed methods own higher latency due to higher iterations and weaker error correcting performance than that of the G-Matrix based method, but they are more hardware-friendly [72] due to their lower computational complexity. In this section, our priority focuses on the latency reduction, which can be achieved through decreasing iterations.

Although the G-Matrix based criterion stops the decoding process when it satisfies the condition:

$$\hat{u}_1^N \mathbf{G}^{\otimes n} = \hat{x}_1^N \tag{3.24}$$

the estimated information bits $\hat{u}_1^N \mathbf{G}^{\otimes n}$ may not always agree with $\hat{x}_1^N$, especially in low SNR scenarios. Our proposed stopping criterion in this section is based on an observation that although $\hat{u}_1^N \mathbf{G}^{\otimes n}$ cannot always be equivalent to $\hat{x}_1^N$, the number of different bits between $\hat{u}_1^N \mathbf{G}^{\otimes n}$ and $\hat{x}_1^N$ can be comparatively stable and reach to a "platform" with little fluctuation. According to this observation, if bits difference fluctuations are small enough, and such different gaps can be kept within a tolerance for a consecutive number of iterations, or even such gap equals to zero, which means that $\hat{u}_1^N \mathbf{G}^{\otimes n} = \hat{x}_1^N$, the decoding process can be stopped. We call this method "bits difference ratio (BDR)" stopping criterion.

3.3.2 Previous BP decoders with stopping criteria

A stopping criterion was proposed in [71] based on the generator matrix $\mathbf{G}^{\otimes n}$, called G-Matrix based scheme. For this criterion, the estimated information bits at the t^{th} iteration $\hat{\mathbf{u}}_t$ are re-encoded by making use of the generator matrix $\mathbf{G}^{\otimes n}$. Then, it is compared to the estimated codeword $\hat{\mathbf{x}}_t$. If $\hat{\mathbf{u}}_t \mathbf{G}^{\otimes n} == \hat{\mathbf{x}}_t$, the decoder can stop and assumes that the decoding is successful. In literature [72], a simplified stopping criterion based on the "worst protected information bits (WIBs)" was proposed. For

WIB stopping criterion, authors assume that the successful detection of a cluster of WIBs is enough to stop the decoding process. Hence, the WIB stopping criterion tracks the alternative signs of a cluster of WIBs, if signs does not change for several iterations, the decoder will stop and declare decoding success. BP decoders with these criteria can stop themselves earlier with low computational complexity. Similarly, A stopping criterion based on the best protected frozen bits called FBER scheme was proposed [73]. FBER stopping criterion can achieve similar performance, in terms of iteration reduction, as that of WIB but lower computational complexity.

Among these existing criteria, G-Matrix based scheme saves the most iterations compared with the other two. It is very efficient in terms of latency reduction. However, in many low SNR scenarios, $\mathbf{u}_t\mathbf{G}^{\otimes n}$ does not equal to $\mathbf{x}_t$ even t reaches to its maximum. To clarify this behavior occurred during the decoding process, we define the BDR at iteration t as:

$$\frac{(K - D_t)}{K} \tag{3.25}$$

where D_t is the number of different bits between $\hat{\mathbf{u}}_t\mathbf{G}^{\otimes n}$ and $\hat{\mathbf{x}}_t$ at the t^{th} iteration. For example, if $\hat{\mathbf{u}}_t\mathbf{G}^{\otimes n}$ equals to $\hat{\mathbf{x}}_t$, then D_t is zero, thus BDR equals to 1. It is indicated in Fig.3.19 that in comparatively high SNR scenarios, the G-Matrix based stopping criterion can be easily satisfied, while in comparatively low SNR scenarios, BDR may not equal to 1 but also gets to a "platform" with little fluctuation. This intuitive behavior gives us the idea that a BP decoding process can stop as ling as the BDR can keep flat for a consecutive iterations, which may save more unnecessary decoding procedure than that of the G-Matrix based scheme.

3.3.3 The proposed BDR based early stopping criterion

As shown in Fig.3.19, it appears that the BDR stabilizes at a steady-state value for each SNR scenario. Hence, we propose a BDR based stopping criterion to make use of this behavior. Here, we keep tracking the value of $\text{BDR}_v - \text{BDR}_{v-1}$, which is the

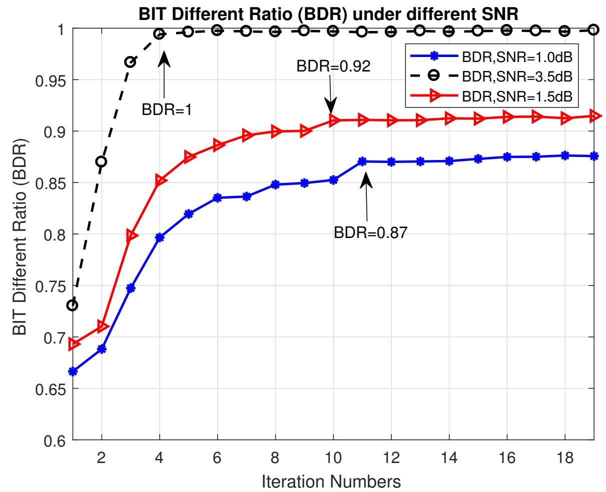

Fig. 3.19: BDR along with iterations, N=128, K=64, $max_t = 19$

difference of BDR between iterations v and $v-1$. The idea of BDR based stopping criterion can be given as:

$$\begin{gathered}|\mathrm{BDR}_v - \mathrm{BDR}_{v-1}| \leq M, \ \text{ for } v = t, t+1, ..., t+P-1 \\ \text{or} \\ |\mathrm{BDR}_v| = 1\end{gathered} \tag{3.26}$$

This proposed stopping criterion can be interpreted as that if the gap of BDR between iterations v and $v-1$ is lower than a threshold M within successive P iterations, the decoder can terminate the decoding procedure. In other words, if the fluctuation of BDR is tolerable (tolerance is M) for consecutive P iterations, it can be concluded that the decoding process probably gets to a "platform" thus more iterations may be redundant. Moreover, if $\mathrm{BDR}_v = 1$, which indicates that $\hat{\mathbf{u}}_v\mathbf{G}^{\otimes n}$ equals to $\hat{\mathbf{x}}_v$ at the v^{th} iteration, the decoding procedure can stop immediately.

We note that the proposed stopping criterion relies on two parameters, M and P. M describes the percentage of fluctuation ($|\mathrm{BDR}_v - \mathrm{BDR}_{v-1}|$) that a decoder can tolerate. The optimization of M in mathematical way is an open topic for future investigation. However, intuitively, it can be expected that a large M means that the proposed stopping criterion can tolerate more fluctuations, which may cause more bits errors. However, a small M leads more redundant iterations because a small M (i.e. 0) may not be satisfied even the t goes to maximum. To find out the impact of P on the proposed stopping criterion, we redraw Fig.3.19 by utilizing the mean value of BDR. Hence, the stopping criterion can be rewritten as:

$$\begin{gathered} |E[\mathrm{BDR}_v] - E[\mathrm{BDR}_{v-1}]| \leq M, \ \text{ for } v = t, t+1, ..., t+P-1 \\ \text{or} \\ |E[\mathrm{BDR}_v]| = 1 \end{gathered} \tag{3.27}$$

where $E[\,]$ is the mean operation. We note that although mean values can reflect the trend of BDR, this value cannot be used in practice. Hence, in real time situation, (3.26) is still used. For example, in Fig.3.20, when SNR=1.0 dB, in the range of 5-15 of abscissas, there has fluctuations, which means that if $M = 0$, the proposed stopping criterion cannot stop before the 15^{th} iteration. However, as seen, the decoding process can claim to be successful at the 9^{th} iteration. Effects of the selection of M are shown in Fig.3.20 where the SNR is 1.0 dB. It is indicated that a larger threshold M may cause the decoder to mistakenly believe it has successfully find the "platform", which leads higher BER. In other words, the decoding process may terminate before BDR get to the "platform". Therefore, M is essentially the fluctuation tolerance. For example, $M = 0.02$ means that the decoder can tolerant 2% of fluctuations between BDR_v and BDR_{v-1}. We can expect that larger tolerance M may cause worse error correction performance, which will be shown by simulations in next section.

Another question is that how many consecutive iterations we need to track in the proposed stopping criterion ? In another word, what the value of P should be? It can be expected that lower P cannot guarantee that the "platform" is stable, while a large value of P may compromise the iteration reducing ability of BP decoding algorithms. Here, similar to the investigation on M, the mean of BDR is used to

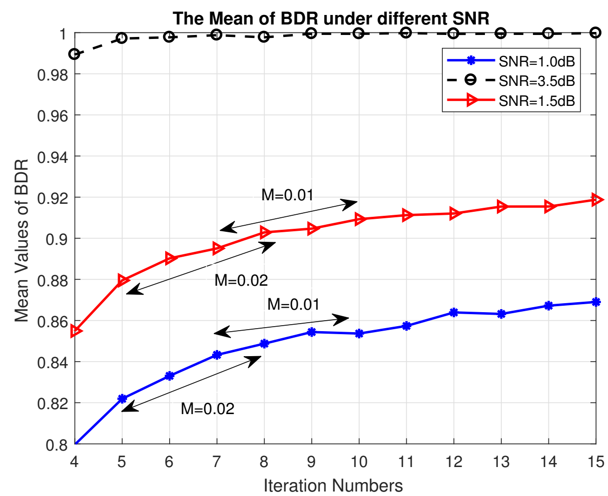

Fig. 3.20: Impact of M on the proposed criterion when SNR=1 dB,1.5 dB,and 3.5 dB

determine the value of P.

If the value of (3.27) changes drastically, it is difficult to guarantee that the BDR has reached to a "platform". Hence, the values of BDR should be comparatively stable within P iterations. However, a long P may never be satisfied for limited iterations, which results in unnecessary decoding process. Fig.3.21 indicates that the small value of of P may result in an instability, which could make the proposed criterion stops early even the "platform" is not stable. For example, it can be seen from Fig.3.21 that when SNR=1.0 dB and $M = 0.01$, from the 6^{th} to 7^{th} iteration, if $P = 2$, the decoding procedure would be stopped at the 7^{th} iteration, which could cause poor BER performance. However, if $P = 4$, the decoding process would be terminated at the 9^{th} iteration, which could guarantee the error correction performance. As shown, although a comparatively lower value of P (e.g.$P = 2$) may work in a comparatively high SNR scenario (e.g. SNR=3.5 dB), $P = 4$ is enough to decide if the BDR is stable in most cases (e.g. SNR=1.0 dB or 1.5 dB). It can be expected that an adaptive P for different SNRs can achieve more effective performance. However, for simplicity, in this section, we use a fixed P value in simulations. Accordingly, a polar BP decoder with the proposed BDR stopping criterion is given in Algorithm.3.3.

Algorithm 3.3 C(N,K) polar decoder with BDR stopping criterion: $\hat{u}_1^N$ = BDR($y_1^N, M, P, \mathbb{F}$)

Log-likelihood ratios of the received vectors y_1^N $LLR(y_i)$, $i = 0, 1, ..., N$;
The index set of the frozen bits $\mathbb{F}$;
Initialization :
Set the maximum iteration T and scale factor α
$\mathrm{BDR}^0 = 0$, $Flag = 0$
For each node (i, j), initialize messages $L_{i,j}^t$ and $R_{i,j}^t$;
if $(j == 1)$ & $(i \in \mathbb{F})$ **then**
  $R_{i,j}^t \leftarrow \infty$, $t = 0, 1, ...T$;
else if $(j == 1 + n)$ **then**
  $L_{i,j}^t \leftarrow LLR(r_i)$, $t = 0, 1, ...T$;
else
  $L_{i,j}^0 = R_{i,j}^0 \leftarrow 0$;
end if
Iterations :
while $1 < t < T$ **do**
  Update: $L_{i,j}^t$ and $R_{i,j}^t \leftarrow$ (3.4);
  Update: $\hat{x}_t$ and $\hat{u}_t \leftarrow$ (3.7) and (3.6);
  $\mathrm{B}_t \leftarrow |\mathrm{BDR}_t - \mathrm{BDR}_{t-1}|$;
  if $\mathrm{BDR}_t == 1$ **then**
    Decoding is successful and output $\hat{u}_1^N$;
  else if $\mathrm{B}_t \leq M$ & Flag $< P$ **then**
    Flag $\leftarrow$ Flag+1;
  else if $\mathrm{B}_t \leq M$ & Flag $== P$ **then**
    Decoding is successful and output $\hat{u}_1^N$;
  else
    Flag $= 0$ & $t \leftarrow t + 1$ & Start the next iteration;
  end if
end while
Output: $\hat{u}_1^N$

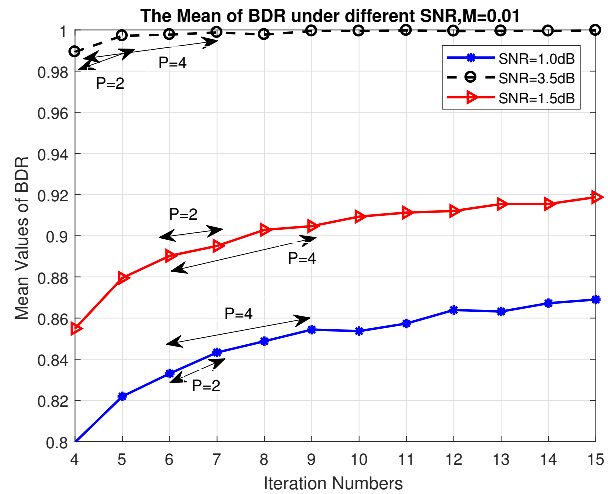

Fig. 3.21: Impact of P on the proposed stopping criterion with different SNRs when $M = 0.01$

3.3.4 Simulation results

In this section, comparisons among the proposed criterion and previous stopping criteria [72, 71, 73] are given. For a fair comparison, different length of polar codes $C(1024, 512)$, $C(128, 64)$ in AWGN channels are used. Additionally, SMS-BP is used with scale factor $\alpha = 0.935$ [91]. The maximum iterations (T) is 60 for $N = 1024$ and 20 for $N = 128$. P is set to 4 and the express journey (XJ) message passing schedule [100] is adopted to each decoding procedure in order to a rapid converge.

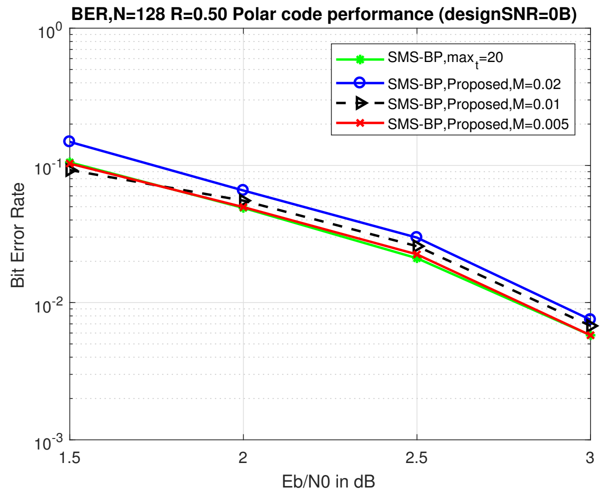

Fig. 3.22: BER performance of $C(128, 64)$ polar codes with the proposed BDR criterion

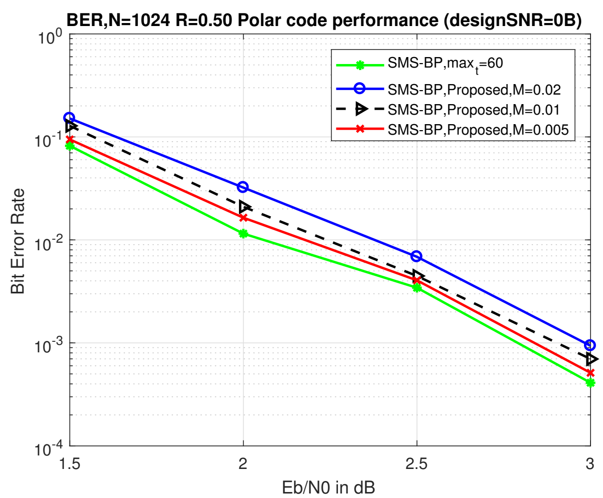

Fig. 3.23: BER performance of $C(1024, 512)$ polar codes with the proposed BDR criterion

Fig.3.22 and Fig.3.23 illustrate BER results of SMS-BP decoders for fixed iterations and BP decoders with BDR criterion using different threshold M. It can be seen from the figures that as what we expected, a larger M causes BER degradation. For example, in Fig.3.23, when the M equals to 0.5%, the BP decoder using the proposed stopping criterion can achieve around 0.3 dB gain compared to that of the case using $M = 2\%$. However, with an appropriate selection of M, the BER performance is almost the same as that of the decoder with fixed iterations. When the length of code N is short, the estimated $\hat{x}_1^N$ is easier to agree with $\hat{u}_1^N \mathbf{G}^{\otimes n}$, which can explain that for the proposed BDR criterion, why the BER degradation of $C(128, 64)$ is slightly lower than that of $C(1024.512)$.

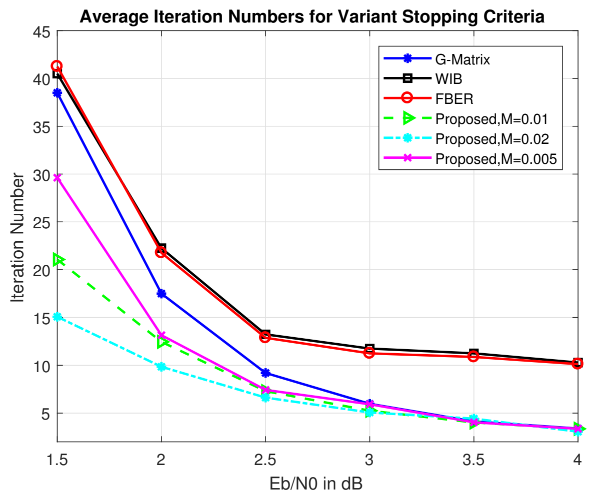

Fig. 3.24: Average iterations along with different SNRs for variant stopping criteria

Fig.3.24 shows average iterations among different criteria for a length 1024 polar code. As shown in Fig.3.24, the proposed stopping criterion can achieve the most iteration reductions among these 4 current schemes regardless of M. Although larger M may compromise BER performances, it also reduces more iterations, which offers users more flexibility to make a trade-off between reliability and latency. However, we note that because the BDR can easily equal to 1 in comparatively high SNR scenarios, which makes our proposed stopping criterion insensitive to the decreasing value of M. Also, when SNRs become higher, $\hat{x}_1^N$ may equal to $\hat{u}_1^N \mathbf{G}^{\otimes n}$ easily in early stages. In these cases, the proposed method achieves the same iteration reduction performance as that of G-Matrix based stopping criterion.

3.4 A hybrid SD for short polar codes using variable step size

3.4.1 Introduction

Polar codes [28], as a type of error correction codes, can be proved to asymptotically achieve the memoryless channel capacity. Using SC, the decoding complexity of polar code can be very simple, summarized as $O(N\log N)$, where N denotes the length of polar code [87]. To further improve the polar decoding performance, some modified SC were proposed [89, 88, 45]. Also, BP [26] can be adopted in polar decoding for higher throughput despite its sub-optimal performance. Although the above polar decoding schemes have lower complexity, they are not capable of achieving ML performance.

As an alternative scheme for polar codes to achieve ML performance, SD has been extensively investigated in spite of its high complexity. The SD for polar codes [51], as inspired by the similar concept that is applied in space-time block code (STBC), is capable of achieving ML performance and exhibiting nearly cubic complexity [99]. Unlike ML decoding that searches all possible outputs, SD only visits candidates in a sphere with radius of r. Although SD noticeably reduces the complexity compared with the conventional ML decoding scheme, it remains too complex to be implemented. Hence, many scholars are seeking modified SD schemes towards complexity reduction. Since SD can be considered as a tree searching problem, most works have simplified the complexity of SD by developing different ways to terminate the tree searching in an early stage. In [53], a low complex SD utilizing the properties of Galois field was proposed. In [54], an optimum PM was introduced to the conventional SD to effectively decrease its complexity and latency. Moreover, it was proved that by adding CRC bits, the CRC-SD can outperform CRC-SCL decoding with increased complexity [101].

Additionally, unlike the conventional SD that decreases sphere radius r, [52] proposed a simple but feasible SD scheme, named as “reduced latency ML” (RML) method. The proposed RML scheme gradually increases the sphere radius until one candidate with the minimum SED is identified. It was shown in [52] that without compromising ML performance, RML decoding method can effectively reduce the complexity and latency compared with existing SD schemes. Nevertheless, such effective RML scheme has two points that can be improved for complexity reduction: first, some nodes visited in the last searching round, might be revisited; second, when the radius r increases, the step size is fixed, making the tree pruning less aggressive. Inspired by RML [52] and the SD with optimum PM [54], in this section, a hybrid low- complex SD for short polar codes is proposed. The proposed scheme introduces the idea of stack, which has been utilized in SC based decoding [89], to RML in order to reduce the redundant node visiting. Also, the proposed method employs variable step sizes obtained from the PM that is modified from the optimum PM proposed in [54] to effectively prune the searching tree of the SD scheme. Simulation results suggest that compared with existing SD schemes, the proposed scheme achieves ML optimality with lower complexity.

Then, some notations we used in this section are claimed. Matrix and vectors are denoted by upper and lower case boldface letters.

- $a_i^{N-1} = [a[i], a[i+1], ..., a[N-1]]$ is a length $N-i$ vector with element $a[i]$, where $0 \leq i \leq N-1$.
- $g[i,j]$ represents the i^{th} row and j^{th} column element of matrix $\mathbf{G}$.
- $\otimes n$ denotes the n^{th} Kronecker power.
- $D(a_i^{N-1})$ denotes the sum of SED from $a[i]$ to $a[N-1]$, and $d_{min}(a[i])$ is the minimum SED and $d_{max}(a[i])$ is the maximum SED that $a[i]$ can achieve, respectively.

- $\dot{a}_i^{N-1} = [\dot{a}[i], \dot{a}[i+1], ..., \dot{a}[N-1]$ represent a failed tree searching process stopped at $\dot{a}[i]$.
- $u_i^{N-1}(l)$, where $1 \leq l \leq L$, denotes the l^{th} vector with length $N-i$ in the stack with size L.

3.4.2 The signal model

Consider a length N polar code with rate $R = K/N$, where $N = 2^n$, and K $(K \leq N)$ indicates the number of information bits. Denote an input sequence $\mathbf{u} \triangleq u_0^{N-1}$ and codeword $\mathbf{x} \triangleq x_0^{N-1}$. When an encoding procedure is finished, the vector $\mathbf{y}$ on receiving side can be written as:

$$\mathbf{y} = \sqrt{E_s}\mathbf{s} + \mathbf{w} \tag{3.28}$$

where $\mathbf{y} \triangleq y_0^{N-1}$, E_s indicates the energy of a transmitted symbol, $\mathbf{s} \triangleq s_0^{N-1}$ refers to BPSK symbols of a codeword $\mathbf{x}$ ($1 \rightarrow$ -1, $0 \rightarrow +1$), and $\mathbf{w}$ represents a length N AWGN with 0 mean and variance $N_0/2$.

Based on (3.28), the ML estimate $\hat{\mathbf{u}}$ can be obtained by minimizing the SED between $\mathbf{y}$ and all possible information bits $\mathbf{u}$:

$$\hat{\mathbf{u}} = \underset{\mathbf{u}}{\operatorname{argmin}} ||\mathbf{y} - \sqrt{E_s}(\mathbf{1} - 2\mathbf{u}\mathbf{G}^{\otimes n})||^2 \tag{3.29}$$

where $\mathbf{1}$ indicates an all ones vector of length N.

It is known that a ML decoding can be transformed to a depth N tree-searching problem. In the searching tree, each node has two children (0 and 1). Each node can be mapped to a partial estimated vector u_i^{N-1}, where $0 \leq i \leq N-1$, equating to a unique path from the root $s[N-1]$ to the corresponding node at depth i. Subsequently, the SED of s_i^{N-1}, where s_i^{N-1} is the corresponding partial BPSK signals that related to u_i^{N-1}, can be written recursively as:

$$D(s_i^{N-1}) = D(s_{i+1}^{N-1}) + (y[i] - \sqrt{E_s}s[i])^2 \tag{3.30}$$

where in (3.30),

$$s[i] = 1 - 2\sum_{k=i}^{N-1} u[k]g[k+1, i+1], \text{ for } i = 0, ..., N-1$$

and $D(s_{N-1}^{N-1}) = 0$. Hence, ML decoding is equated with finding the nodes path with minimum $D(s_0^{N-1})$.

3.4.3 RML decoding via SD tree searches

From existing works, we know that conventional SD schemes gradually decrease the radius r until there is no vector within r [51]. SD performs well in high SNR scenarios. Otherwise, latency and computational complexity are very high. To address these disadvantages, RML decoding was proposed [52]. The low efficiency of SD partially results from the value of radius. To cope with this problem, instead of gradually decreasing the radius, RML decoding gradually increases the radius r in parallel or serial manners. In RML decoding, r grows continuously by a fixed step size α, and this step needs to be added on a path obtained from PM in (3.31) until the first candidate within the radius r is identified.

$$M_0(u_i^{N-1}) = N - i \tag{3.31}$$

where $0 \leq i \leq N-1$.

As observed, the value $\sqrt{E_s}s[i]$ in (3.30) is only taken from $\sqrt{E_s}$ or $-\sqrt{E_s}$. Hence, in an ideal case, the SED from any leaf node to the root should be equated with or larger than the lower-bound of SED [52], D^N_{min}, as defined below:

$$D^N_{min} \triangleq D_{min}(s_0^{N-1}) = \sum_{i=0}^{N-1} d_{min}(s[i]) \tag{3.32}$$

where:

$$d_{min}(s[i]) = \min\{(y[i] - \sqrt{E_s})^2, (y[i] + \sqrt{E_s})^2\}$$
$$\text{for } \; i = 0, ..., N-1 \tag{3.33}$$

RML decoding performs several tree searching process with variant radius r, the squared radius r in the w^{th} tree search is expressed as:

$$r_w^2 = D^N_{min} + w \cdot \alpha \tag{3.34}$$

where w starts from 1, and α denotes the fixed step size. The searching process continues and r_w^2 keeps growing until a valid codeword is identified. The SED for ML leads to the N-length ML distance $D_{ML} \le {r_k}^2$ if a valid estimate is found in the k^{th} search. Accordingly, a further increase in r will unnecessarily enlarge the search space by just adding solutions with larger SED than the one identified already [52].

The difference between the conventional SD and RML decoding scheme with the respect of the number of visited nodes is presented in Fig.3.25. For example, if we assume $\alpha = 0.25$, $D^N_{min} = 0.4$, $D_{ML} = 0.7$. For the conventional SD, 40 nodes are visited. For RML decoding, r_1^2 is firstly set to 0.65, which resulted in a failure after 7 visited nodes. Subsequently, the r_2^2 increases by one step size α. Then, the ML path is visited since r_2^2 is larger than D_{ML}. It takes 17 more node visiting. Hence, after counting the 8 nodes caused by D_{min}, RML decoding costs 32 node visiting in total, which saving 8 node visiting compared with the conventional SD scheme. Since these unnecessary node visiting are saved, the corresponding computational complexity is reduced. Moreover, since RML decoding can be implemented parallelly, the latency can be further reduced compared with the conventional SD.

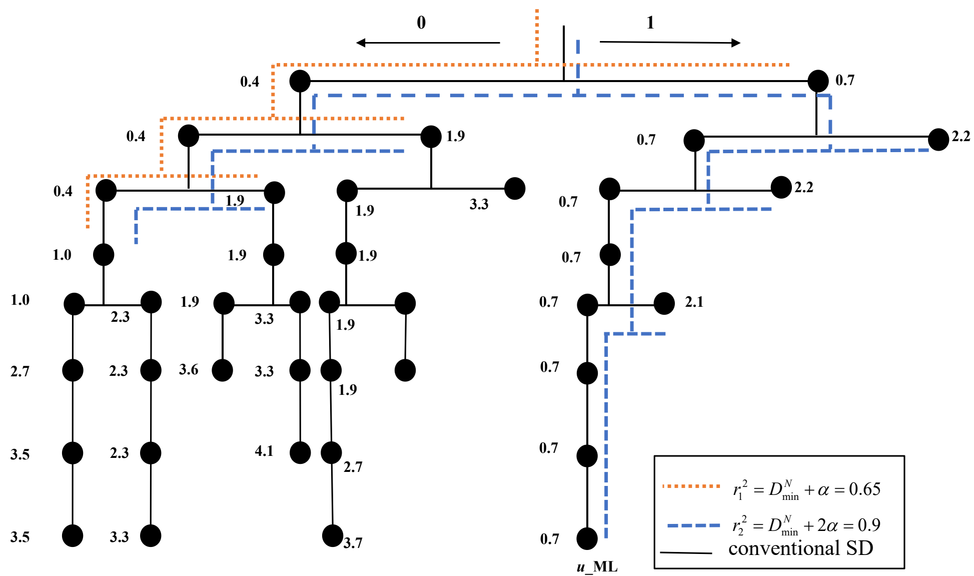

Fig. 3.25: Searching trees of RML decoding and the conventional SD scheme

3.4.4 The proposed SD scheme

Consider a failed searching $\dot{u}_i^{N-1}$ terminated at $\dot{u}[i]$, and $\dot{s}_i^{N-1}$ is the corresponding partial BPSK symbols. For RML decoding, after a failed search, the scheme starts over with a larger radius, and expands the vector that owns the longest length until no path has smaller SED than the current radius r. It is a straightforward strategy, but the path that steps are added only depends on it length. Moreover, RML does not have a mechanism to store the visited nodes, resulting in unnecessary calculations. Inspired by [54], to reduce the computational complexity without compromising ML optimality, in our proposed scheme, a stack and an PM derived from [54] are introduced to the proposed hybrid SD scheme. By utilizing the new PM, after each failed search, a variable step size according to such PM can be added. The optimum PM in [54] is rewritten as:

$$M_1(u_i^{N-1}) = \sum_{j=i}^{N-1}(y[j]s[j] - |y[j]|) \tag{3.35}$$

where $0 \leq i \leq N-1$, (3.35) suggests which path has the maximal possibility to become the ML result. We note that for better understanding, the proof of the optimality of (3.35) is rewritten in the appendix. However, during the decoding procedure, paths with different length may have very similar PM values. From Fig.3.26, we can see that some paths stored in the stack have the same M_1 value, but their length are different. Intuitively, the longer path with similar M_1 values should have more chances to be the final result. Therefore, in this section, we propose a new PM that adds a very small correction part related to the length of paths after the original PM M_1 to distinguish the paths that have similar M_1 but different length. The new PM M_2 is written as:

$$M_2(u_i^{N-1}) = A\frac{M_1(u_i^{N-i})}{2\sum\limits_{i=0}^{N-1} y[i]} + B\frac{N-i}{N} \tag{3.36}$$

where A, B are constants, and in order to let the optimum PM M_1 dominate the metric, we set $A \gg B$.

No.	M_1	Sequence	Path length
1	-9.8995	$[x[0], x[1], x[2], ..., x[21]]$	22
2	-9.8995	$[x[0], x[1], x[2], ..., x[26]]$	27
3	-9.8995	$[x[0], x[1], x[2], ..., x[10]]$	11
4	-9.9022	$[x[0], x[1], x[2], ..., x[24]]$	25
⋮	⋮	⋮	⋮
N-1	-22.2535	$[x[0], x[1], x[2], ..., x[41]]$	42
N	-23.2025	$[x[0], x[1], x[2], ..., x[17]]$	18

PM

Fig. 3.26: Illustration of a stack using PM M_1

According to this knowledge, the variable step size α_w at the w^{th} searching, can be derived, as expressed below:

$$\begin{aligned}
\alpha_w &= d_w^{max}(s[\tilde{i}]) - d_w^{min}(s[\tilde{i}]) \\
&= \max\{(y[\tilde{i}] - \sqrt{E_s})^2, (y[\tilde{i}] + \sqrt{E_s})^2\} \\
&\quad - \min\{(y[\tilde{i}] - \sqrt{E_s})^2, (y[\tilde{i}] + \sqrt{E_s})^2\} \\
&= 4\sqrt{E_s}|y[\tilde{i}]| \qquad (3.37)
\end{aligned}$$

where $\tilde{i} \in \{0, ..., N-1\}$ denotes the corresponding depth of candidate $u_{\tilde{i}}^{N-1}$ at the top of stack in current searching (i.e. the w^{th} searching) among all candidates $u_i^{N-1}(l)$ for $l = 1, ...L$ in the stack after sorting in a descending order based on M_2, where L is defined as the size of stack.

By employing (3.37), a variable step size α_w is introduced to the current radius r to ensure that the expanded nodes cover the path that exhibits the highest possibility to become the final solution. Hence, the current radius r after adding step size α_w is expressed as:

$$r_w = r_{w-1} + 4\sqrt{E_s}|y[\tilde{i}]| \qquad (3.38)$$

A comparison between the proposed SD and RML is drawn in Fig.3.27. After the first failed searching with $r = D_{min}^N = 0.4$, RML decoding continuously increased r to 0.9 based on a fixed step size α and revisited 7 nodes (the orange line). On contrast, the proposed SD increased the r_2^2 to 0.7 based on the step size α_2 obtained from M_2. Subsequently, using the stored visited path in the stack, the proposed scheme visits 10 more nodes and finds the ML solution (the blue line). Hence, after accounting the first 8 nodes visiting of calculating D_{min}^N, the proposed SD visited 25 nodes in total, which has lower node visiting than that of RML. However, compared with the RML decoding that can be implemented in parallel ways, the computational complexity reduction of the proposed SD is at the cost of latency.

The procedure of the proposed SD scheme is summarized as follows:

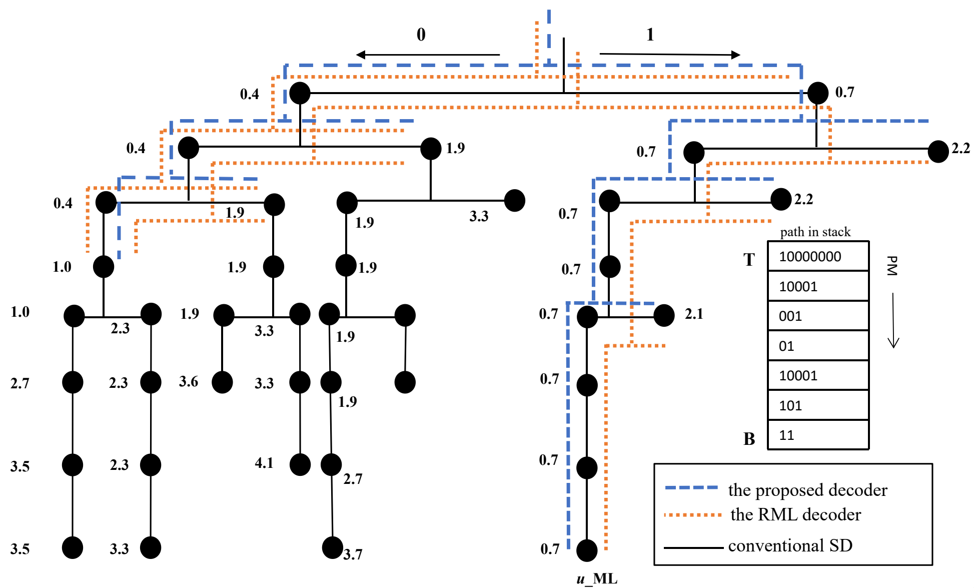

Fig. 3.27: Searching trees of RML and the proposed SD

Step 1. Initialization: a. Set the beginning r to D^N_{min}. b. Initialize an empty stack with size L. c. Push a null path $D(\emptyset)$ into the stack. d. Calculate all possible α_w according to the received $y[i]$ for $i = 0, ..., N-1$ by (3.37).

Step 2. Popping: the path $u_i^{N-1}(1)$ on the top of the stack is popped out if its SED is smaller than r^2, otherwise, go to **Step 6**. If the length of u_i^{N-1} equals to N ($i = 0$), record the u_0^{N-1} as the output $\mathbf{u}$ and then terminate the decoding procedure.

Step 3. Expand u_i^{N-1} to two new paths $[0, u[i], u[i+1], ...u[N-1]]$ and $[1, u[i], u[i+1], ...u[N-1]]$, subsequently, calculate the corresponding SED and PM using (3.30) and (3.36).

Step 4. Pushing: push both paths $[0, u[i], u[i+1], ..., u[N-1]]$ and $[1, u[i], u[i+1], ..., u[N-1]]$ back to the stack if their corresponding SEDs are smaller than current r_w^2.

Step 5. Sorting: sort the path stack according to (3.36) in a descending order. If the path stack size is larger than L, keep the top L paths and discard others.

Step 6. Radius Update: when the SED of all paths in the stack is larger than the current radius r_w^2, update r according to (3.38). Then, go to the **Step 3**.

3.4.5 Simulation results

In this part, variant length short polar codes with code rate $R = 0.6$ using BPSK modulation are examined. The comparison between low complex ML (SD, RML) decoding methods in [54, 52, 53] and our proposed approach in AWGN channels is drawn. For the proposed scheme, the study on different lengths of stack size is conducted. In M_2, A and B are set to 0.95 and 0.05 respectively. In the first subsection, the block error rate (BLER) comparison is drawn. Then, the computational complexity (numbers of nodes visiting) and the latency comparison is implemented.

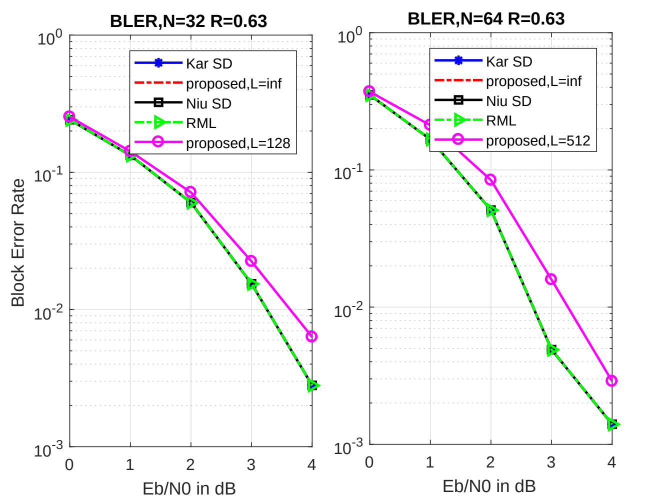

Fig. 3.28: BLER of different polar decoding schemes for short length polar codes (some lines are overlapped)

The BLER performance among existing low complex ML decoding schemes with different polar codes length configuration is given in Fig.3.28. Note that all existing low complex ML decoding schemes can achieve ML performance [54]. It is suggested that the proposed SD can also achieve the ML performance when the stack size is infinity. Furthermore, with comparatively small stack size, the proposed decoding scheme exhibits a lower complexity at the cost of BLER degradation. Moreover, different values of A and B in (3.36) will effect the overall performance of the proposed SD scheme, in terms of BLER and complexity performance. However, the optimization of (3.36) can be regarded as an open topic for further investigation.

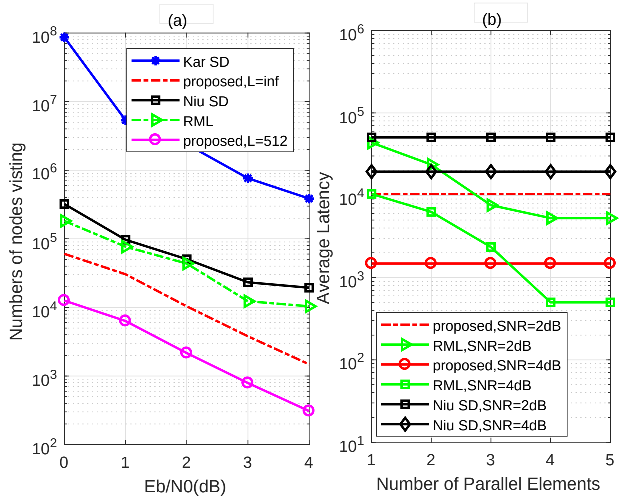

Fig. 3.29: (a). Numbers of nodes visiting and (b). Average latency for different low complex ML schemes for a $C(64,38)$ polar code

The computational complexity and latency comparisons among different low complex ML decoding schemes are drawn in Fig.3.29. The average number of nodes visiting using various polar decoding schemes are employed to assess the average computational complexity. Since RML decoding can be implemented parallelly, the latency comparison between the proposed scheme and RML decoding is also investigated. Compared with existing schemes, the proposed decoding can significantly reduce the computational complexity. Further, at the cost of BLER degradation, the computational complexity of the proposed scheme can be reduced more. Moreover, since the proposed scheme need update the radius after each failed search, compared with RML decoding, the computational reduction is at the cost of latency, which can be reflected in Fig.3.29.(b). However, results show that the proposed decoder has comparable latency when then number of parallel elements used in RML decoding is small.

Although the complexity of our proposed scheme is reduced, the complexity and latency is still high compared with SC based decoding, like SC (with complexity $O(N\log N)$), SCS [89] and SCL (with complexity $O(DN\log N)$, where D is the list size, usually smaller than 100) [45] decoding. However, compared with the schemes aiming at achieving ML decoding performance, the proposed SD can reduce significant computational complexity.

3.5 Comparsions among the proposed polar decoding schemes

According to the proposed modified polar decoding schemes in above sections, we know that all proposed schemes can achieve better performance in different performance metrics than their original versions or some existing works. In this section, for better understanding, the author implements a comprehensive comparison between our proposed polar decoding methods in this chapter and state-of-the-art decoding algorithm of polar codes, namely Fast-simplified-SCL decoding (F-SCL) [95] in terms of error performance, decoding latency (in a quantitative manner such as the number of decoding time-steps), and computational complexity. We note that since our proposed SD scheme is only suitable for short polar codes due to its high complexity, the performance of this method are not included.

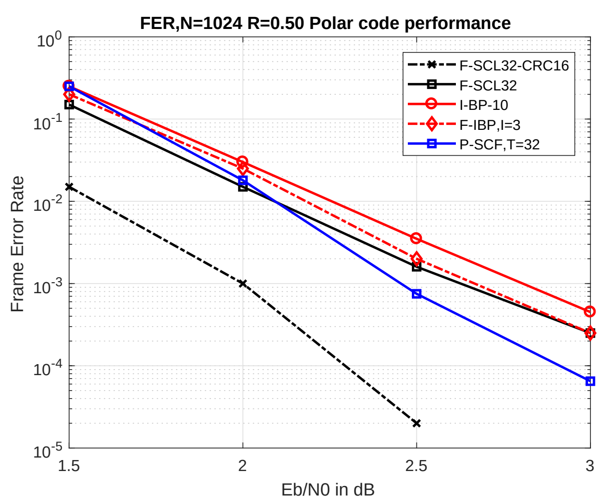

Fig. 3.30: FER comparison among different polar decoding methods

It is illustrated from Fig.3.30 that all proposed decoding can approach or sightly outperform the non-CRC aided F-SCL decoding. However, the performance of CRC-aided F-SCL can outperform our proposed decoding methods (The CRC was 16 bits and the generation polynomial was $x^{16} + x^{15} + x^2 + x^1$).

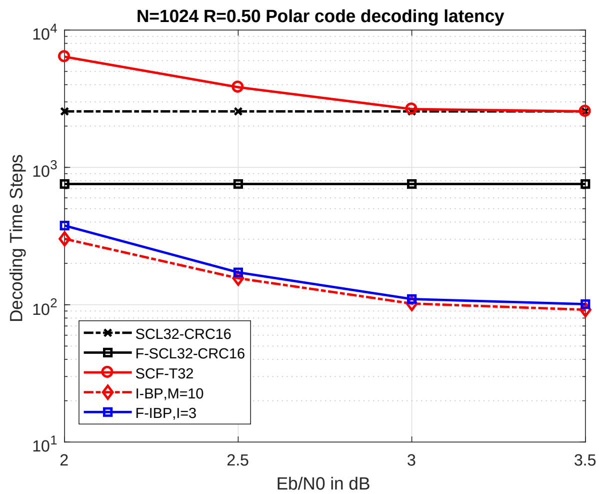

Fig. 3.31: Average decoding latency comparison among different polar decoding methods

Then, we measure the decoding latency of the proposed methods in terms of the number of decoding time-steps. The average decoding latency of I-BP in the number of time steps can be given as: $T_{avg}2n$, where T_{avg} is the average number of iterations. After adding the feedback structure, the average latency can be expected increased, which can be concluded as: $I_{avg}T_{avg}2n$, where I_{avg} is the average number of feedback iterations I. Then, the average decoding latency of the proposed SCF can be roughly calculated as T_{avg} times as the conventional SC decoding, if no simplified SC is considered. Moreover, the average decoding latency of F-SCL can be found in [95]. The number T_{avg} and I_{avg} are obtained from experiments. The comparison of the average decoding latency is given in Fig.3.31.

The investigation of the accurate computational complexity comparison among the above polar decoding methods is open for future research. However, based on existing works, we can roughly estimate each polar decoding scheme's complexity. For instance, since the complexity of SC decoding is $O(NlogN)$, the complexity of the proposed SC-F should be at most $O(T_{avg}NlogN)$. The complexity of SCL based

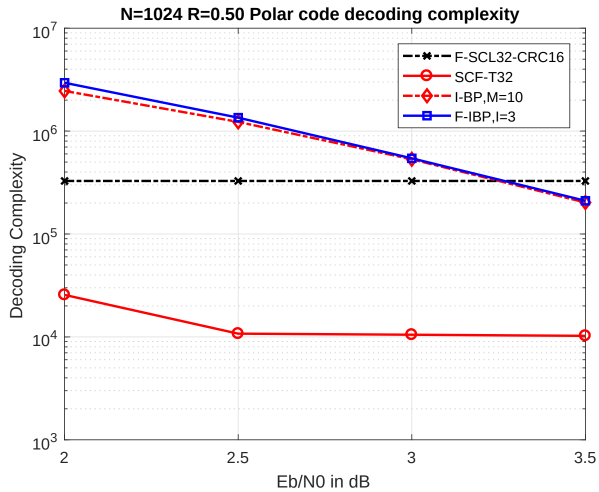

Fig. 3.32: Decoding complexity comparison among different polar decoding methods

Table 3.3: Comparison Among Different Modified Polar Decoding Schemes

	Error performance	Decoding latency	Computational complexity
F-SCL-CRC	Best[1]	Low[2]	$O(LNlogN)$ High
SCL	Good	$2(n-1)+K$ High	$O(LNlogN)$ High
I-BP	Sub-optimal	$T_{avg}2n$ Lowest	$O(MT_{avg}NlogN)$ Highest
F-IBP	Good	$I_{avg}T_{avg}2n$ Low	$O(I_{avg}MT_{avg}NlogN)$ Highest
P-SCF	Good	$T_{avg}2(n-1)+K$ Highest	$O(T_{avg}NlogN)$ Lowest
1.All comparison are relative results according to the above simulation results 2.Experimental results are according to [95]			

decoding can be generalized to $O(LNlogN)$. Then, the complexity of I-BP should be $O(MT_{avg}NlogN)$, where M is the number of candidates, and the complexity of F-IBP should be $O(I_{avg}MT_{avg}NlogN)$. Here, we show the corresponding complexity comparison in Fig.3.32. Moreover, we conclude the corresponding comparison in Table.3.3.

According to the above analysis, we know that each proposed polar decoding own their unique advantages and trade-offs. Fortunately, these modified polar decoding, as well as some other polar decoding methods, can be smoothly applied in the proposed polar-coded OFDM-IM system as long as their have soft-valued input, which provides huge flexibility to our designed system.

3.6 Summary

In section 3.1, a novel SC-F decoding based on GA and stack was proposed. By utilizing stricter error bits selecting criteria, the proposed SC-F can accurately select unreliable bits, leading to a better error correcting performance. Moreover, by including more potential incorrect bits into the stack based on the ML rule, the decoding process may correct more than one errors, leading higher possibility to obtain correct sequence. Simulation results show that the proposed method can improve the FER performance with lower complexity compared with conventional SC-F and SCL methods.

Then, in section 3.2, two enhanced BP decoding algorithms for polar codes were proposed. These schemes employ specific designed interleavers or offsets to effectively enhance the FER performance without changing the structure of BP decoders. Moreover, a feedback structure was proposed based on the proposed enhanced BP decoders. This structure iteratively exchanges the information obtained during the BP decoding. The proposed BP schemes keep most advantages of the conventional BP at the cost of increasing complexity. The only modification is the way to generate permuted input sequences for BP decoders, which can be implemented in advance. Moreover, M-BP and I-BP decoding schemes can be implemented in both serial and parallel ways, thereby conducting effective trade-off between cost and efficiency. Lastly, with the proposed feedback structure, at the cost of increasing complexity and latency, the FER performance of BP decoders can be further enhanced, and this gain is more noticeable in fading channels. However, how to optimize the parameter σ_0, threshold β, and decrease the latency of the proposed BP decoding with feedback structure require further studies.

In section 3.3, a novel stopping criterion for BP polar decoders based on the BDR was proposed. The proposed stopping criterion can significantly reduce the number of iterations via recognizing the successful decoding. Moreover, by choosing different thresholds M, the proposed criterion can save more iterations by compromising the BER performance, which is suitable for some applications with low latency requirement. The mathematical optimization of parameter M and P can be regarded as open investigations.

Last, in section 3.4, a low complex hybrid SD decoding for short polar codes using variable step was proposed. The proposed SD consists of two parts. First, the proposed scheme gradually increases the radius instead of shrinking the radius. Second, the proposed scheme utilizes variable step derived from a modified optimum PM and a stack to avoid node revisiting and unnecessary calculations. Simulation results suggest that for short polar codes, the proposed scheme is capable of maintaining ML optimality and exhibiting lower complexity. Besides, by changing the size of stack, polar decoders with different error correcting capability and complexity can be obtained, exhibiting flexibility and trade-off between complexity and decoding performance. However, the proposed scheme still has somethings to improve. First, compared with RML, the proposed SD has higher latency. Second, compared with other low complex polar decoding, the proposed scheme still has high computational complexity. Third, the variable step size obtained from higher order modulation needs further investigation.

After introducing above modified polar decoding schemes, in the next chapter, the author will move to OFDM based systems which are another inevitable part for wireless communication systems besides channel coding. The OFDM based techniques can obtain benefit from applying polar codes. The next chapter start from introducing conventional OFDM and then move to OFDM-IM. The author believe that by introducing these preliminaries, it would be easier to understand the proposed polar-coded OFDM-IM system.

4 THE THEORY OF OFDM BASED SYSTEMS

Besides channel coding, for a practical wireless communication system, a reliable transmission scheme is also required. In this chapter, the author introduces the fundamental of transmission schemes which have potentialities to be applied in next generation communication networks, including OFDM and OFDM-IM. This chapter starts from the introduction of OFDM, then, the concept of OFDM-IM is given. At the end of this chapter, the author compares OFDM and OFDM-IM from several aspects.

4.1 OFDM systems

This section presents the introduction of OFDM systems, including the fundamental principles of OFDM and OFDM transceivers.

4.1.1 Fundamental principles of OFDM

For an analog OFDM system with N sub-carriers shown in Fig.4.1, assume that the complex symbol X_n is a signal point from the constellation that is modulated on the n^{th} sub-carrier. The transmitted OFDM signal can be expressed as follows [102]:

$$x(t) = \sum_{n=0}^{N-1} X_n \exp(j2\pi f_n t), \quad 0 \leq t \leq T, \tag{4.1}$$

where $f_n = f_0 + n/T$ and $T = NT_s$ is the OFDM symbol interval and T_s is the data symbol period.

Based on (4.1), we know that although sub-carriers may have different phases and amplitudes, they are mutually orthogonal over the symbol interval T if the sub-carrier

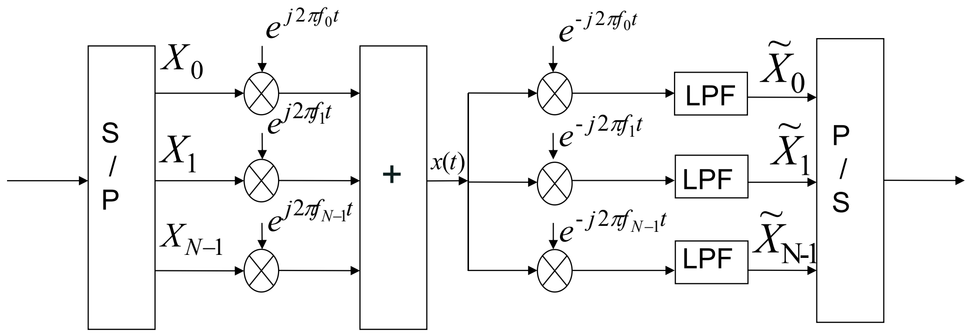

Fig. 4.1: Simple block diagram of OFDM.

spacing is a multiple of $1/T$, as:

$$\frac{1}{T}\int_0^T \exp(j2\pi f_n t)\exp(-j2\pi f_m t)dt = \begin{cases} 1, & m = n, \\ 0, & m \neq n, \end{cases} \tag{4.2}$$

where $|f_n - f_m| = k/T$, $k = 0, \ldots, N-1$.

At the receiver, the received signal $s(t)$ should be fed to N correlators whose outputs are sampled at the end of each symbol interval $t = T$, which is given in Fig.4.1. Since the sub-carriers are orthogonal, the correlator outputs can be simply obtained as follows:

$$\begin{aligned} \tilde{X}_k &= \frac{1}{T}\int_0^T x(t)\exp(-j2\pi f_k t)dt, \\ &= \frac{1}{T}\int_0^T \Big[\sum_{n=0}^{N-1} X_n \exp(j2\pi f_n t)\Big]\exp(-j2\pi f_k t)dt, \\ &= \sum_{n=0}^{N-1} X_n \Big[\frac{1}{T}\int_0^T \exp(j2\pi f_n t)\exp(-j2\pi f_k t)dt\Big], \\ &= X_k, \end{aligned} \tag{4.3}$$

for $k = 0, \ldots, N-1$.

Analog implementation of OFDM requires multiple local oscillators, which is not a practical solution. However, the digital implementation of OFDM systems can be easily done using the fast Fourier transform (FFT), which is simply the efficient computational tool of the discrete Fourier transform (DFT).

The baseband OFDM signal in (4.1) can be synthesized by the inverse discrete Fourier transform (IDFT). Sampling the signal $x(t)$ with sample rate T/N yields the following result:

$$x_k = x(kT/N) = \sum_{n=0}^{N-1} X_n \exp(j\frac{2\pi}{N}nk), \qquad k = 0, \ldots, N-1. \tag{4.4}$$

which is essentially the IDFT of original symbol X_n. Therefore, to recover these original symbols, the receiver performs the DFT on received samples x_k, as:

$$X_n = \sum_{k=0}^{N-1} x_k \exp(-j\frac{2\pi}{N}nk), \qquad n = 0, \ldots, N-1. \tag{4.5}$$

In practice, IDFT/DFT can be replaced by IFFT/FFT. The IFFT can dramatically decrease the computational complexity compared with the IDFT/DFT [103].

4.1.2 OFDM transceivers

OFDM systems split high-speed data streams into low-speed data streams, which increase the duration of symbol period on each sub-carrier. The longer symbol duration is helpful to eliminate the ISI due to time dispersive channels. Unlike the conventional FDM that data are transmitted by uncorrelated sub-channels protected by guarded bands between adjacent sub-carriers, OFDM overlaps sub-carriers because of the orthogonality. Therefore, OFDM is spectral efficient. A typical OFDM transceiver is shown in Fig.4.2.

As illustrated in Fig.4.2, at an OFDM transmitter, the K bits data d_0^{K-1} are mapped to N constellation symbols S_0^{N-1}. Then, after serial to parallel converter (S/P), the frequency domain signals S_0^{N-1} are transformed to time domain signals s_0^{N-1} by an IFFT unit. This operation is called OFDM modulation. Then, after IFFT operations, the parallel symbols stream are transformed into serial format (P/S), and

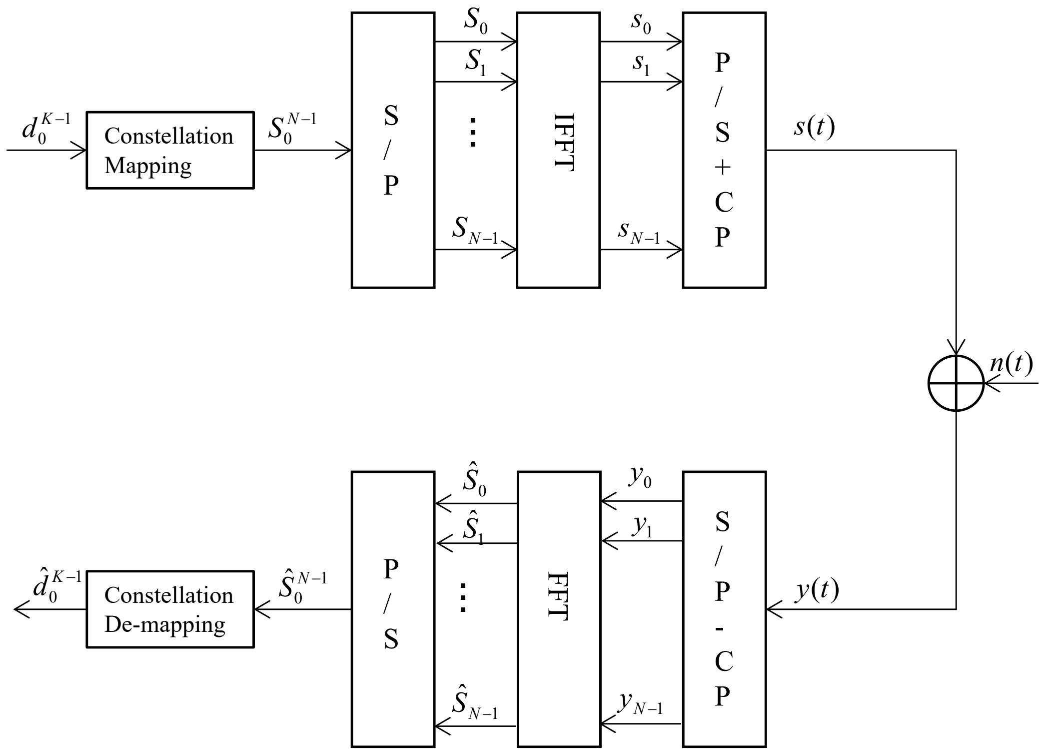

Fig. 4.2: Block diagram of an OFDM transceiver

CP is inserted into original symbols. CP is a set of samples that are copied from the data in the last T_g duration of each OFDM symbol, where T_g should be larger than the time spread delay caused by multi-path propagation. In this way, if the time spread delay is shorter than T_g, signals will not suffer ICI during the demodulation process.

At the receiving side, CP are removed from the received OFDM signals $y(t)$. Then, the parallel symbols are fed to a FFT block to transform the received samples from the time domain to the frequency domain. Then, the constellation de-mapping is implemented to obtain the estimated data stream $\hat{d}_0^{K-1}$. The author notes that in practice, a digital to analog converter (DAC) and an analog to digital converter (ADC) are required at transmitters and receivers, respectively. Moreover, as an illustration, the author omits some blocks that are necessary in practical OFDM realization in the block diagram for simplicity, such as: channel estimation, (de)interleaving, timing and synchronization.

4.2 OFDM-IM systems

In last decade, OFDM has been widely applied in wireless communication networks, providing high data rate transmission. Thanks to its attractive features, OFDM has been adopted to several standards since 1990s, such as digital audio broadcasting (DAB) [104], high-bit-rate digital subscribe line (HDSL) [105], asymmetric digital subscriber line (ADSL) [106]. Currently, OFDM is the core technique of wireless local area networks (WLAN) [107], wireless local and metropolitan area networks (WMAN) [108, 109], and 4G-LTE networks. With the increasing requirements of new generation wireless communication systems, modified OFDM are also developed. Therefore, OFDM-IM attracts attention because of its unique advantages compared with its ancestor, which is suitable for some applications in next generation wireless communication networks [110].

In this section, the author briefly introduces the concept of OFDM-IM. As a modified OFDM technique inspired by SM, OFDM-IM can achieve a balance between error performance and spectral efficiency as well as high energy efficiency compared with classical OFDM thanks to the information bits carried by the indices of OFDM sub-carriers under both ideal and realistic channels [69]. This section presents the introduction of OFDM-IM by introducing transmitters and receivers, respectively.

4.2.1 Transmitters

A transmitter structure of OFDM-IM is illustrated in Fig.4.3.(a). For each OFDM-IM frame, first, m source bits are equally divided into G sub-blocks, and each one has p bits, thus $m = Gp$. Then, each block of p bits need to be modulated by an OFDM-IM modulator, which is given in Fig.4.3.(b). Each block has n available sub-carriers to perform index modulation, where the author denotes N_F, where $N_F = Gn$, as the total available sub-carriers. In OFDM-IM, each sub-block selects k out of n available sub-carriers as active using the first p_1 bits through an indices selector according to:

$$p_1 = \lfloor \log_2 \mathbb{C}_n^k \rfloor \tag{4.6}$$

where $\lfloor \cdot \rfloor$ is the floor function and $\mathbb{C}$ is the combinatorial operation. The author notes that the conventional OFDM can be regarded as a special case of OFDM-IM with $n = k$. The selection of active sub-carriers can be implemented by a reference look-up table when n and k are small or the combinatorial method [69] when n and k are large.

Since the first group of p_1 bits are utilized for index modulation, the rest p_2 bits, where $p = p_1 + p_2$, for each sub-block are modulated by a M-ary constellation parallelly. Then, each OFDM-IM sub-block creator obtains a n-length OFDM block by considering symbols $\{S_g(\eta)\}_{\eta=1}^{k}$ and indices $\mathbf{I}_g$, for $g = 1, ..., G$, respectively. $\mathbf{I}_g$ indicates which sub-carriers are occupied by symbols $\{S_g(\eta)\}_{\eta=1}^{k}$, and which sub-carriers are idle. Then, an OFDM-IM block creator concatenates these G sub-blocks to obtain a N_F length OFDM frame. The author notes that after this point, a $n \times G$ block interleaver might be utilized to improve the performance of OFDM-IM [67, 111]. However, it is not necessary for a conventional OFDM-IM. Finally, IFFT operations, P/S converter, and CP insertion are performed like the classical OFDM for the transmission through fading channels. Here, the total number of bits transmitted by OFDM-IM in one frame can be written as:

$$m = pG = (\lfloor \log_2 \mathbb{C}_n^k \rfloor + K \log_2 M)G \tag{4.7}$$

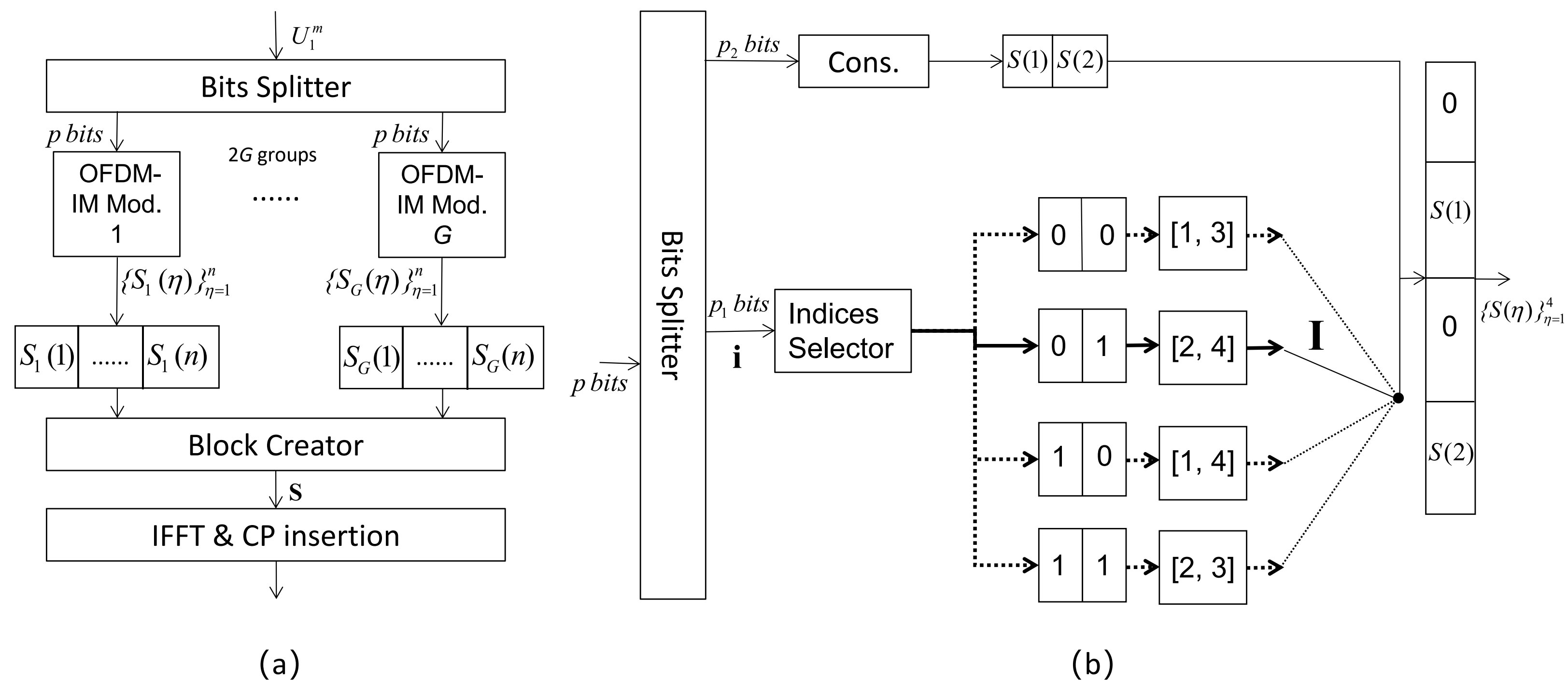

Fig. 4.3: System model of (a). an OFDM-IM transmitter, (b). an example of an OFDM-IM modulator for $n = 4$, $k = 2$

4.2.2 Receivers

The receiver of OFDM-IM is required to determine the indices of active sub-carriers as well as the corresponding symbols that are conveyed by these active sub-carriers. A receiver of OFDM-IM is shown in Fig.4.4. After reverse operations (CP removal, N_F points FFT), the received sequence $\mathbf{y}$ needs to be split into G sub-blocks $\mathbf{y}_g$ for $g = 1, .., G$. The author notes that the detection of these G sub-blocks are implemented parallely and independently. For OFDM-IM, generally, two detection schemes can be utilized. One is the optimal but high-complex ML detector, which performs a joint search by considering all realizations of sub-carrier activation patterns (SAPs) and data symbols [110]. For each sub-block, the ML detector for OFDM-IM is given by:

$$\{\hat{S}_g(\eta)\}_{\eta=1}^{n} = \underset{\{S_g(\eta)\}_{\eta=1}^{n}}{\operatorname{argmin}} \sum_{\eta=1}^{n} |y_g(\eta) - H_g(\eta)S_g(\eta)|^2 \tag{4.8}$$

where $H_g(\eta)$ denotes the channel frequency response (CFR) on the η^{th} sub-carrier of the g^{th} sub-block. More details for ML decoding in OFDM-IM can be found in [112]. The other one is the low-complex *a posteriori* probability based near-optimal detector, which independently calculates the *a posteriori* probability for each sub-carrier. The channel detector handles indices first and then detect transmitted symbols based on the detected indices information. The author will discuss more details for the detection of OFDM-IM in the chapter where the polar-coded OFDM-I/Q-IM system is proposed.

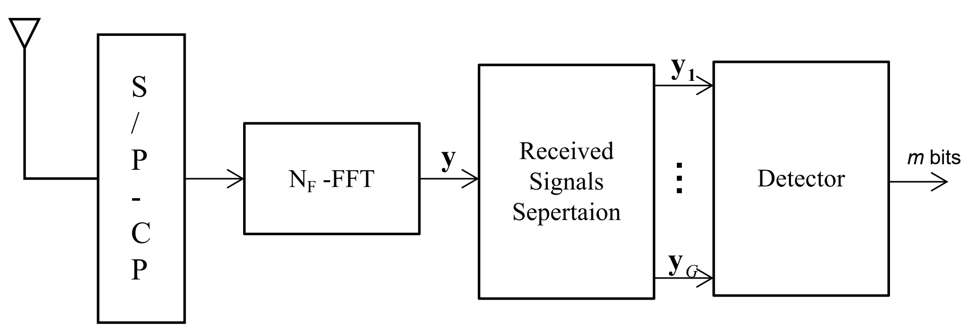

Fig. 4.4: Block diagram of an OFDM-IM receiver

OFDM-IM provides a very interesting result in terms of BER performance. According to the simulation result in [69], compared with OFDM, the classical OFDM-IM achieves worse performance when SNR is low and better performance when SNR is mid to high. Also, the OFDM-IM usually achieves lower spectral efficiency than that of OFDM when modulation order is high. Moreover, compared with ML detectors, the BER performance of OFDM-IM using low-complex *a posteriori* probability based detectors only have slight degradation. To further improve the spectral efficiency and error performance, modified OFDM-IM schemes appeared. Some of them can achieve performance enhancement without increasing complexity, which makes OFDM-IM surpass OFDM in many scenarios of the next generation wireless communication networks. Therefore, polar-coded OFDM-IM systems can be regarded as a valuable investigation.

4.2.3 Comparisons between OFDM and OFDM-IM

A detailed tutorial article of OFDM-IM techniques can be found in [110]. According to such existing works, the author concludes the advantages and disadvantages of OFDM-IM compared with OFDM in this section.

In general, OFDM-IM was proposed as an extended version of OFDM. Therefore, compared with emerging waveforms such as generalized frequency division multiplexing (GFDM) [113], filtered bank multi-carrier (FBMC) [114], and universal filtered multi-carrier (UFMC) [115], OFDM-IM has a less complicated structure, and it can be seen as a smooth transition from OFDM. Compared with the conventional OFDM, the advantages of OFDM-IM are concluded as follows:

- OFDM-IM owns trade-off between error performance and spectral efficiency because OFDM-IM can adjust the number of activated sub-carriers accordingly to reach the target spectral efficiency or error performance. In other words, OFDM-IM can generate variable sized frames, which provides high flexibility for the network slicing in the next generation communication networks.

- OFDM-IM has flexibility in terms of energy efficiency and error performance. On the one hand, OFDM-IM can achieve higher energy efficiency by setting some of sub-carriers as idle. On the other hand, since some of sub-carriers are inactive, the power of active sub-carriers can be increased under the constraint of total power, which is expected to achieve better error performance.
- OFDN-IM has better BER performance than that of the classical OFDM when the spectral efficiency is low to mid utilizing low-complex *a posteriori* or ML detectors.
- OFDM-IM has better performance compared with OFDM in terms of ergodic achievable rate.
- OFDM-IM has better performance in terms of PAPR and inter-carrier interference (ICI) because of inactive sub-carriers.
- OFDM-IM performs well in multiple input multiple output (MIMO), multi user (MU), and high mobility setups as well as to optical wireless (OW), device to device (D2D) and under water acoustic (UWA) communication systems.
- OFDM-IM has multiple modified versions proposed in recent years, which increase its flexibility as well as error performance without increasing complexity.

Since OFDM-IM can provide above advantages, it has been an attractive candidate for next generation networks. However, compared with OFDM, OFDM-IM still has following disadvantages:

- When modulation orders are high, the spectral efficiency of the classical OFDM-IM is lower than that of the conventional OFDM due to the index modulation. However, some enhanced OFDM-IM schemes have been proposed to overcome this drawback.

- Coded/uncoded OFDM-IM usually performs worse than that of the classical OFDM in low SNR scenarios. Also, this disadvantage might be solve by applying enhanced OFDM-IM schemes.

- The computational complexity of the ML detector for OFDM-IM is high compared with the OFDM. The low-complex *a posteriori* probability based detector achieves lower complexity while losing some error performance.

- OFDM-IM and OFDM have similar PAPR performance when the input are Gaussian symbols. Moreover, OFDM beats OFDM-IM in terms of achievable rate for Gaussian input symbols.

4.3 Summary

In this chapter, OFDM based techniques, including conventional OFDM and OFDM-IM, were reviewed. Further, the author provided the advantages and disadvantages of OFDM-IM compared with OFDM. Thanks to the unique advantages, OFDM-IM has been regarded as a potential candidate for the 5G wireless communication system, competing with its ancestors. Moreover, the flexibility and well performance in variety of user applications and channel conditions makes OFDM-IM very attractive for M2M and D2D systems. Therefore, based on OFDM-IM, the author will introduce a polar-coded OFDM-I/Q-IM system in Chapter 7. Nevertheless, before introducing such novel system, the author will first introduce polar codes to conventional OFDM systems, and propose two modified polar-coded OFDM systems based on existing techniques. These works that can be implemented in practical systems enhance the corresponding error performance.

5 MODIFIED POLAR-CODED OFDM SYSTEMS

OFDM systems are suitable for selective fading conditions without complicated equalizers because OFDM converts a high-speed message stream to several low-speed streams modulated on sub-carriers, thus each sub-carrier can be treated as undergoing flat fading. Moreover, in order to make OFDM systems work normally in practical scenarios, channel coding is usually adopted. As one of the selected coding schemes using in 5G communication networks, it is worth to investigate polar-coded OFDM systems. In this chapter, the author will introduce two modified polar-coded OFDM systems, which can achieve better error performance than that of the system where polar codes and OFDM are simply concatenated. Therefore, these two works are presented in this chapter as two separate sections.

5.1 Polar decoding for wireless system with noisy channel estimates

5.1.1 Introduction

Polar codes, introduced by E.Arikan [28], are the first type of capacity-achieving codes over B-DMCs. Nevertheless, in OFDM communication systems, after OFDM modulation, signal transmissions are equivalent to be transmitted over flat fading channels. Moreover, channel estimates are usually inaccurate, leading to BER degradation. Exploiting channel compensations can effectively enhance the BER performance of error correction codes over fading channels [116]. In this part, a channel reliability compensator $\boldsymbol{C}$ for BP decoding in polar-coded OFDM with imperfect channel estimates is proposed. This compensator $\boldsymbol{C}$ re-regulates the initial LLRs of the conventional BP decoding by introducing the variance of channel estimate errors σ_m^2. It is shown that utilizing the proposed compensator $\boldsymbol{C}$ for BP is helpful for BER performance enhancement. However, similar to turbo codes, "min-sum" (MS) based decoding methods cannot benefit from the proposed channel reliability compensation [117]. Simulation results reveal that the proposed $\boldsymbol{C}$ can significantly enhance the BER performance of polar codes with noisy channel estimates without rising any complexity.

5.1.2 The system model

The channel model and receiver structure are illustrated in Fig.5.1. It is assumed that a BPSK modulated polar-coded sequence $\mathbf{x} = [x_1, ...x_N]$ with $x_i \in \{+\sqrt{E_s}, -\sqrt{E_s}\}$, where $1 \leq i \leq N$, and E_s is the transmitted power, is sent over an independent Rayleigh fading channel. After noise contamination, the corresponding transmitted sequence is written as:

$$r_i = h_i x_i + n_i \tag{5.1}$$

where the fading coefficient h_i and AWGN component n_i are independent complex-valued, Gaussian distributed random variables with zero mean. The variance of h_i and n_i are assumed as $E[|h_i|^2] = 2\sigma_h^2$ and $E[|n_i|^2] = 2\sigma_n^2$, respectively, where $E[x]$ denotes the expectation value of x.

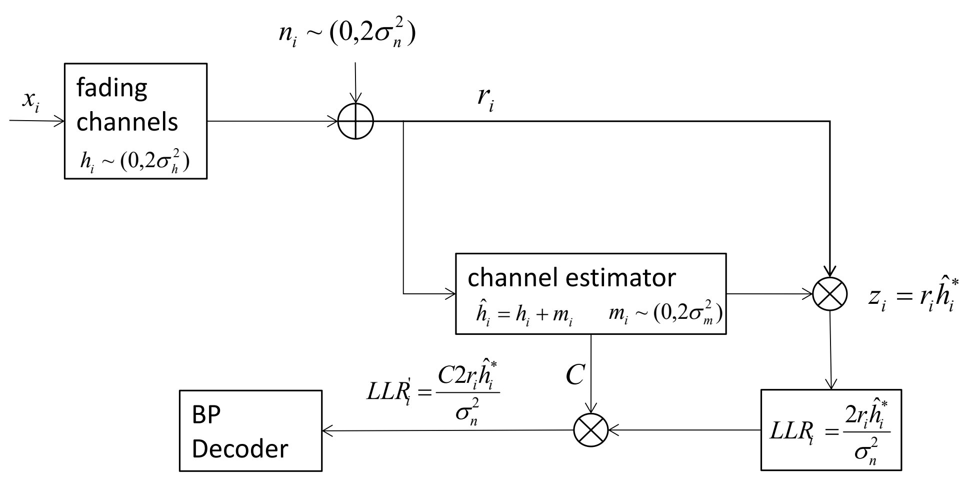

Fig. 5.1: Block diagram of the receiver and channel model

In practice, channel estimators are available at receivers for data recovery, whereas the estimation is usually inaccurate. Thus, the noisy channel estimate $\hat{h}_i$ is defined as:

$$\hat{h}_i = h_i + m_i \tag{5.2}$$

where m_i indicates a Gaussian distributed complex variable with $E[|m_i|] = 0$ and $E[|m_i|^2] = 2\sigma_m^2$. $E[\hat{h}_i] = 0$, h_i and m_i are assumed to be independent. Accordingly, $\sigma_{\hat{h}}^2 = \sigma_h^2 + \sigma_m^2$. σ_m can be ascertained if parameters, such as SNR and channel Doppler frequency, are available [118]. In this paper, it is assumed that σ_m is known by the receiver, employed to enhance the BER performance of BP polar decoding. Subsequently, after channel estimation, the variable applied for decoding is denoted as:

$$z_i = y_i \hat{h}_i^* = z_{i,R} + z_{i,I} \tag{5.3}$$

where $z_{i,R}$ and $z_{i,I}$ denote the real and imaginary part of z_i, respectively. Since BPSK modulated signals only exhibit real parts, imaginary parts $z_{i,I}$ are omitted, $z_{i,R}$ is directly expressed as z_i in following sections.

If the fading coefficient h_i is optimally estimated, received symbols z_i can be treated as the symbols that are only affected by Gaussian white noise, and the PDF that receives z_i conditioned on x_i in AWGN channels is expressed as:

$$p_{z_i|x_i}(z_i) = \frac{\sqrt{E_s}}{N_0} \exp\left(-\frac{(z_i - \sqrt{E_s}x_i)^2}{\frac{N_0}{2}}\right) \tag{5.4}$$

If $x_i \in \{+\sqrt{E_s}, -\sqrt{E_s}\}$, initial LLRs of BP decoders with channel estimate can be written as:

$$LLR_i = \ln\left(\frac{\frac{\sqrt{E_s}}{N_0}\exp\left(-\frac{(z_i-\sqrt{E_s}x_i)^2}{\frac{N_0}{2}}\right)}{\frac{\sqrt{E_s}}{N_0}\exp\left(-\frac{(z_i+\sqrt{E_s}x_i)^2}{\frac{N_0}{2}}\right)}\right) = \frac{4\sqrt{E_s}}{N_0} z_i = \frac{2z_i}{\sigma_n^2} = \frac{2r_i\hat{h}_i^*}{\sigma_n^2} \tag{5.5}$$

However, due to noisy channel estimates, initial LLRs in (5.5) is not as accurate as that with perfect channel estimation. Therefore, in this part, a channel compensator $\boldsymbol{C}$ for BP is proposed to improve the accuracy of initial LLRs, which is expected to enhance the BER performance of BP polar decoding in fading channels.

It is known that in AWGN channels, BP for polar codes is not sensitive to inaccurate channel estimates since min-sum based decoding functions are insensitive to multiplicative factors [119]. However, the conventional BP is sensitive to multiplicative factors. Given the mentioned knowledge, $\boldsymbol{C}$, a multiplicative factor for the original inaccurate LLRs, is defined.

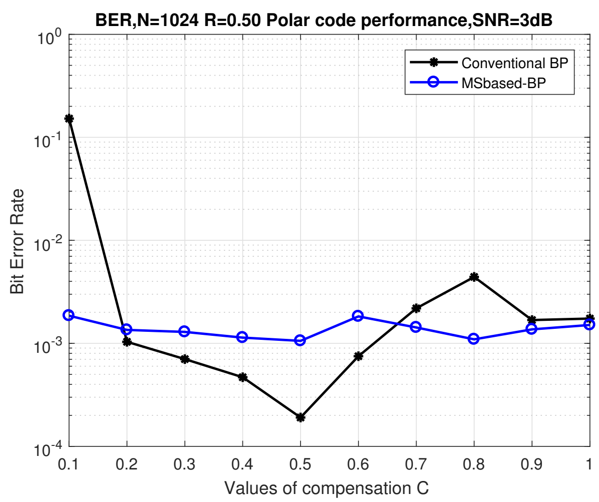

Fig. 5.2: BER performance for a (1024,512) polar code with variant channel compensator $\boldsymbol{C}$ for two kinds of BP decoders with $E_b/N0$=3 dB

Fig.5.2 suggests that compared with MS-based BP decoders [91], the conventional BP is susceptible to the variance of compensation factor $\boldsymbol{C}$. Thus, applying an appropriate $\boldsymbol{C}$ can help conventional BP enhance its BER performance.

5.1.3 The proposed channel compensator $\boldsymbol{C}$ for BP

In fading channels with estimate $\hat{h}$, the PDF of z_i conditioned on transmitted BSPK modulated symbol x_i is defined as [120]:

$$p_{z_i|x_i}(z_i) = \frac{1}{2\pi\sigma_{\hat{h}}^2\sigma_r^2(1-|\mu|^2)}\exp[\frac{\Re[z_i\mu_i]}{\sigma_{\hat{h}}\sigma_r(1-|\mu|^2)}] \times K_0(\frac{|z_i|}{\sigma_{\hat{h}}\sigma_r(1-|\mu|^2)}) \tag{5.6}$$

where $K_0(x)$ denotes the 0^{th}-order Hankel function of x, $\Re(x)$ refers to the real part of x. Moreover, μ_i is denoted as the cross-correlation coefficient of r_i and $\hat{h}_i$, which is defined as:

$$\begin{aligned}\mu_i &= \frac{E[r_i \hat{h}_i^*]}{\sqrt{E[|r_i|^2]E[|\hat{h}_i|^2]}} \\ &= x_i \frac{2\sigma_h^2}{\sqrt{(|x_i|^2 2\sigma_h^2 + 2\sigma_n^2)(2\sigma_h^2 + 2\sigma_m^2)}} \\ &= |\mu| e^{-j\epsilon_i}\end{aligned} \tag{5.7}$$

Since x_i is a BPSK modulated symbol, thus, $|\mu_i|$ is a real value and $\epsilon_i \in \{0, \pi\}$. Subsequently, based on (5.6) and (5.7), the corrected initial LLRs of decision variable z_i with noisy channel estimate $\hat{h}_i$ is written as:

$$LLR_i' = \ln \frac{P(z_i | x_i = -\sqrt{E_s})}{P(z_i | x_i = -\sqrt{E_s})} = \frac{2|\mu|}{\sigma_r \sigma_n (1 - |\mu|^2)} z_i \tag{5.8}$$

By considering (5.7), $\sigma_{\hat{h}}^2 = \sigma_h^2 + \sigma_m^2$, and $\sigma_n^2 = N_0/2$, the corrected LLRs are rewritten as:

$$LLR_i' = \frac{4\sqrt{E_s}}{N_0} z_i \sigma_h^2 [\sigma_m^2 (\frac{2E_s}{N_0} \sigma_h^2 + 1) + \sigma_h^2]^{-1} \tag{5.9}$$

where $\sigma_h^2[\sigma_m^2(\frac{2E_s}{N_0}\sigma_h^2 + 1) + \sigma_h^2]^{-1}$ is called the channel compensator $\boldsymbol{C}$.

(5.9) reveals that the channel compensator introduces the variance of estimate error σ_m^2. With the proposed channel compensator $\boldsymbol{C}$, corrected initial LLRs can be achieved. Moreover, when $\sigma_m^2 = 0$, (5.9) can be simplified to $\frac{4\sqrt{E_s}}{N_0} z_i$, which is equivalent to (5.5).

5.1.4 Simulation results

In this section, BER simulation results of BP decoding with the proposed $\boldsymbol{C}$ are given and evaluated. In the presented simulation results, $\sigma_h^2 = 1$. Furthermore, code length is 1024 and rate is fixed to 0.5. The noisy channel estimate is simulated, and m_i is calculated from a Gaussian random generator. The maximum iteration for BP is 60. Furthermore, the BER performance of BP in AWGN channels with perfect channel state information (CSI) is also included.

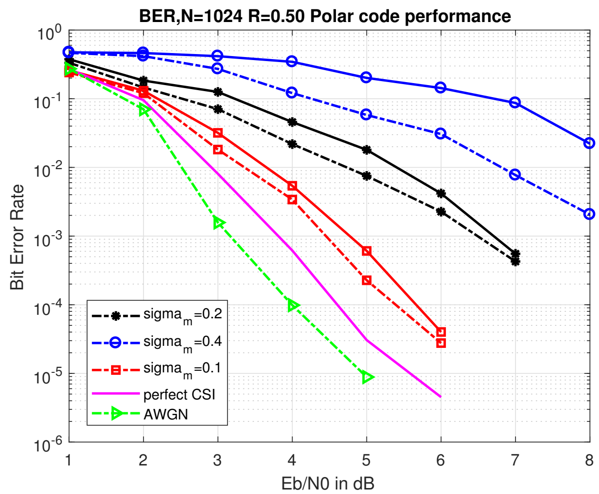

Fig. 5.3: BER performance of polar codes using corrected $LLRs$ (dashed) versus $LLRs$ in (5.5) (solid) with variable $\sigma_m^2 = 0, 0.1, 0.2, 0.4$.

The BER performance of BP decoding in Rayleigh fading channels using the proposed channel compensator $\boldsymbol{C}$ is illustrated in Fig. 5.3. The code length is 1024. It is suggested that when σ_m^2 increases, benefits gained from $\boldsymbol{C}$ are more noticeable. When $\sigma_m^2 = 0.4$, compared with the BP using initial LLRs in (5.5), the performance gain using the proposed compensator is nearly 1.5 dB at probability of 10^{-2}.

It is known that better channel estimates (lower σ_m^2) can be obtained by using different channel estimate algorithms under high SNRs [69]. To make our simulation results more practical, instead of a fixed value of σ_m^2 for all SNRs, it is assumed here that $\sigma_m^2 = \alpha\sigma_n^2$, where α denotes a constant scale factor. Fig.5.4 reveals that with variable α, the BER performance using the proposed compensator $\boldsymbol{C}$ (dashed) is always better than that of the case without introducing σ_m^2 (solid). The gain is about 1.5 dB at probability 10^{-3} when $\alpha = 1$.

Fig.5.5 draws the comparison between BP decoding utilizing the proposed $\boldsymbol{C}$

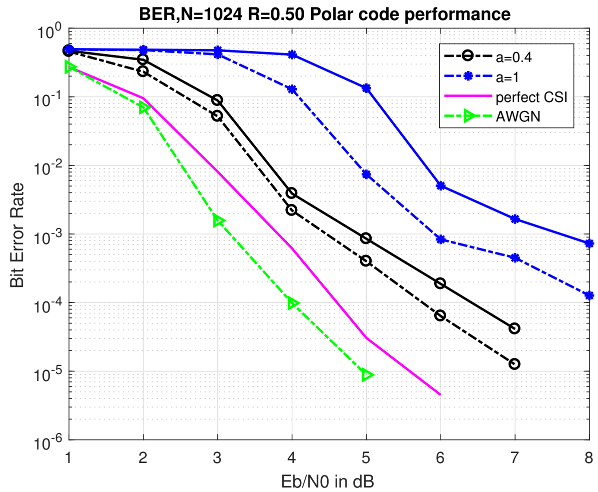

Fig. 5.4: BER performance of polar codes using corrected $LLRs$ (dashed) versus $LLRs$ in (5.5) (solid) for variable $\sigma_m^2 = \alpha\sigma_n^2$ with $\alpha = 0, 0.4, 1$.

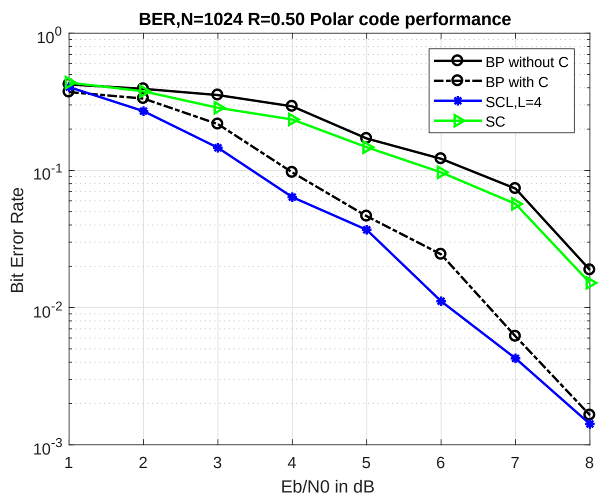

Fig. 5.5: BER performance of BP with (dashed) and without (solid) corrected $LLRs$ versus different SC based polar decoders (SC, SCL)

and other major stream polar decoding algorithms, including: SC and SCL [45], with $\sigma_m^2 = 0.4$. It is known that SCL can act as a benchmark for polar decoding. Nevertheless, SC based decoding algorithms are not capable of exploiting the proposed $\boldsymbol{C}$ for its insensitivity to multiplicative factors [119]. Given this, in noisy estimate scenarios, the proposed BP decoding can achieve a very similar BER performance to SCL (list size $L = 4$), which exhibits higher latency. Furthermore, the gain obtained from utilizing $\boldsymbol{C}$ does not rises the complexity of BP decoders.

5.2 Turbo receiver for polar-coded OFDM systems with unknown CSI

5.2.1 Introduction

We know that in November 2016, polar coding was agreed to be used in eMBB control channels for the 5G NR interface [55], which makes related research in polar codes more attractive. Nevertheless, in practice, communication channels are usually frequency selective. However, polar codes are mostly designed for AWGN channels, which may be insufficient when using in frequency selective channels. Although there are some investigations for polar code construction in memory channels [64, 65, 66], it is more practical to modify receivers rather than polar encoders. We know that OFDM is a multi-carrier modulation technique which converts frequency selective fading into flat fading [61], and OFDM is also the chosen one as waveform for 5G [63]. This decision gives us the idea to combine polar codes with OFDM techniques. Moreover, currently, OFDM has been implemented in 4G LTE and WiMAX cellular network standards [121], which provides us a lot of ideas to learn from.

In this part, a novel turbo receiver for polar codes, which combines a expectation maximization (EM) demodulator and BP polar decoders [1] in OFDM systems to improve the error-correcting performance of polar decoding in frequency selective channels. Simulation results show that by utilizing the proposed receiver, corresponding BER performances can be significantly improved compared with the case that implements demodulation and decoding separately. Moreover, the performance of using the proposed receiver with unknown CSI can approach the performance with perfect CSI. Similar research has been investigated by using LDPC codes [122]. In this part, the turbo receiving structure is realized by using polar codes.

5.2.2 The system model

Assume a polar coded OFDM system with Q sub-carriers, transmitting data through frequency selective channels. The system model at transmitting side is given in Fig.5.6. First, information bits $\mathbf{u}$ are coded by a polar encoder. Then, polar codewords $\mathbf{c}$ are modulated by M-phase shift keying (M-PSK). These M-PSK symbols $\mathbf{X}$ are transmitted across P OFDM slots. Therefore, PQ M-PSK symbols are transmitted in total. It is assumed that the fading processes remain static during each OFDM word (time slot) while varying from one OFDM word to another. Then, after IFFT, time-domain OFDM words $\mathbf{x}$ are sent to fading channels.

At the receiver, signals after matched filtering and symbol-rate sampling are operated by FFT, obtaining:

$$\mathbf{Y}[p] = \mathbf{X}[p]\mathbf{H}[p] + z[p], \text{ for } p = 1, ..., P \tag{5.10}$$

where

$$\mathbf{X}[p] = \text{diag}\{X[p,0], X[p,1], ..., X[p,Q-1]\}_{Q\times Q}$$
$$\mathbf{H}[p] = \{H[p,0], ..., H[p,Q-1]\}^T_{Q\times 1}$$

where $\mathbf{H}[p]$ is a length Q vector including complex channel frequency responses at the pth OFDM slot. The $\mathbf{H}$ in time domain at the kth sub-carrier and pth slot can be written as:

$$H[p,k] = \sum_{l=0}^{L-1} h[l;p]e^{-j2\pi kl/Q} = \mathbf{w}_f^H(k)\mathbf{h}(p) \tag{5.11}$$

where $\mathbf{h}(p) = [\alpha(0;pT), ..., \alpha(L-1;pT)]^T$ is the L-length channel response of all taps in time domain. T is the duration of one OFDM slot. The $\alpha(l;pT)$ is the complex fading amplitude of the lth tap, and

$$\mathbf{w}_f(k) = [e^{-j0}, e^{-j2\pi k/Q}, ..., e^{-j2\pi k(L-1)/Q}]^H_{L\times 1}$$

are related FFT coefficients. Therefore, (5.10) can be rewritten as:

$$\mathbf{Y}[p] = \mathbf{X}[p]\mathbf{W}_f\mathbf{h}[p] + z[p], \text{ for } p = 1, ..., P \tag{5.12}$$

with

$$\mathbf{X}[p] = \mathrm{diag}\{X[p,0], X[p,1], ..., X[p,Q-1]\}_{Q\times Q}$$
$$\mathbf{W}_f = [\mathbf{w}_f(0), \mathbf{w}_f(1), ..., \mathbf{w}_f(Q-1)]^H_{Q\times L}$$

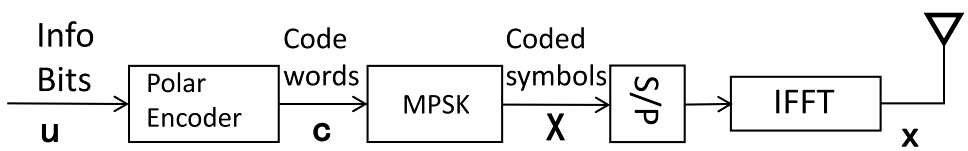

Fig. 5.6: Block diagram of a polar-coded OFDM transmitter

5.2.3 The turbo receiver for polar-coded OFDM

In this section, design of the proposed turbo receiver for polar-coded OFDM is introduced. A polar code based turbo receiver includes two stages, the *soft demodulator* and *soft* polar decoder. To obtain soft values, BP decoding is used. By utilizing soft demodulators and decoders, the extrinsic information can be iteratively exchanged between these two parts to gradually improve the performance of the proposed system.

In practice, CSI are usually unknown and needs to be estimated at receiving sides. Therefore, we assume an unknown fading channel, and utilize the maximum *a posteriori* expectation-maximization (MAP-EM) algorithm for demodulation. An illustration of the proposed turbo receiver for polar-coded OFDM systems is shown in Fig.5.7. It consists two parts: The *soft* MAP-EM demodulator and BP decoder. Both of them are iterative algorithms. The soft MAP-EM demodulator receives signals $\mathbf{Y}$ after FFT operations, and the extrinsic LLRs λ_2 from the BP polar decoder. It computes the extrinsic *a posteriori* LLRs of coded words λ_1 and sends them to BP. Then, the decoder obtains corresponding LLRs and computes as the output extrinsic LLRs of coded words or the hard decision if it reaches the last turbo iteration.

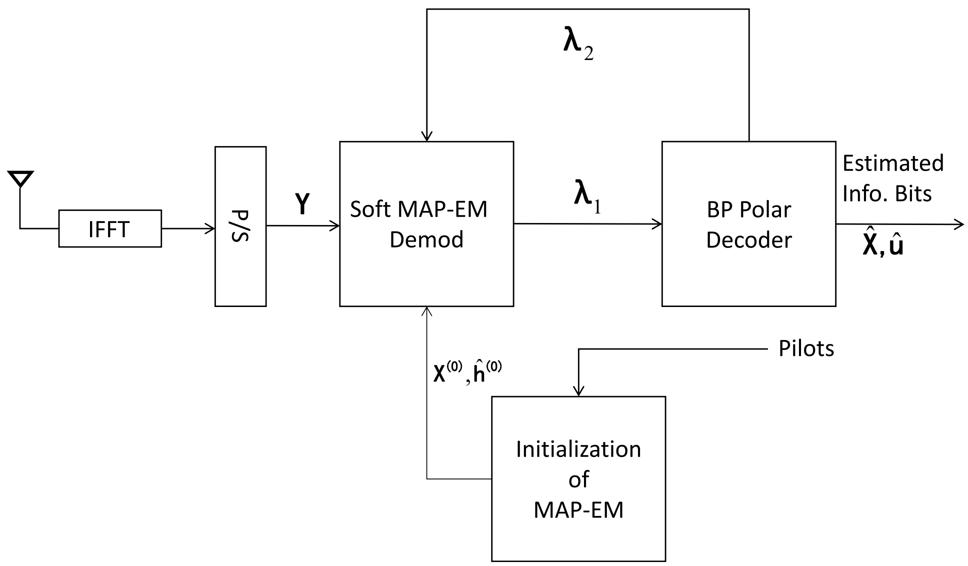

Fig. 5.7: Block diagram of the proposed turbo receiver

5.2.3.1 The MAP-EM demodulator :

For notation simplicity, in the following discussion, we assume that $P = 1$, and BPSK is used for modulation. It should be noted that the $\mathbf{h}$ defined above is supposed to have only time responses of L_f nonzero taps. Moreover, since CSI is not available at first, the $\mathbf{h}$ needs to be redefined to consist time responses of all taps within the maximum multi-path spread, which is $\mathbf{h} = [h(1), ..., h(L'_f)]^T$, with $L'_f = \lceil \tau_m Q \Delta_f + 1 \rceil \geqslant L_f$, where τ_m is the maximum multi-path spread. Hence, the corresponding FFT coefficients need to be rewritten as $\mathbf{w}_f(k) = [e^{-j0}, e^{-j2\pi k/Q}, ..., e^{-j2\pi k(L'_f-1)/Q}]^H_{L'_f \times 1}$.

Therefore, the received signal $\mathbf{Y}$ should be rewritten as

$$\mathbf{Y} = \mathbf{X}\mathbf{W}_f\mathbf{h} + \mathbf{z} \tag{5.13}$$

where:

$$\mathbf{X} = \mathrm{diag}\{X[0], X[1], ..., X[Q-1]\}_{Q\times Q}$$
$$\mathbf{W}_f = [\mathbf{w}_f(0), ..., \mathbf{w}_f(Q-1)]^H_{Q\times L'_f}$$

with $\mathbf{Y}$ and $\mathbf{z}$ the length Q vectors which contain the received signals and ambient Gaussian noise at all Q sub-carriers, respectively.

Without CSI, the MAP detection problem is defined as:

$$\hat{\mathbf{X}} = \underset{\mathbf{X}}{\mathrm{argmax}} \ln P(\mathbf{X}|\mathbf{Y}) \tag{5.14}$$

and this problem can be solved by an EM algorithm.

E-step: the expectation is computed with respect to the hidden channel response $\mathbf{h}$ conditioned on $\mathbf{X}$ and $\mathbf{Y}$. It is shown that the $\mathbf{h}$ follows a complex Gaussian distribution conditioned on $\mathbf{X}$ and $\mathbf{Y}$, which is denoted as:

$$\mathbf{h}|(\mathbf{Y}, \mathbf{X}^{(i)}) \sim N_c(\hat{\mathbf{h}}, \hat{\sum}_h) \tag{5.15}$$

with:

$$\hat{\mathbf{h}} = (\mathbf{W}_f^H \mathbf{X}^{(i)H}\mathbf{X}^{(i)}\mathbf{W}_f + \sum_h^{\dagger})^{-1}\mathbf{W}_f^H\mathbf{X}^{(i)H}\mathbf{Y} \tag{5.16}$$

$$\hat{\sum}_h = \sum_h - (\mathbf{W}_f^H \mathbf{X}^{(i)H}\mathbf{X}^{(i)}\mathbf{W}_f + \sum_h^{\dagger})^{-1} \times \mathbf{W}_f^H\mathbf{X}^{(i)H}\mathbf{X}^{(i)}\mathbf{W}_f \sum_h \tag{5.17}$$

where $\sum_h$ denotes the covariance matrix of the channel response $\mathbf{h}$. $\sum_h$ can be written as: $\sum_h = E[\mathbf{h}\mathbf{h}^H] = \text{diag}\{\sigma_1^2, ..., \sigma_{L'_f}^2\}$, where σ_l^2 is the average power of the lth tap, which can be known with the help of pilots. $\sum_h^\dagger = \text{diag}\{\gamma_1, ..., \gamma_{L'_f}\}$ is the pseudo-inverse of $\sum_h$, which is defined as:

$$\gamma_l = \begin{cases} 1/\sigma_l^2, \ \sigma_l^2 \neq 0 \\ 0, \qquad \sigma_l^2 = 0 \end{cases} \quad l = 1, 2, ..., L'_f \tag{5.18}$$

By using (5.15) and (5.13), the Q function is calculated as:

$$\begin{aligned} \text{Q}(\mathbf{X}|\mathbf{X}^{(i)}) &= -E_{\mathbf{h}|(\mathbf{Y},\mathbf{X}^{(i)})}\{||\mathbf{Y} - \mathbf{X}\mathbf{W}\mathbf{h}||^2\} + \text{C} \\ &= -E_{\mathbf{h}|(\mathbf{Y},\mathbf{X}^{(i)})}\{||(\mathbf{Y} - \mathbf{X}\mathbf{W}\hat{\mathbf{h}}) + (\mathbf{X}\mathbf{W}\hat{\mathbf{h}} - \mathbf{X}\mathbf{W}\mathbf{h})||^2\} + \text{C} \\ &= -E_{\mathbf{h}|\mathbf{Y},\mathbf{X}^{(i)}}\{(\hat{\mathbf{h}} - \mathbf{h})^H\mathbf{W}^H\mathbf{X}^H\mathbf{X}\mathbf{W})(\hat{\mathbf{h}} - \mathbf{h})\} - ||\mathbf{Y} - \mathbf{X}\mathbf{W}\hat{\mathbf{h}}||^2 + \text{C} \\ &= -||\mathbf{Y} - \mathbf{X}\mathbf{W}\hat{\mathbf{h}}||^2 - \text{trace}\{\mathbf{X}\mathbf{W}\hat{\sum}_h\mathbf{W}^H\mathbf{X}^H\} + \text{C} \\ &= -\sum_{k=0}^{Q-1} q(X[k]) + \text{C} \end{aligned} \tag{5.19}$$

where C is a constant, $q(X[k]) = \{||Y[k] - X[k]\mathbf{w}_f^H(k)\hat{\mathbf{h}}||^2 + [X[k]\hat{\sum}_h(k)X[k]]\}$, with $\hat{\sum}_h(k) = [\mathbf{w}_f\hat{\sum}_h\mathbf{w}_f^H]_{k+1,k+1}$, where $[\mathbf{A}]_{i,j}$ denotes the (i, j)th elements in matrix $[\mathbf{A}]$.

Then, based on the function Q, the M-step can be concluded as:

$$\begin{aligned} \mathbf{X}^{(i+1)} &= \underset{\mathbf{X}}{\text{argmax}}[Q(\mathbf{X}|\mathbf{X}^{(i)}) + \ln P(\mathbf{X})] \\ &= \underset{\mathbf{X}}{\text{argmax}}[-\sum_{k=0}^{Q-1} q(X[k]) + \sum_{k=0}^{Q-1} \ln P(X[k])] \\ &= \sum_{k=0}^{Q-1} \underset{\mathbf{X}}{\text{argmin}}[q(X[k]) - \ln P(X[k])] \end{aligned} \tag{5.20}$$

It is shown that the M-step can be decoupled into Q independent minimization steps. Each step is solved by enumerating all possible symbols $\mathbf{X}$ from set Ω, where Ω represents the set of all M-PSK symbols. Therefore, the total complexity of the

M-step is $O(|\Omega|)$.

In each turbo iteration, EM optimization iterates I_{EM} times. At the end of EM process, the extrinsic *a posteriori* LLRs of code words are calculated and fed to the BP decoder. Using M-PSK modulation, the *a posteriori* LLRs λ_1 of the jth ($j = 1, 2, ..., \log_2|\Omega|$) code word at the kth sub-carrier, $c^j[k]$ is calculated as the output of the EM demodulator, which is computed as follows:

$$\begin{aligned}
\lambda_1(c^j[k]) &= \ln\frac{P(c^j[k]=+1|\mathbf{Y})}{P(c^j[k]=-1|\mathbf{Y})} - \ln\frac{P(c^j[k]=+1)}{P(c^j[k]=-1)} \\
&= \frac{\sum_{X\in C_j^+} P(X[k]=X|\mathbf{Y})}{\sum_{X\in C_j^-} P(X[k]=X|\mathbf{Y})} - \lambda_2(c^j[k]) \\
&= \frac{\sum_{X\in C_j^+} \exp[-q(X)+\ln P(X)]}{\sum_{X\in C_j^-} \exp[-q(X)+\ln P(X)]} - \lambda_2(c^j[k]) \qquad (5.21)
\end{aligned}$$

where C_j^+ denotes the set of X where the jth polar code word is mapped to $+1$ and C_j^- is defined similarly. For BPSK, the above equation can be simplified as:

$$\lambda_1(c^j[k]) = \frac{\exp[-q(X=+1)+\ln P(X=+1)]}{\exp[-q(X=-1)+\ln P(X=-1)]} - \lambda_2(c^j[k])$$

The extrinsic *a posteriori* LLRs λ_2 are given by polar decoders from the previous iteration. Then, the extrinsic *a posteriori* LLRs λ_1 computed by EM demodulator are fed to the polar decoder, which in turns obtains the extrinsic LLRs λ_2, and gives to the MAP-EM demodulator iteratively. In such way, one turbo iteration can be completed. At the last turbo iteration, hard decision of information bits are computed and output by the polar decoder.

5.2.3.2 Initialization of MAP-EM demodulators :

The performance of MAP-EM highly depends on initial values of $\mathbf{X}^{(0)}$ and $\hat{\mathbf{h}}^{(0)}$. Except the first turbo iteration, $\mathbf{X}$ in (5.20) is simply taken as $\mathbf{X}^{(i)}$ from the previous iteration. Then, the mean value $\hat{\mathbf{h}}$ is updated based on (5.16). However, The initial value of $\hat{\mathbf{h}}^{(0)}$ is obtained by using the aid of pilots bore on transmitting OFDM symbols. In this section, the simplest LS channel estimation method is used to obtain $\hat{\mathbf{H}}$ and then FFT is applied to have the initial value of $\hat{\mathbf{h}}^{(-1)}$, which is given as follows:

$$\begin{aligned}\hat{\mathbf{H}}_{LS} &= \mathrm{int}[(\mathbf{X}_{pilot}^{-1}\mathbf{Y})^H] \\ \hat{\mathbf{h}}^{(0)} &= [\mathrm{FFT}(\hat{\mathbf{H}}_{LS})]_{L'_f\times 1}\end{aligned} \tag{5.22}$$

where int[ ] denotes the interpolation operation, and $[\mathbf{A}]_{L'_f\times 1}$ represents the first L'_f elements of $[\mathbf{A}]$. More details of the LS channel estimation can be found in [99]. After obtaining $\hat{\mathbf{h}}^{(0)}$, The $\mathbf{X}^{(0)}$ is demapped as:

$$\mathbf{X}^{(0)} = \mathrm{Demap}\{\mathrm{diag}(\mathbf{W}_f\hat{\mathbf{h}}^{(-1)})^H\mathbf{Y}\} \tag{5.23}$$

5.3 Simulation results

In this section, the BER performance comparison between the proposed turbo receiver and a separated processing receiver is implemented in frequency selective channels. In the simulation, the number of sub-carriers $Q = 256$, the length of polar code $N = 128$, OFDM symbols number $P = 10000$, and the rate of code $R = 0.75$. LS channel estimation is used to obtain the initial value of $\hat{\mathbf{h}}$. Furthermore, the number of iterations I_{turbo} for turbo receivers are variant while the number of iterations for MAP-EM demodulator I_{EM} equals to 4. BP, which is a soft input soft output (SISO) decoding, is used. The iteration T_{max} for BP is 20.

The BER performance among turbo receivers with variant I_{turbo} and that of the corresponding receiver without using the turbo receiving method is compared in Fig.5.8. It is illustrated that 1. turbo receivers are significantly helpful to improve the BER performance. It is shown that by using the proposed joint detection and decoding method, around 5dB gain can be achieved at probability 5×10^{-2}. 2. Increasing I_{turbo} is helpful to decrease the BER performance. 3. Using turbo receivers

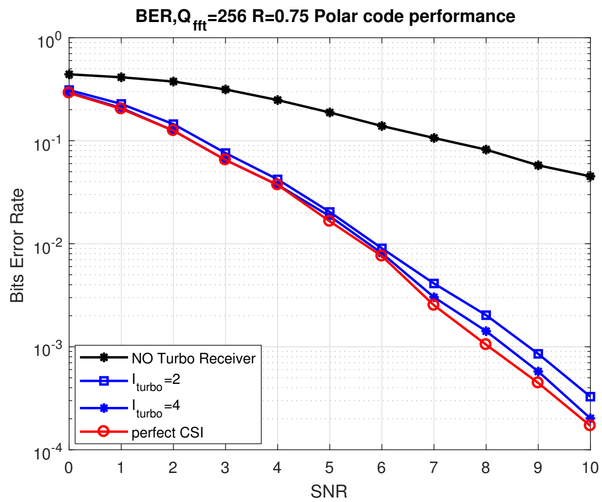

Fig. 5.8: BER performance between the polar-coded OFDM with and without turbo receivers with variant number of I_{turbo}

can obtain a similar BER performance as that of using the perfect CSI. 4. Although increasing I_{turbo} is helpful, the performance enhancement is gradually vanishing.

5.4 Summary

In this chapter, the author proposed two modified polar-code OFDM systems by including: 1. a channel compensator for polar decoding using in fading channels with noisy channel estimates. 2. a turbo receiver based on EM detectors and BP decoders.

First, a fading channel compensator $\boldsymbol{C}$ was proposed for BP polar decoding. It is assumed that an inaccurate channel estimate has been provided, and the variance of estimate errors is available. Using the variance σ_m^2, initial LLRs can be corrected and the corresponding BER performance can be noticeably enhanced. Simulation results reveal that by taking σ_m^2 into consideration, the SNR gain obtained by conventional BP reaches 1.5 dB without any rise in computational complexity.

Then, a novel turbo receiver for polar-coded OFDM was proposed to fight against the frequency selective fading. The turbo receiver iteratively exchanges the soft information between MAP-EM detectors and BP decoders. By utilizing these soft information, the BER performance of such system can be significantly improved.

Simulation results show that compared with the performance of separate implementation, the proposed turbo receiver can significantly improve the BER performance even without CSI. Moreover, by choosing appropriate iteration numbers, the performance given by turbo receivers is comparable to that of receivers with perfect channel estimation.

In next chapter, the author will introduce polar codes to OFDM-IM based systems to solve their high PAPR problems. The proposed scheme in next chapter utilizes polar codes to achieve PAPR reduction as well as error correction. Additionally, the author notes that all proposed techniques for polar-coded OFDM systems in this chapter can be utilized in the polar-coded OFDM-IM based systems proposed in the next chapter without significant modifications.

6 A SLM SCHEME FOR PAPR REDUCTION IN POLAR-CODED OFDM-IM SYSTEMS WITHOUT USING SIDE INFORMATION

6.1 Introduction

The OFDM-IM is a modified version of OFDM [69], which owns an interesting trade-off between energy efficiency and system performance from the adjustment of the number of active sub-carriers in the system. Therefore, the OFDM-IM has acted as one of the potential waveform formats of the 5G communication system [110]. Nevertheless, like the OFDM, as a multi-carrier modulation scheme, the OFDM-IM also faces its high PAPR, resulting in in-band and out-of-band distortion when it passes through high power amplifiers (HPAs) [61]. To reduce PAPR, several schemes have been proposed to address this problem. Conventional PAPR reduction methods can be classified into the following three categories [99]: 1. The limiting technology covers clipping and block-scaling methods, that directly clip the high power signal, which is straightforward but may cause distortions. 2. The scrambling method covers the SLM [123] and PTS [124] schemes, which can effectively reduce the PAPR. However, high complexity is a major problem. 3. Constructing a kind of code that owns PAPR reduction capability [125]. However, the construction of such codes for long length signals is very complicated. Beside the PAPR reduction, for a practical communication system, the error correction code is also an inevitable part, which is applied for errors control. By introducing such error correction codes to OFDM-IM systems, it is very interesting to investigate the PAPR reduction capability of such concatenated system.

In OFDM systems, some articles introduced existing error correction codes to deal with the PAPR reduction problem [126, 127]. Nevertheless, these papers only simply combined existing PAPR reduction schemes with error correction codes (e.g. Turbo codes). Therefore, it is worth to investigate whether there has a kind of scheme that owns the potentiality to have error correction and PAPR reduction capability, which helps the system skip the conventional PAPR reduction process. In [128], a concatenated coding scheme was proposed. In this scheme, RM codes, which reduces PAPR, and LDPC codes, which controls errors, are implemented in frequency and time domain, respectively. By using this kind of hybrid code, the PAPR can be reduced and the error control performance can be maintained. However, compared with the conventional LDPC code, the proposed method has BER degradation due to the introduction of the PAPR reduction coding scheme. Also, since the design of such PAPR reducing code is complicated, this method can be only used when the block length is short.

As the first capacity-achieving error correction code, polar coding [28] is considered as a mile stone in coding and information theory for its low complex encoding and decoding procedures. In November 2016, polar codes have acted as the channel coding scheme for the eMBB control channels of the 5G NR interface through 3GPP [55]. Recently, a new PAPR reduction scheme was proposed in polar-coded OFDM system [129]. In this method, random PAPR reduction bits are injected to original polar codes. These PAPR reduction bits that occupied the frozen bits positions are unknown for receiver thus these bits have to be decoded as information bits, which equivalent to increase the code rate. Hence, such method decreases PAPR by increasing the number of information bits, which compromises the error correction performance.

In is chapter, a novel SI free SLM scheme is proposed based on polar-coded OFDM-IM systems. The proposed method takes advantage of the unique properties of polar codes. It is observed that in the conventional polar encoder, frozen bits are commonly assigned as “0”. However, polar codes can reduce the PAPR of signals by randomly rotating these frozen bits. This scrambling procedure is similar to the SLM scheme. Compared with the conventional polar-coded OFDM-IM system, the proposed method effectively reduces the PAPR. Also, compared with polar codes concatenated SLM scheme in OFDM-IM systems (Polar-OFDM-IM), since the frozen bits are known by receivers and transmitters, polar decoding can be implemented directly without inverse phase rotation procedure required by the conventional SLM scheme, which decreases the latency at receivers. Simulation results reveal that the proposed novel SLM scheme based on polar codes can achieve the performance in PAPR reduction similar to that of the Polar-OFDM-IM scheme without compromising the error correction performance. Moreover, for conventional scrambling PAPR schemes (e.g.SLM, PTS), the SI, which indicates the index of the selected phase rotation factor, is an inevitable part. Losing these bits can cause an irrevocable decoding error. These important bits needs to be carefully protected, which compromises transmission efficiency. Many SI free schemes have been proposed to solve this problem [130, 131, 126, 132]. A common idea to avoid SI transmission is to introduce some PMs that can distinguish different phase rotation factors. In this chapter, we propose a novel receiver for the proposed SLM scheme without transmuting SI. This receiver takes advantage of SCL polar decoding scheme [45]. By using PM values caused by different frozen bits sets, the proposed receiver can correctly choose the frozen bits that the transmitted polar codeword used and decode the information bits without using SI. Simulation results show that the proposed receiver can achieve very close performance as that of the ideal case, where SI are perfectly received, in both AWGN and frequency selective channels.

6.2 Preliminary knowledge

6.2.1 The polar code and system model

Here, the author use the definition and terminologies of polar codes in last chapters by doing the following notations modifications: here, we define the length of codeword as N and the number of information bits is K. The $N-K$ length frozen bits are expressed as F_1^{N-K} with indicies set $\mathbf{A}^c$, where $\mathbf{A}$ is the indices set of information bits. A polar codeword $\mathbf{X}$ can be obtained by a matrix product:

$$\mathbf{X} = \mathbf{u}G_{2,\mathbf{A}}^{\bigotimes n} \oplus F_1^{N-K} G_{2,\mathbf{A}^c}^{\bigotimes n} \tag{6.1}$$

where $G_{2,\mathbf{A}}^{\bigotimes n}$ denotes the sub-matrix of $G_2^{\bigotimes n}$ formed by the rows with the indices in $\mathbf{A}$ and so does $G_{2,\mathbf{A}^c}^{\bigotimes n}$. "$\oplus$" denotes the mod 2 operation. We note that if the frozen bits F_1^{N-K} are all zero, denoting as: $\mathbf{F}_0$, the generation process can be simplified to:

$$\mathbf{X} = \mathbf{u}G_{2,\mathbf{A}}^{\bigotimes n} \tag{6.2}$$

Then, we consider an OFDM-IM transmission scheme given in the IM part of Fig.6.1. In this section, we only focus on index modulation part, the candidates generation part for PAPR reduction will be introduced in the next section. Here, a total of N length polar codewords $\mathbf{X}$ are divided by a bit splitter into G groups, each of which contains p bits, where $p = p_1 + p_2$. We assume the size of IFFT is N_{fft} and each group owns n available sub-carriers, thus $N_{fft} = Gn$. The first p_1 bits are used for IM, which selects k active sub-carriers from n available sub-carriers, thus the number of p_1 equals to $\lfloor \log_2 \mathbb{C}_n^k \rfloor$. The remaining p_2 bits are mapped to constellation symbols. Unlike the OFDM, in the OFDM-IM system, not all sub-carriers need to carry symbols, the information are carried by active sub-carriers and their indices. For OFDM-IM, the set that indicates the active sub-carriers is mapped from the G

Table 6.1: A Look-Up Table Example For $k = 2$, $n = 4$

Pattern	Bits **i**	Indices **I**
P_1	[0, 0]	[1, 3]
P_2	[0, 1]	[2, 4]
P_3	[1, 0]	[1, 4]
P_4	[1, 1]	[2, 3]

groups of p_1 bits, which is represented by

$$\mathbf{i} = \bigcup_{g=1}^{G} \mathbf{i}_g \Leftrightarrow \mathbf{I} = \bigcup_{g=1}^{G} \mathbf{I}_g \tag{6.3}$$

$$\mathbf{i}_g = [i[1], i[2], ..., i[p_1]], \ \ \mathbf{I}_g = [I[1], I[2], ..., I[k]] \tag{6.4}$$

where $i[\beta] \in \{0, 1\}$ is a bit for index selector, and $I[\eta] \in \{1, 2, ..., n\}$ denotes an active sub-carrier. For OFDM-IM, **i** and **I** is one-to-one mapping. "$\Leftrightarrow$" means a mapping relationship. For example, let assume a length-128 random polar codeword with BPSK modulation (N_{fft} is 128), and $G = 32$. In this case, n for each sub-block is 4 and $p = 4$. Then, if we decide to use 2 sub-carriers to transmit symbols (thus $k = 2$), the number of p_1 for IM should be $\lfloor \log_2 \mathbb{C}_4^2 \rfloor = 2$, and the rest $p_2 = 2$ bits needs to be mapped to BPSK symbols and modulated on 4 available sub-carriers. Hence, for the 1^{st} sub-block, the p_1 length random sequence $\mathbf{i}_1$ has four possible values $[0, 0], [0, 1], [1, 0], [1, 1]$. Then, the sequence $\mathbf{i}_1$ needs to be mapped to $\mathbf{I}_1$ in order to indicate which 2 out of 4 sub-carriers are active while the rest 2 sub-carriers will be idle. This mapping procedure can be implemented based on a look up table [69], which is shown in Table.6.1.

After index modulation using the first p_1 bits, the g^{th} OFDM sub-block can be denoted as:

$$\mathbf{S}_g = \begin{cases} S_g(\eta), & \eta \in \mathbf{I}_g \\ 0, & \text{otherwise} \end{cases} \tag{6.5}$$

where $S_g(\eta)$ is obtained from a constellation Θ for $\eta = 1, ..., k$. After concatenating

$\mathbf{S}_g$, the OFDM block $\mathbf{S}$ is transformed to time domain using the IFFT operations.

In the proposed polar code based SLM scheme, V candidates S_v with different PAPR are generated by polar codes. In the next section, the proposed SLM scheme will be given in detail. After IFFT, CP is inserted to the time domain signal $\mathbf{s}$. After digital to analog converter and HPA, the signal is transmitted over the channel. The transmission rate of an OFDM-IM is:

$$R = \frac{(p_1 + p_2)}{n} = G(\frac{\lfloor \log_2 \mathbb{C}_n^k \rfloor + k\log_2 M}{N_{fft}}) \tag{6.6}$$

where $\lfloor \ \rfloor$ is the floor function M is the order of constellation, and $\mathbb{C}$ is the combinatorial operation.

At the receiving side, after the removal of CP, a FFT operation needs to be applied on the received vector. Then, the received $\mathbf{y}$ is divided into G groups. The OFDM-IM receiver needs to detect both the indices of active sub-carriers and the corresponding data symbols. The optimal ML detector owns high complexity. To achieve near optimal performance, two low complex IM detectors (IMDs) are proposed, including the low complex ML and the LLR detection method [110]. The initial LLR values for polar decoding are constructed by two parts, the LLRs of indices bits, $\mathbf{LLR}_{id}$, and LLRs of transmitted bits, $\mathbf{LLR}_s$. We consider the estimated received indices bits sequence for each sub-block as

$$\mathbf{r}_{id,g} = [\hat{X}_{id,g}[1], \hat{X}_{id,g}[2], ..., \hat{X}_{id,g}[p_1]] \tag{6.7}$$

where $\hat{X}_{id,g}[\beta]$ is the estimated indices bits. Then, the initial LLR values for these indices bits can be represented as

$$\mathbf{LLR}_{id,g} = \frac{2\sqrt{E_b}}{\sigma_k^2}\mathbf{r}_{id,g} \tag{6.8}$$

where $\sqrt{E_b}$ is the energy per bit. It is assumed that the noise variance in the time domain is σ^2, which is related with the noise variance in the frequency domain via $\sigma_k^2 = (k/n)\sigma^2$ due to the normalization factor $\sqrt{(k/n)}$ of the FFT at the receiver [133]. In this section, the detail of such detector will not be introduced. Interested readers can refer to [69]. Then, the LLRs of the estimated received indices bits $\mathbf{LLR}_{id}$ and the corresponding received vector for transmitted bits $\mathbf{LLR}_s$ are combined together and send to a polar decoder.

6.3 The proposed polar code based SLM scheme for PAPR reduction

In general, frozen bits in a polar code are certain and usually zeros. Nevertheless, by rotating these frozen bits, more randomness can be introduced to a conventional polar code, presumably leading to a lower PAPR in OFDM systems. Also, by utilizing the PM provided by SCL polar decoder, the transmitted frozen bits vector can be correctly distinguished, thus the inefficient SI can be avoided. In this section, we propose a SLM scheme by introducing the transmitter and receiver, respectively.

6.3.1 The transmitter design

The proposed polar code based SLM scheme can be implanted in a conventional polar encoder, as illustrated in Fig.6.1.

In an OFDM-IM transmitter, first, information bits $\mathbf{u}$ should be transformed to a polar codeword $\mathbf{X}_0$ according to (6.1) using all zero frozen bits. In the proposed scheme, the transmitter generate a number of frozen bits sequence $\mathbf{F}_v$, for$v = 1, ..., V-1$, which are a set of length $N-K$ random vectors, expressed as:

$$\mathbf{F}_v \triangleq \{F_1^{N-K}\}_v = [F_v[1], F_v[2], ..., F_v[N-K]] \tag{6.9}$$

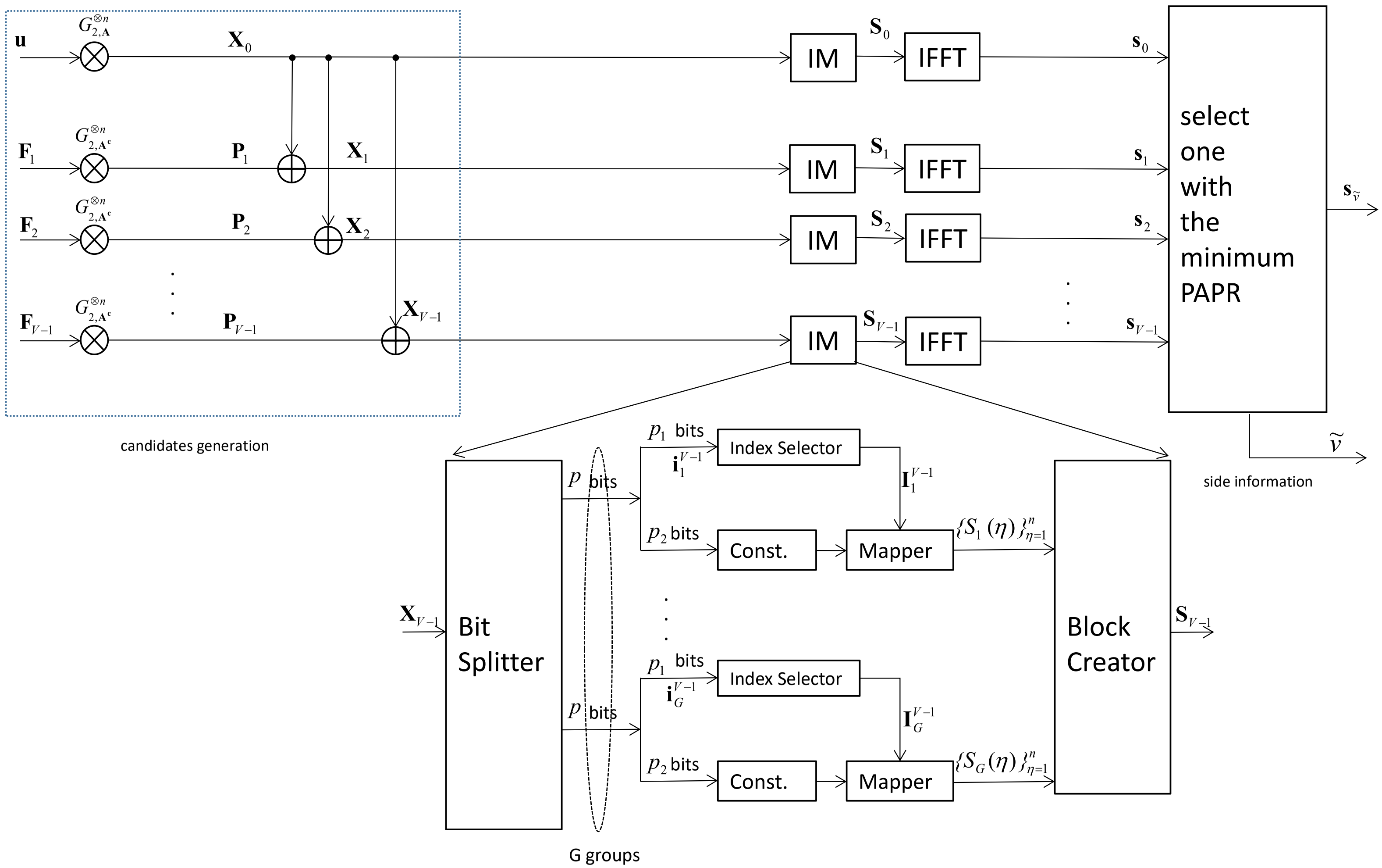

Fig. 6.1: Block diagram of the proposed polar code PAPR reduction scheme

where $F_v[j] \in \{0,1\}$, for $1 \le j \le N-K$. After matrix product using $G_{2,\mathbf{A}^c}^{\bigotimes n}$, a group of length N vectors $\mathbf{P}_v$ are obtained. In this section, we call these random frozen bits vectors as "phase rotation" vectors, which is inspired by the same terminology in the SLM scheme [123]. We note that the indices set $\mathbf{A}^c$ are predetermined, which are decided by polar encoding methods. More details regarding to polar codes construction algorithms can be found in [134].

After mod 2 operations "$\oplus$" with $\mathbf{X}_0$, polar codewords with different phase rotation vectors $\mathbf{P}_v$ result in a set of V modified input vectors $\mathbf{X}_v$ for $0 \le v \le V-1$, as:

$$\mathbf{X}_v = [X_v[1], X_v[2], ..., X_v[N]] \tag{6.10}$$

We note that the first candidate $\mathbf{X}_0$ equals to the polar codeword using all zeros frozen bits. Then, a set of polar coded vectors $\mathbf{X}_v$ go through IM part, including index modulation and constellation mapping. Then, the parallel modified symbol vectors $\mathbf{S}_v$ are transformed to time domain using V blocks of IFFT, yields:

$$\mathbf{s}_v = \mathrm{IFFT}[\mathbf{S}_v], \text{ for } v = 0, ..., V-1 \tag{6.11}$$

where $\mathbf{s}_v = [s_v[1], s_v[2], ..., s_v[N]]^T$ with components:

$$s_v[n] = \frac{1}{N}\sum_{k=1}^{N} S_v[k]e^{j2\pi kn/N} \tag{6.12}$$

for $n = 1, 2, .., N$. Then the system selects one candidate $\mathbf{s}_{\tilde{v}}$ which owns the minimum PAPR as:

$$\tilde{v} = \underset{0\le v\le V}{\mathrm{argmin}} \mathbf{PAPR}\{\mathbf{s}_v\} \tag{6.13}$$

to transmit. This PAPR reduction procedure can be regarded as a kind of SLM scheme based on polar codes. The definition of PAPR of candidate vectors $\mathbf{s}_v$ is defined as [93]:

$$\Gamma_{\mathbf{s}_v} = \text{PAPR}\{\mathbf{s}_v\} \triangleq \frac{\max\limits_{1\leq n\leq N} |\mathbf{s}_v[n]|^2}{P_{\mathbf{s}_v}} \tag{6.14}$$

where $P_{\mathbf{s}_v}$ denotes the average power of $\mathbf{s}_v$, which is calculated as:

$$P_{\mathbf{s}_v} = \frac{1}{N}E[\mathbf{s}_v^H \mathbf{s}_v] = \frac{1}{N}E[||\mathbf{s}_v||^2] \tag{6.15}$$

where $E[\,]$ denotes the expected value and the superscript H denotes the Hermitian transpose.

In the conventional scrambling PAPR reduction scheme (i.e. SLM or PTS), the transmitter should let the receiver know which phase rotation vector is applied. In other words, the index of $\tilde{v}$ should be transmitted as SI. The number of bits that should be transmitted is $\log_2 V$ for each data block. In the proposed polar code based SLM scheme, similar to the conventional SLM scheme, the transmitter also needs to send the index of $\tilde{v}$. Some researchers have proposed methods capable of avoiding SI transmission [135, 136]. However, it is assumed in this subsection that the receiver knows the table of phase rotation vectors in advance and the transmitter is required to send the $\log_2 V$ bits SI. The SI free method for the proposed PAPR reduction scheme will be introduced in the next subsection.

It is noteworthy that since the phase rotation $\mathbf{P}$ generation in Fig.6.1 can be implemented in advance, the proposed PAPR reduction method has the same complexity as the polar code concatenated SLM scheme at the transmitter. Also, because of the parallelism, the proposed polar code based SLM scheme owns almost the same latency as the polar coded OFDM-IM system. Note that advanced or low complex SLM schemes [61, 137] can also be easily applied on the proposed scheme, which provides more flexibility to our proposed method. On the receiving side, given in Fig.6.2, after obtaining the used frozen bits set index $\tilde{v}$ correctly, the proposed scheme directly decodes the received vector using the corresponding frozen bits $\mathbf{F}_{\tilde{v}}$ by regular polar decoding algorithms, such as SC [28], SCL [45], or BP [38]. Hence, compared with the conventional SLM concatenated polar coded OFDM system, the required inverse phase rotation procedure can be skipped, which reduces the complexity and latency on the receiving side.

6.3.2 The receiver design

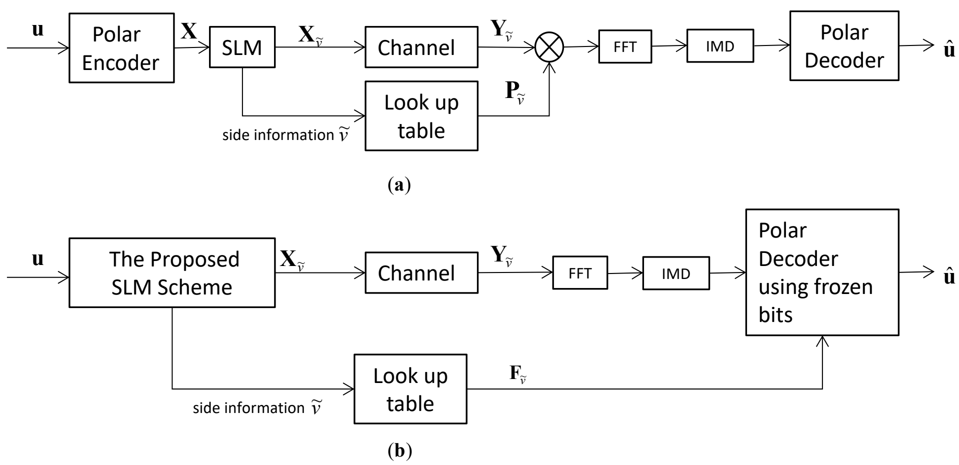

Fig. 6.2: Transceiver of (a).the Polar-SLM scheme. (b).the proposed scheme

In the conventional SLM PAPR reduction scheme. The SI needs to be transmitted to the receiver in order to obtain the used phase rotation vector $\mathbf{P}_{\tilde{v}}$. After the inverse operation by utilizing $\mathbf{P}_{\tilde{v}}$, the polar codeword can be decoded by regular polar decoding algorithms. In this subsection, we introduce a SI free receiver for the proposed SLM scheme, which is based on SCL polar decoders.

The block diagram of the SI receiver for the proposed SLM scheme is illustrated in Fig.6.3. At the receiver, after invoking the FFT demodulation operation, we denote the serial received signal, including the bits for IM, $\mathbf{r}$ as: $\mathbf{r} \triangleq r_1^N = [r[1], r[2], ..., r[N]]$.

We assume that the receiver has the table of all possible $\mathbf{F}_v$ with $0 \le v \le V-1$. First, the selected index $\tilde{v}$ needs to be confirmed. To solve this problem, the signal $\mathbf{r}$ is firstly decoded parallelly by a set of SCL polar decoders with different frozen bits set $\mathbf{F}_v$ with $0 \le v \le V-1$. We will show that the list size l at this round is good

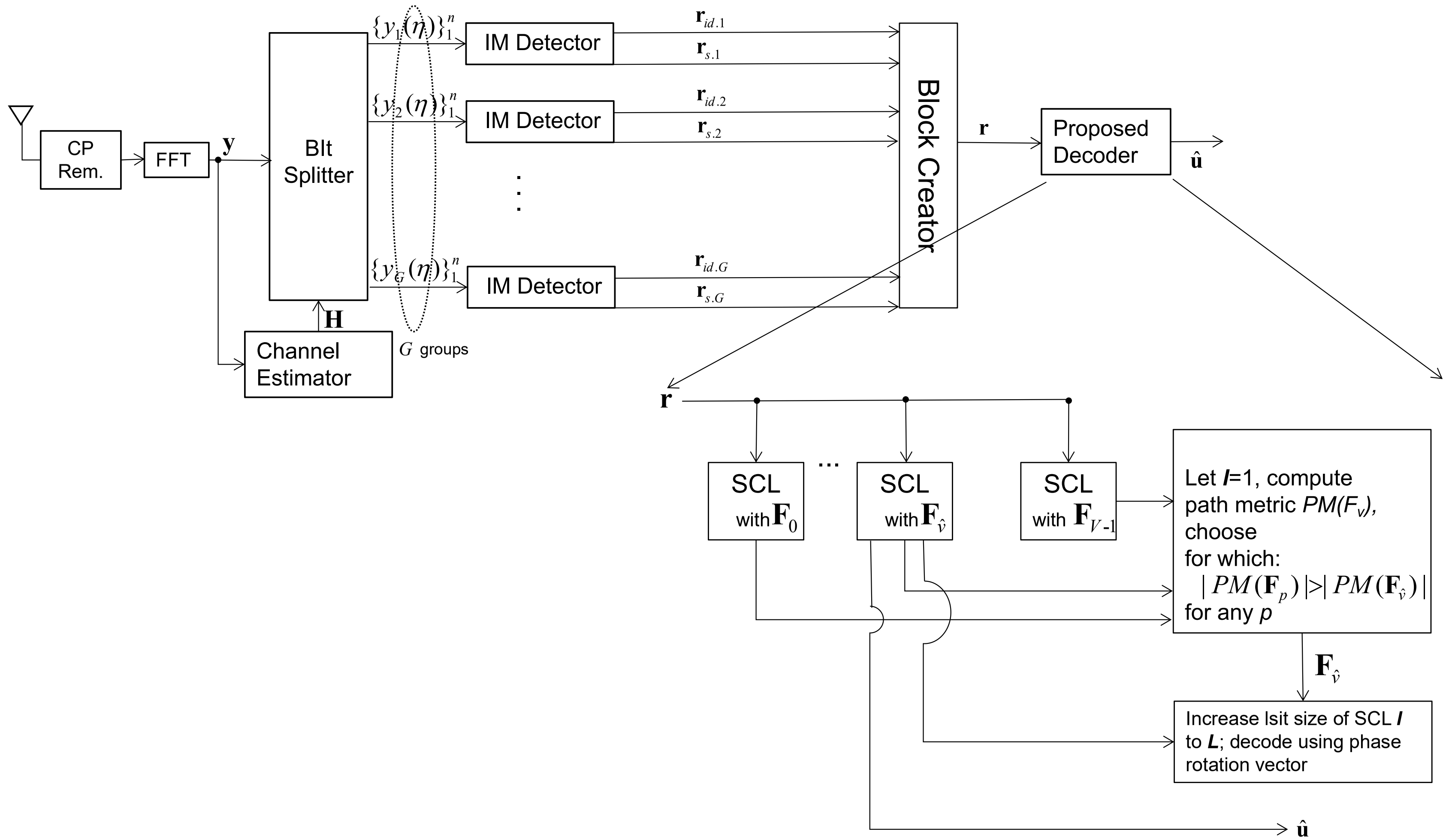

Fig. 6.3: Block diagram of the receiver for the proposed SLM scheme

to be set to 1 because by using larger size l, there has no significant difference on the accuracy of $\mathbf{F}_v$ detection but increasing corresponding computational complexity. Thus, to select the correct index $\tilde{v}$, $l = 1$ is enough. After the first round decoding, each SCL decoder using different $\mathbf{F}_v$ can obtain a unique PM value. Generally, the l^{th} PM for the i^{th} bit is calculated as:

$$PM_l^i = \begin{cases} PM_l^{(i-1)} \\ \text{if } i \in \mathbf{A} \text{ or } \mathbf{A}^c \text{ and } \hat{u}_l[i] = h(L[u_i]) \\ PM_l^{(i-1)} - |L[u_i]| \\ \text{if } i \in \mathbf{A} \text{ or } \mathbf{A}^c \text{ and } \hat{u}_l[i] \neq h(L[u_i]) \\ +\infty \\ \text{if } i \in \mathbf{A}^c \text{ and } h(L(u_i)) \neq P_v[i] \end{cases} \tag{6.16}$$

with $1 \leq l \leq L$ and $1 \leq i \leq N$, where L is the list size of a SCL decoder, $h(x) = \frac{1}{2}(1 - \text{sgn}(x))$, and

$$L[u_i] = \ln(\frac{P(u_i = 0|\mathbf{r}, \hat{u}_1^{i-1})}{P(u_i = 1|\mathbf{r}, \hat{u}_1^{i-1})}) \tag{6.17}$$

is the LLR of bit u_i calculated by the SCL decoding algorithm. More details of the SCL decoding method can be found in [45]. By using different $\mathbf{F}_v$, every SCL decoder owns different PM values. Here, the receiver selects the $\hat{v}^{th}$ decoder corresponding to $\mathbf{F}_{\hat{v}}$ so that:

$$|PM(\mathbf{F}_{\hat{v}})| < |PM(\mathbf{F}_p)| \text{ for any } p \tag{6.18}$$

where $0 \leq p \neq \hat{v} \leq V - 1$. Therefore, by using different PM values, the index of the used $\mathbf{F}_{\tilde{v}}$ can be found. We note that this unique PM value is caused by the pre-known positions of frozen bits and error propagation of SCL decoding. In other words, the proposed SI free scheme makes use of the structure of polar decoding schemes, so the conventional scrambling PAPR reduction (i.e. SLM or PTS) schemes without using polar codes cannot enjoy this advantage.

Table 6.2: Rate of Selecting Incorrect $\mathbf{F}_{\hat{v}}$ in Different Channels with $R = 0.5$

dB \ V	8(AWGN)	16(AWGN)	8(Fading)	16(Fading)
0.5	1.1×10^{-3}	2.4×10^{-3}	-	-
1.5	2.3×10^{-5}	4.2×10^{-5}	-	-
2.5	0	0	-	-
7	-	-	2.7×10^{-3}	3.6×10^{-3}
8	-	-	4.0×10^{-4}	4.8×10^{-4}
9	-	-	1.2×10^{-4}	2.0×10^{-4}

In Table.6.2, we show the rate of proposed SI receiver fails to find the correct $\mathbf{F}_{\tilde{v}}$. From the table, we can learn that the proposed receiver can effectively find the used $\mathbf{F}_{\tilde{v}}$ in different types of channels. The effectiveness of the proposed receiver can be partially explained by the error propagation effect of SC based decoding [79]. Here, we briefly introduce such effect starting from a review of SC decoding. We note that SCL can be regarded as a modified SC decoding with L-sized stack using PM in (6.16).

Then, the $\hat{v}^{th}$ SCL decoder increases the list size l to L, where L is a positive number ($L \geq 1$). This step is to guarantee the error correction performance. Therefore, the estimated information bits $\hat{\mathbf{u}}$ can be obtained through the $\hat{v}^{th}$ SCL decoder.

SC decoding is a type of sequent decoding. Hence, SC first computes an estimate of $u[1]$, denoted by $\hat{u}[1]$ based on only $\mathbf{r}$. Then, the SC starts to estimate $\hat{u}[2]$. Since $u[i]$, $i \in \mathbf{A}^c$ is known by receiver, thus the SC only needs to compute $\hat{u}[i]$, $i \in \mathbf{A}$. The hard decision of $\hat{u}[i]$ can be obtained from $h(L[u_i])$, and it can be calculated through a decoding graph which contains two types of nodes, f and g. Here, in Fig.6.4, we give an example of this graph for a $N = 8$ SC decoding, where $L_n^{(i)} \triangleq L[u_i]$. Each node has two input LLRs, denoted as L_1 and L_2, and the output LLR is written as L. The g block implements extra operation called as partial sum, denoted by u. The min-sum operation [79] for two types of rules are

$$f(L_1, L_2) = \text{sgn}(L_1)\text{sgn}(L_2)\min(|L_1|, |L_2|) \tag{6.19}$$

$$g(L_1, L_2, u) = (-1)^u L_1 + L_2 \tag{6.20}$$

The partial sum of stage $(s-1)$ can be obtained from the corresponding sum at stage s, where $1 \leq s \leq n$, written as

$$u_{s-1}^{(2i-1-[(i-1) \bmod 2^{s-1}])} = u_s^{(2i-1)} \oplus u_s^{(2i)} \tag{6.21}$$

$$u_{s-1}^{(2^{s-1}+2i-1-[(i-1) \bmod 2^{s-1}])} = u_s^{(2i)} \tag{6.22}$$

where $u_n^{(i)} \triangleq \hat{u}[i]$.

Since SC is a type of sequent decoding, erroneous bit decisions can be caused by the error propagation due to previous erroneous bit decisions. For example, we assume an all zero codeword with $\mathbf{A} = \{3, 4, 7, 8\}$ is transmitted and $\hat{u}[3]$ is determined erroneously. Then, if we assume that the two LLRs used for next bit calculation, namely $L_2^{(2)}$ and $L_2^{(6)}$ are larger than zero and $L_2^{(2)} > L_2^{(6)}$. By utilizing the g node update rule with $\hat{u}[3] = 1$, the result $L_2^{(6)} - L_2^{(6)}$ is smaller than 0, which leads to an erroneous decision. Since the proposed SI free decoder uses all possible $\mathbf{F}_v$, most frozen bits from decoders with incorrect $\mathbf{F}_v$ must be determined erroneously, which will cause serious error propagations. Hence, the PM values from the incorrect SCL decoders should be larger than that from the correct one. Therefore, our proposed SI free decoder is very likely to select the correct $\mathbf{F}_{\tilde{v}}$.

The average PM values of $L = 4$ SCL decoders with different $\mathbf{F}_v$ is shown in Fig.6.5 after 1000 trials. In this figure, we assume $V = 8$ and $\tilde{v} = 1$. From Fig.6.5, we know that the absolute PM values of SCL decoders with incorrect $\mathbf{F}_v$ is much larger than that of the decoder with correct $\mathbf{F}_{\tilde{v}}$ due to serious error propagations. Moreover, increasing the size l at the first stage has no significant impact to the

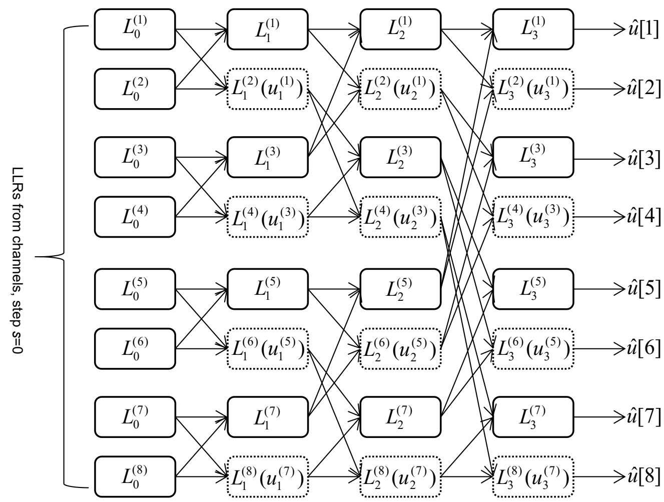

Fig. 6.4: Decoding graph of a SC for $N = 8$, the f and g nodes are rerpesented solid and dash blocks and in the parenthesis are the partial sums used by each g node

detection accuracy of $\mathbf{F}_{\tilde{v}}$. It is because for SCL decoding, adjacent candidates in the stack usually have only one or two bits difference, resulting in similar PM values. It is also verified in Fig.6.5 that the difference between candidates in one SCL decoder (i.e. decoder 1) is much smaller than that between different decoders (decoder 1 and 2).

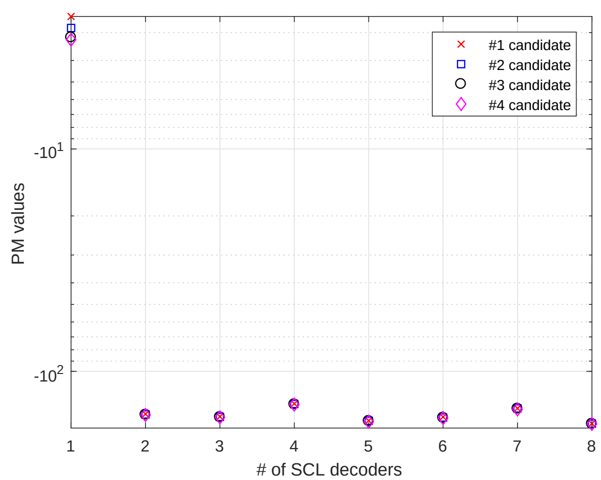

Fig. 6.5: Illustration of the average PM values of $L = 4$ SCL decoders with different $\mathbf{F}_v$

After selected the correct $\mathbf{F}_{\tilde{v}}$, the $\hat{v}^{th}$ SCL decoder increases the list size l to L, where L is a positive number ($L \geq 1$). This step is to guarantee the error correction performance. Therefore, the estimated information bits $\hat{\mathbf{u}}$ can be obtained through the $\hat{v}^{th}$ SCL decoder.

Then, we analyze the complexity of the proposed SLM scheme. In order to more intuitively reflect the complexity of our proposed scheme, we do a comparison between the proposed SLM and the conventional SLM scheme in polar-coded OFDM-IM system. The complexity comparison can be separated into two part: the transmitter side and the receiver side.

For the transmitting side, the proposed SLM scheme has similar computational complexity as that of the polar-coded SLM scheme in OFDM-IM systems. To generate V candidates, both schemes require V IFFT operations, which complexity is generalized to $O(VNlogN)$ [138]. On the receiving side, if we consider the ideal case where both schemes need transmit SI and the SI is perfectly received. The proposed SLM scheme based on polar codes have lower latency and computational complexity compared with the conventional one because the proposed SLM scheme does not require inverse phase rotation multiplications, which complexity is $O(N)$.

Additionally, compared with the conventional proposed system with SI and the PAPR reduction scheme in [129] using SCL decoding, it is obvious that the corresponding complexity of the proposed SI free receiver increased. On the one hand, for the conventional SCL decoding, the decoding complexity can be generalized to $O(LNlogN)$ [87]. On the other hand, the complexity of the proposed SI free receiver is roughly $O((V + L)NlogN)$. Nevertheless, since the proposed receiver is a parallel structure, the latency does not increase compared with the conventional receiver. Also, if the hardware resources is a main concern, this structure can also be flexibly modified to serial format at the cost of latency.

6.4 Simulation results

In the present section, some simulations are implemented and evaluated. First, simulation is conducted to compare the PAPR reduction performance of the proposed SLM scheme (expressed as "Proposed"), the novel PAPR reduction method in [129] (denoted as "Novel"), and the conventional SLM scheme (C-SLM). In the simulation, the phase rotation vectors are randomly selected from $\{0, 1\}$. The codeword length N is selected from 128 and 256. BPSK modulation is used. The impacts of the number of candidates V on the proposed scheme and C-SLM are compared. Also, even the results for the OFDM system without any PAPR reduction scheme (Unmod) is covered.

Subsequently, the BER performance of the proposed scheme, Novel scheme, polar-coded OFDM-IM, and that of the conventional SLM OFDM-IM scheme not using any error control coding are compared. In these simulations, the length of polar codes is $N = 128$, length-16 CP is used, the FFT size is 128, SC decoding [28] is used, and the AWGN channel is assumed.

Last, the performance of the proposed SI free receiver is compared and evaluated. In this section, we utilize simulations to compare the BER performance of the proposed SI free receiver and the proposed SLM scheme using SI. It is assumed that for the proposed SLM scheme with SI, those side information are always correctly received (denoted as Ideal). Also, the error correction performance of the proposed receiver using variant number of candidates V is also included. In our simulations, the codeword length is 128, $R = 0.5$, $L = 4$, and the cases in AWGN and frequency selective channels are considered and shown respectively.

The performance of any PAPR reduction scheme is usually ascertained by the complementary cumulative distributive function (CCDF) of its PAPR [139] since the PAPR of an OFDM signal can be considered as a random variable. The CCDF is defined as the probability that the PAPR of an OFDM block $\mathbf{s}$ exceeds a given threshold γ (usually given in decibels) [93], as:

$$\begin{aligned} F^c_{\Gamma_{\mathbf{s}}}(\gamma) &= 1 - F_{\Gamma_{\mathbf{s}}}(\gamma) \\ &= 1 - Pr[\text{PAPR}\{\mathbf{s}\} \leq \gamma] \\ &= Pr[\text{PAPR}\{\mathbf{s}\} > \gamma] \end{aligned} \tag{6.23}$$

where $F_{\Gamma_{\mathbf{s}}}(\gamma) = Pr[\Gamma_{\mathbf{s}} \leq \gamma]$ denotes the cumulative distributive function of $\Gamma_{\mathbf{s}}$.

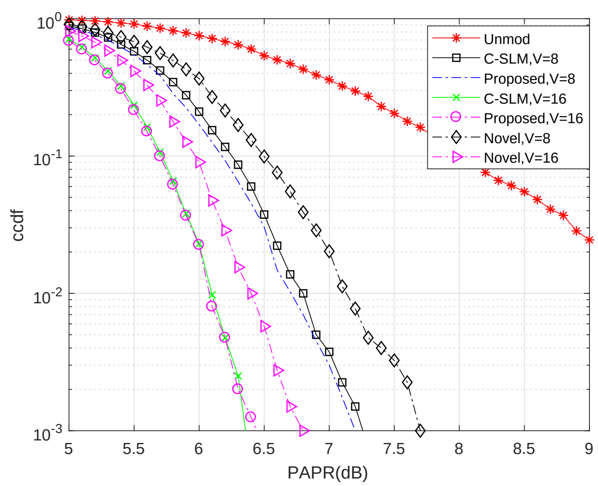

Fig. 6.6: Comparison of CCDFs for three PAPR reduction schemes, with 8 and 16 candidates for N=128

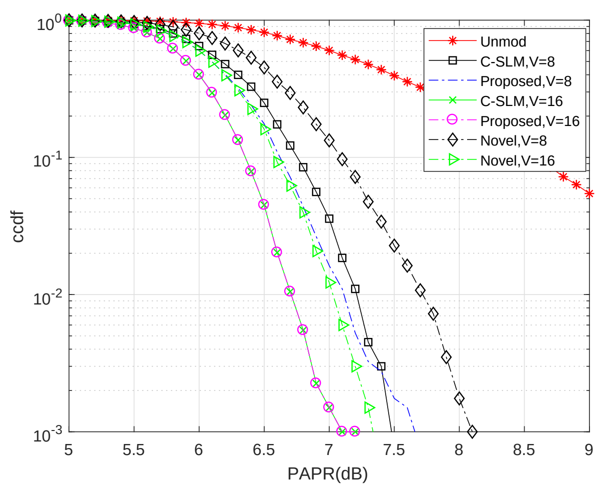

Fig. 6.7: Comparison of CCDFs for three PAPR reduction schemes, with 8 and 16 candidates for N=256

The PAPR reduction performance of the proposed scheme and the C-SLM scheme is presented in Fig.6.6 and Fig.6.7, using different candidates number V ($V \in \{8, 16\}$) when $N = 128$ and $N = 256$, respectively. In these simulations, the code rate is 0.5. Moreover, as a reference the Novel PAPR reduction performance of the method in [129] is also included. We can see that all schemes exhibit prominent PAPR reduction capability. As long as the phase sequences are carefully designed, the C-SLM is theoretically expected to perform at least the same PAPR performance as the proposed scheme. However, based on the simulation results, we surprisingly found that given in Fig.6.6 and Fig.6.7, when the parameter V is small, our proposed scheme can achieve even better PAPR reduction than that of the C-SLM. It is because for the proposed OFDM-IM based system, the random frozen bits $\mathbf{F}_v$ not only affect the transmitted signal but also changes the bits for IM, which indirectly affect the distribution of the active sub-carriers. This can be regarded as an extra benefit only enjoyed by OFDM-IM, and this operation is equivalent to a set of interleavers which is helpful for PAPR reduction while this benefit will be vanished with the increase of candidates [93]. Then, compared with the "Novel" scheme which treats a small part of frozen bits as information to reduce PAPR, our proposed scheme takes advantage of all frozen bits, resulting in better PAPR reduction performance. Also, as seen, the increase of candidate number helps obtain a better PAPR reduction performance. Further, we can expect that the code rate will affect the PAPR reduction capability of the proposed SLM scheme, it is because that when the code rate is high, the number of available frozen bits is small, which introduce less randomness to the candidate sequences (assume that the code rate is 1, there is no position for frozen bit). However, a very high code rate for polar codes is not practical in real communication systems. Moreover, it is suggested in the next subsection that apart from the competitive PAPR reduction performance, the proposed scheme owns the same BER performance as that of the SLM concatenated polar-coded OFDM-IM system (Polar-OFDM-IM).

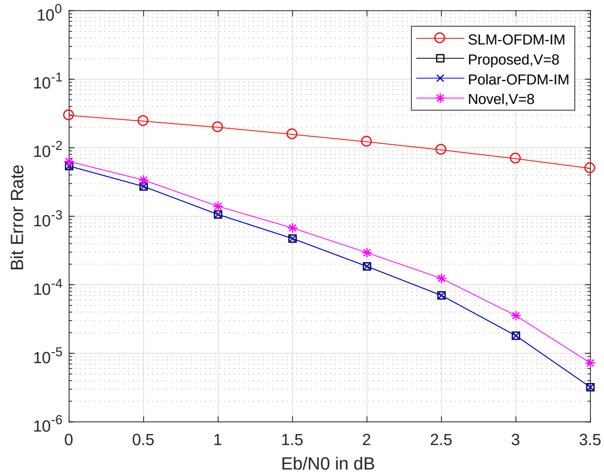

Fig. 6.8: Comparison of the BER performance of the proposed scheme, Novel scheme, Polar-OFDM-IM, and C-SLM (SLM-OFDM-IM) in an AWGN channel

The BER among the proposed PAPR reduction scheme, the "Novel" scheme, the SLM-OFDM-IM (no channel coding is used), and the Polar-OFDM-IM system is illustrated in Fig.6.8. For all compared schemes, for simplicity, perfect SI receiving is assumed. For the proposed and "Novel" scheme, we assume code rate equals to 0.5 and $V = 8$. After obtaining the SI, for the proposed scheme, the receiver decodes information bits using the estimated frozen bits $\mathbf{F}_{\hat{v}}$. For the "Novel" scheme, the bits that are occupied the frozen positions used for PAPR reduction is treated as information bits and decoded together with messages, which equivalent to code rate increase. First, it is shown that compared with the pure polar-coded SLM scheme in OFDM-IM system, the proposed system has the same performance and lower receiving complexity, which is shown in Fig.6.2. Second, it is suggested that due to the error correction property of polar codes, the proposed scheme achieves significant gain than that of the C-SLM scheme in OFDM-IM systems, which exhibits no capability of the error control. Last, the proposed SLM scheme achieves better BER performance than that of the "Novel" scheme with the same number of candidates. Therefore, the proposed SLM scheme based on polar codes combines two advantages (error correction and PAPR reduction) that are required in OFDM-IM systems with lower complexity.

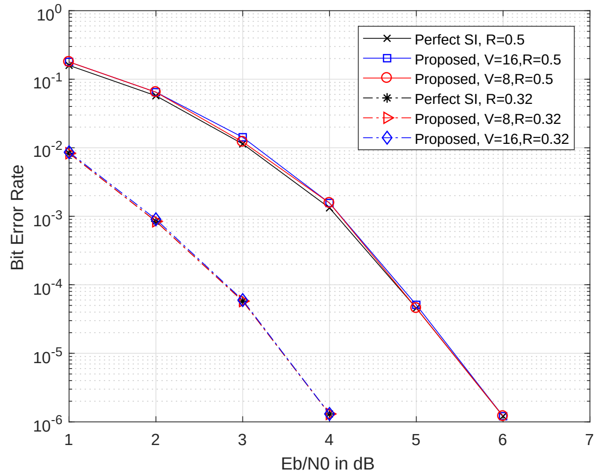

Fig. 6.9: Comparison of the BER performance between the proposed and ideal receivers using variant V in AWGN channels

Fig.6.9 illustrates the BER performance between the proposed SLM schemes utilizing the SI free receiver (denoted as Proposed) and utilizing the conventional receiver with perfect SI (denoted as Ideal) in AWGN channels. As seen, the proposed SI free receiver can achieve a very close BER performance as that of the ideal case. It is shown that in Fig.6.9, in high SNR scenario, the gap between the proposed SI free scheme and the ideal case is negligible. Further, we know that for the conventional SLM scheme, increasing the number of candidates V can enhance the PAPR performance but does not influence the performance of error correction. However, for our proposed receiver, increasing the number of candidates V may cause error performance degradation because the distance (i.e Euclidean distance) among each candidate is closer, which result closer PM values that are used to distinguish the possible $\mathbf{F}_v$. How to optimize this trade-off can be regarded as an open topic for future research. In this section, to partially solve this problem, we can decrease the rate of polar codes, which introduces more randomness to the candidates. From Fig.6.9, we can see that for low code rate (0.32), the BER degradation is almost vanished. For medium code rate (0.5), the BER degradation is still acceptable. We note that a low to mid code rate is practical for polar codes because high code rate will cause serious performance degradation, which makes channel coding ineffective.

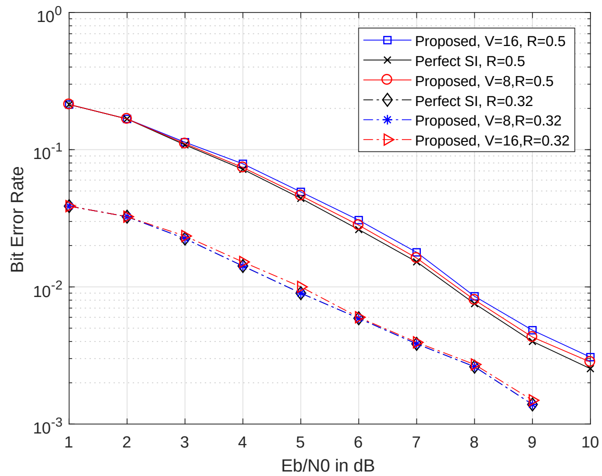

Fig. 6.10: Comparison of the BER performance between the proposed and ideal receivers using variant V in frequency selective channels

Fig.6.10 illustrates the BER performance between the proposed SLM schemes using the SI free receiver,and the perfect SI in frequency selective channels. In each transmit block, a length-16 CP is used and the maximum delay spread of the channel is 8. As seen, our proposed SI free receiver has more degradation in frequency selective channels compared with the ideal case in terms of BER performance than that in AWGN channels. It is illustrated in Table.6.2 that for the proposed receiver, the rate of selecting incorrect $\mathbf{F}_v$ in frequency selective channels is much higher than that in AWGN channels, resulting in more burst errors. Fig.6.10 shows that by using polar codes with rate 0.5, the proposed receiver has around 0.1dB gap compared with the ideal case at probability 1×10^{-2}. However, it is still a close performance compared with the ideal case. Also, similar to the case in AWGN channels, the increase of V compromises the error performance, and this gap can be mitigated by decreasing the code rate.

6.5 Summary

In this chapter, we proposed a novel SLM scheme based on polar codes for PAPR reduction in OFDM-IM systems. Moreover, for transmission efficiency, we also proposed a corresponding receiver without using side information for the proposed SLM scheme. First, for the proposed SLM scheme itself, the problem of high PAPR in OFDM systems can be solved by rotating frozen bits of a Polar code. This method does not require separate PAPR reduction blocks. Besides, as an error correction code, the Polar code can also achieve impressive error correction performance. According to simulation results, the proposed SLM scheme can achieve the performance close to that of the SLM scheme. In the meantime, compared with the Polar code concatenated SLM scheme, the proposed scheme does not compromise the error correction capability with lower complexity on the receiving side. Using the proposed SLM scheme based on Polar codes, the PAPR reduction and error control can be solved jointly. Second, for the proposed receiver, by utilizing a set of parallel SCL decoders, no side information is required when using the proposed SLM scheme. Simulation results show that compared with the ideal receiver, which perfectly obtains the side information, our proposed receiver can achieve a very close BER performance. Moreover, this advantage can be also kept in frequency selective channels. The computational complexity reduction for our proposed receiver can be seen as a future topic for investigation.

In next chapter, the author will propose a general design guideline for polar-coded OFDM-I/Q-IM systems, which can achieve better error performance than that of the conventional polar-coded OFDM.

7 POLAR-CODED OFDM WITH INDEX MODULATION

7.1 Introduction

Polar codes, introduced by Arikan in 2009 [28], can achieve symmetric capacity of B-DMC for the input letters with equal probability. In some scenarios, it has been shown that the bit-error-rate (BER) performance of polar codes can be similar to that of turbo or LDPC codes with lower complexity by utilizing SCL decoding scheme [87]. Furthermore, the polar codes aided by CRC can achieve even better performance than other channel coding schemes [50]. For these reasons, polar coding has been adopted to the 5G NR interface by the 3GPP [55].

Beside applying polar coding, to meet the requirements of the next generation of high-speed wireless communication networks, also new waveform formats have been proposed. The OFDM-IM is a modified version of OFDM by extending the concept of SM to the frequency domain. The idea of OFDM-IM was firstly proposed in [69], and an overview of this technique can be found in [70, 140]. Compared with the conventional OFDM, OFDM-IM offers a trade-off between energy efficiency and system performance with the adjustment of the number of active sub-carriers in the system [68]. Hence, OFDM-IM is suitable for some businesses in next generation communication networks. Since OFDM-IM has unique advantages, as an extended version of OFDM, it is also considered as a promising candidate for 5G [110]. However, OFDM-IM performs weaker than OFDM in low SNR [69]. Hence, some modified OFDM-IM schemes with better performance have been proposed. In [133], the number of active sub-carriers was adaptive, which increased the SE of OFDM-IM. In [67], interleavers were adopted to enhance the performance of OFDM-IM at the cost of higher latency. In [68] and [141], two methods with higher diversity gain were introduced, which significantly improved the performance of OFDM-IM while reducing

SE. In [112], OFDM-I/Q-IM, which can be considered as a generalized OFDM-IM, was proposed. Compared with the conventional technique, OFDM-I/Q-IM not only has higher SE but also achieves better BER performance. Hence, OFDM-I/Q-IM can be considered as a promising candidate for the next generation of high-speed wireless communication networks.

The application of polar codes in conventional OFDM systems has been discussed in [142]. It has been shown the design of a polar-coded OFDM system is very straight forward. However, a major drawback of polar-coded OFDM systems is that increasing the transmission rate in these systems leads to substantial performance degradation [143]. Because of some advantages of OFDM with index modulation, it seems intuitively that polar-coded OFDM-IM or polar-coded OFDM-I/Q-IM systems can outperform their OFDM counterpart. However, combining polar codes with any type of OFDM-IM is a challenging problem, whereas the design of polar-coded OFDM is very straightforward. It is shown that the idea of applying polar codes in the conventional OFDM-IM scheme [69, 144, 145, 146] is limited to the case in which a BPSK modulator is employed as a symbol mapper; while, in practice, the design of most systems is based on higher order modulations to reach higher spectral efficiency. Hence, in this chapter, we focus on OFDM-I/Q-IM since it has more flexibility in the allocation of bits in a polar-coded system and also better performance compared to OFDM-IM. We try to provide a general design guideline for polar-coded OFDM-I/Q-IM.

Application of polar codes in OFDM-I/Q-IM systems presents new challenges, and dealing with these is the main focus of this section. One of the challenges is to combine polar coding with restricted length with OFDM-I/Q-IM modulators employing different constellations symbols. The other challenge is to include the *a posteriori* information provided by the index detector for polar decoding to take further advantage of the structure signaling. Hence, in order to propose a polar-coded OFDM-IM system, the following step will be taken:

- In the proposed system, at the transmitter, in order to make the polar code compatible with OFDM-I/Q-IM, we employ a random frozen bits appending scheme. In the design of polar-coded OFDM-I/Q-IM, this novel scheme not only helps us to make the polar code compatible with OFDM-I/Q-IM but also improves the BER performance of the system.

- At the receiver, the channel detectors, based on the received signal and the a priori information, provide soft information for both the index detector and the polar decoder. Next, the index detector produces the *a posteriori* information for the index bits, by utilizing the information from the channel detectors and the lookup tables for mapping. Then, the information provided by the index detector is fed to the polar decoder. Finally, the proposed polar decoder, which is based on the belief propagation (BP) algorithm, computes the *a posteriori* information for the information bits based on the code constraints, the input information given by the channel detectors and utilizing the information provided by the index detector.

The remainer of this chapter is organized as follows. Section 7.2 gives the preliminary knowledge, which is the background of OFDM-I/Q-IM. We give the proposed polar-coded OFDM-I/Q-IM system in section 7.3 by introducing its transmitter and receiver, respectively. Simulation results of the proposed system are presented and evaluated in section 7.4. The summary of this chapter is given in section 7.5.

7.1.1 OFDM with in-phase/quadrature index modulation

By independently implementing index modulation on the in-phase and quadrature components of OFDM signals, OFDM-I/Q-IM achieves more transmit diversity than conventional OFDM-IM. Moreover, thanks to the higher SE, OFDM-I/Q-IM is able to transmit polar-coded signals, which may have restricted length and variant constellations. Hence, in this chapter, we apply OFDM-I/Q-IM to the proposed system to achieve better performance and flexibility. This sub-section gives a brief introduction on OFDM-I/Q-IM.

The block diagram of an OFDM-I/Q-IM transmitter is given in Fig.7.1.(a). For OFDM-I/Q-IM, the available number of sub-carriers is denoted as: N_{fft}. First, m information bits U_1^m are divided into $2G$ groups, each of which has p bits, thus $m = 2Gp$. Each group of p bits are sent to an OFDM-I/Q-IM modulator to generate an in-phase or quadrature component of an OFDM sub-block with n available sub-carriers, where $n = N_{fft}/G$. Unlike conventional OFDM-IM that maps a complex symbol to an available sub-carrier, OFDM-I/Q-IM implements index modulation on in-phase and quadrature dimensions separately. The p bits of an OFDM-I/Q-IM sub-block are divided into two parts: the first p_1 bits are used for index modulation, and the remaining p_2 bits are mapped to constellations on in-phase or quadrature dimension. Let take the first p bits on in-phase dimension as an example, the p_1 bits $\mathbf{i}_1^I = [i_1^I(1), ..., i_1^I(p_1)]$, where $i_1^I(\alpha) \in \{0, 1\}$, are sent to an index selector to generate an indices indicator $\mathbf{I}_1^I$, which indicates to activate k sub-carriers out of n available ones, while the rest of $n - k$ sub-carriers are null. For the g^{th} $(1 \leq g \leq G)$ sub-block, the indices of k active sub-carriers in the in-phase and quadrature dimensions are denoted as:

$$\mathbf{I}_g^I = [I_g^I(1), ..., I_g^I(k)],\ \mathbf{I}_g^Q = [I_g^Q(1), ..., I_g^Q(k)] \tag{7.1}$$

where $I_g^I(\gamma), I_g^Q(\gamma) \in \{1, ..., n\}$ for $\gamma = 1, ..., k$. The indices selection is implemented by using the look-up table or combinational methods [69]. Then, based on the first p_1 bits of $\mathbf{i}_g$, the remaining p_2 bits are mapped to M-PAM symbols in in-phase/quadrature dimensions. After index modulation using the first p_1 bits, the in-phase/quadrature part of the g^{th} OFDM sub-block can be denoted as:

$$\mathbf{S}_g^I = \begin{cases} S_g^I(\eta), & \eta \in \mathbf{I}_g^I \\ 0, & \text{otherwise} \end{cases}, \mathbf{S}_g^Q = \begin{cases} S_g^Q(\eta), & \eta \in \mathbf{I}_g^Q \\ 0, & \text{otherwise} \end{cases} \tag{7.2}$$

where $S_g^I(\eta)$ and $S_g^Q(\eta)$ are independently obtained from a M-PAM constellation Θ for $\eta = 1, ..., n$. Then, the in-phase/quadrature parts in (7.2) are combined to generate a complex OFDM sub-block:

$$\mathbf{S}_g = \mathbf{S}_g^I + j\mathbf{S}_g^Q,\ g = 1, 2, ...G. \tag{7.3}$$

An OFDM-I/Q-IM encoder with $n = 4$, $k = 2$ using Table.7.1 is given in Fig.7.1.(b). In this example, if the first p_1 bits is $[0, 1]$, then the symbols $S(1)$ and $S(2)$ generated by the p_2 bits should occupy the 2^{nd} and 4^{th} sub-carriers while the rest ones are idle.

After concatenating $\mathbf{S}_g$, the OFDM block is transformed to time domain by using N_{fft} points IFFT. After P/S converter and CP insertion. The vector is sent to a frequency selective channel. The transmission rate of the OFDM-I/Q-IM is:

$$R = \frac{2(p_1 + p_2)}{n} = 2G(\frac{\lfloor \log_2 \mathbb{C}_n^k \rfloor + k\log_2 M}{N_{fft}}) \tag{7.4}$$

where $\lfloor\ \rfloor$ is the floor function and $\mathbb{C}$ is the combinatorial operation.

At the receiver, after the removal of CP, a FFT operation needs to be implemented. The OFDM-I/Q-IM receiver needs to detect both the indices of active sub-carriers and the corresponding data symbols. For each sub-block, by considering a joint detection for the indices of active sub-carriers and the transmitted symbols carried on, the ML detector for OFDM-I/Q-IM is given by [112]:

$$\{\hat{S}_g(\eta)\}_{\eta=1}^n = \underset{\{S_g(\eta)\}_{\eta=1}^n}{\operatorname{argmin}} \sum_{\eta=1}^{n} |y_g(\eta) - H_g(\eta)S_g(\eta)|^2 \tag{7.5}$$

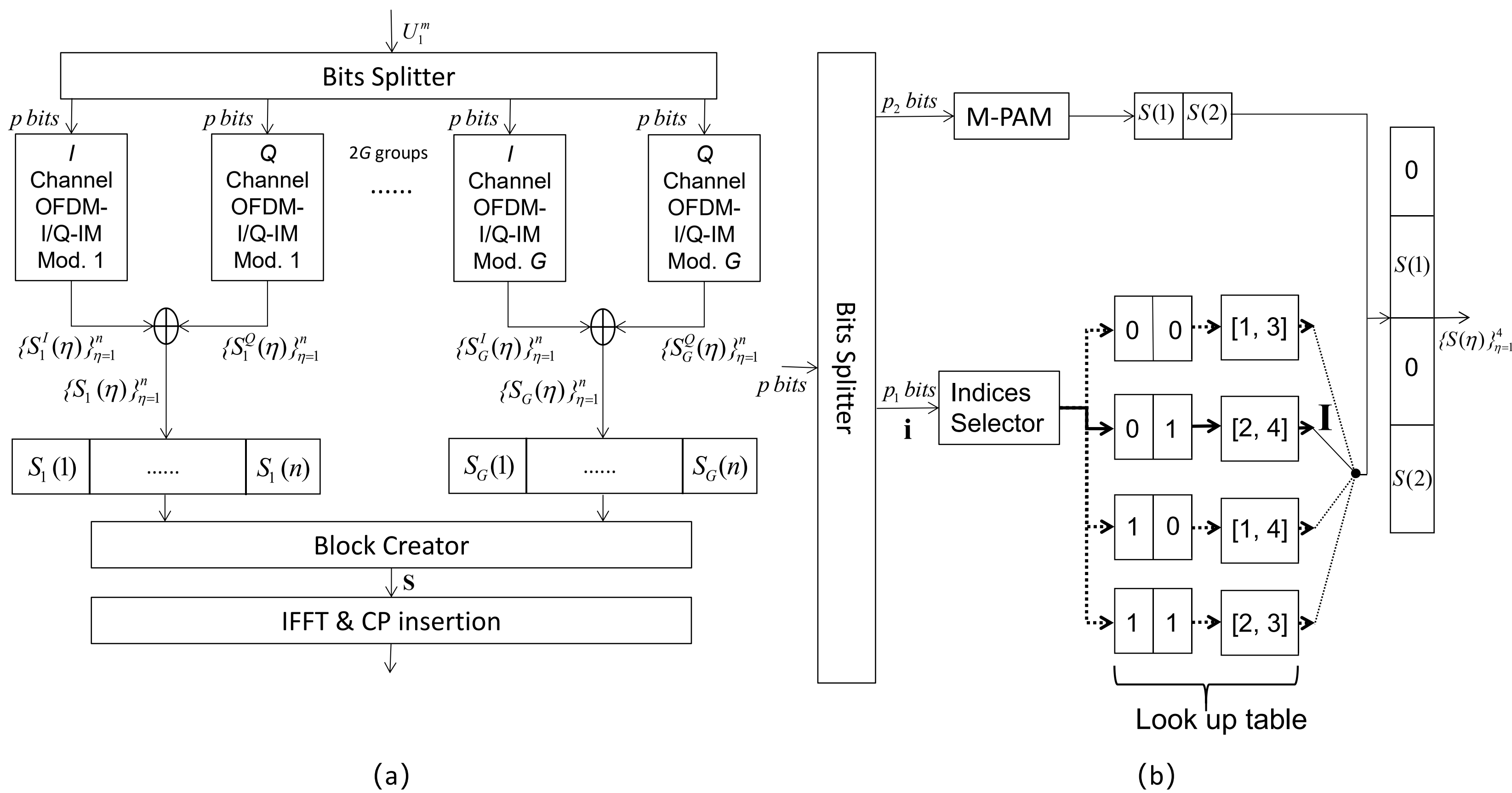

Fig. 7.1: System model of (a).an OFDM-I/Q-IM transmitter (b). an example of an OFDM-I/Q-IM modulator for $n = 4$, $k = 2$

where $H_g(\eta)$ denotes the channel frequency response (CFR) on the η^{th} sub-carrier of the g^{th} sub-block. More details for ML decoding in OFDM-I/Q-IM can be found in [112]. The searching space of the ML detection per bit is given by the order of $O(\binom{n}{k} + M^k)$ [147]. Hence the optimal ML detector has high complexity. To achieve near optimal performance, two low-complex detectors have been proposed, including the low-complex ML and the *a posteriori* probability detection methods [110]. In this chapter, the *a posteriori* probability detection method is used and the corresponding process will be introduced in the next section. The OFDM-I/Q-IM can obtain around 4-6 dB performance gains in mid-high SNR compared with the conventional OFDM scheme [112].

7.2 The proposed polar coded OFDM-I/Q-IM system

The powerful polar codes allow us to achieve channel capacity performance. In this section, the polar-coded OFDM-I/Q-IM is proposed, and the design guideline of the system is introduced in terms of the transmitter and receiver, respectively.

7.2.1 The transmitter design

Block diagram of the proposed polar-coded OFDM-I/Q-IM transmitter is given in Fig.7.2. The system aims to transmit m-bits message U_1^m. These bits are processed by a polar encoder to have a length N codeword X_1^N. Then, they are divided into $2G$ groups, each of which contains b bits. These b bits need to be further divided into two parts, which contain b_1 and b_2 bits for index modulation and constellation mapping, respectively.

We note that the amount of bits carried by a pure OFDM-I/Q-IM must be $2G(k\log_2 M + \lfloor \log_2 \mathbb{C}_n^k \rfloor)$, which is not always equal to the length of a polar code (We note that although in some works, polar codes can be constructed with variant length [148, 149], these methods suffered performance degradation.). Therefore,

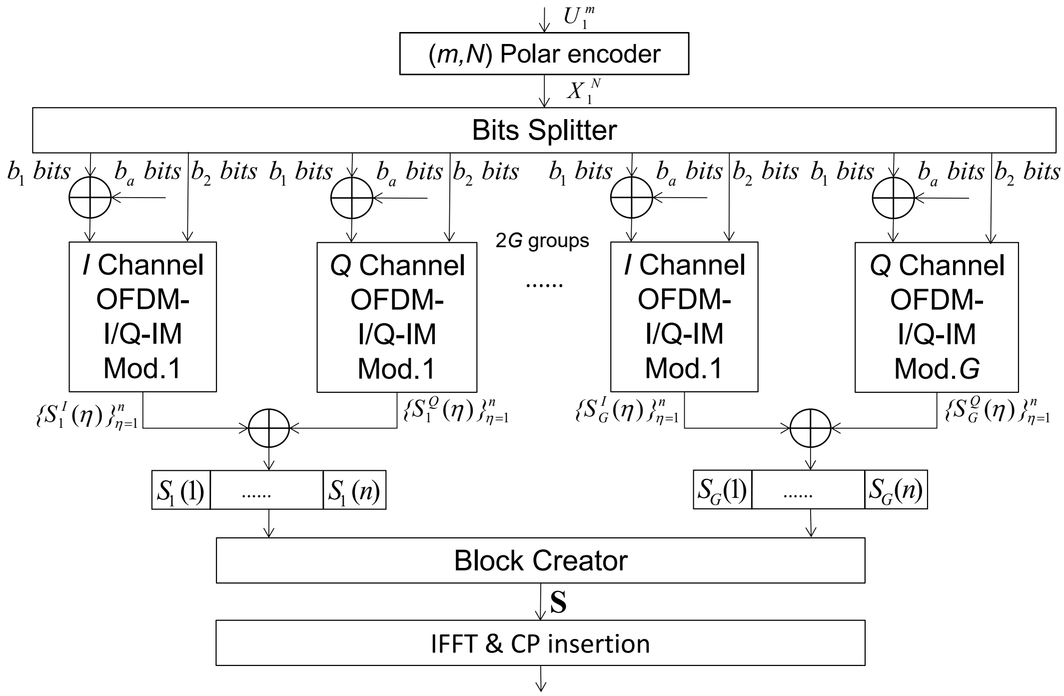

Fig. 7.2: Block diagram of the proposed polar-coded OFDM-I/Q-IM transmitter

compared with a pure OFDM-I/Q-IM, when applying polar coding, the selection of b_1 and b_2 have to be carefully implemented when splitting bits. For a polar-coded OFDM-I/Q-IM, the available b_1 and b_2 needs to be selected based on the following rule:

$$G(b_1 + b_2) \geq k\log_2^M + \lfloor \log_2 \mathbb{C}_n^k \rfloor \tag{7.6}$$

Proof: first, we assume the length of a polar code is 2^v, thus $G(b_1 + b_2) = 2^{v-1}$. Then, since each b_2 bits need to be modulated by M-PAM, we have $\frac{2^{v-1}}{G} - b_1 = k\log_2 M$. Moreover, the first group of b_1 bits are required for index modulation. In a pure OFDM-I/Q-IM system, b_1 is required to be exactly equal to $\lfloor \log_2 \mathbb{C}_n^k \rfloor$. Nevertheless, as long as $b_1 \leq \lfloor \log_2 \mathbb{C}_n^k \rfloor$, the b_2 bits can be successfully used for index modulation. Therefore, we use this loose constraint in the proposed polar-coded OFDM-I/Q-IM. Combining the above three conditions, we can obtain (7.6). For an example, considering a length $N = 128$, $N_{fft} = 64$, and 4-QAM polar-coded OFDM-I/Q-IM system. If $G = 16$, we can set $b_1 = b_2 = 2$ bits, $n = 4$, and $k = 2$. In such

Table 7.1: A Look-Up Table Example For $k = 2$, $n = 4$, $p_1 = 2$

Pattern	Bits $\mathbf{i}$	Indices $\mathbf{I}$
P_1	[0, 0]	[1, 3]
P_2	[0, 1]	[2, 4]
P_3	[1, 0]	[1, 4]
P_4	[1, 1]	[2, 3]

scenario, the value b_1 for index modulation is exactly equivalent to p_1 that is used in pure OFDM-I/Q-IM systems, and Table.7.1 can be used.

However, considering a pure OFDM-I/Q-IM case with $G = 8$, thus $n = 8$, if we set $k = 6$, the corresponding p_1 should be 4 bits. However, since the length of polar code is $N = 128$, for a 4-QAM system, the amount of available bits for index modulation is only 32, thus b_1 has to be 2 bits, resulting in b_1 ¡ p_1. To activate 6 out of 8 available sub-carriers with less bits, instead of all 16 patterns, only 4 sub-carrier activation patterns (SAPs) can be selected, which is shown in Table.7.2. However, to maintain the compatibility of OFDM-I/Q-IM with polar codes, in this chapter, we propose a scheme that appends $b_a = p_1 - b_1$ random frozen bits $\mathbf{U}_f$ at the end of the original b_1 length index vector. We take a 2-bit-length vector $\mathbf{i}^I = [i^I(1), i^I(2)]$ in the in-phase dimension as an example. To align with the pure OFDM-I/Q-IM that requires 4 bits for IM, two frozen bits needs to be appended at the end of $\mathbf{i}^I$, given by:

$$\mathbf{i}^I = [i^I(1), i^I(2), U_f(\zeta), U_f(\zeta + 1)] \tag{7.7}$$

where $U_f(\zeta) \in \{0, 1\}$ is the ζ^{th} frozen bit, and $1 \leq \zeta \leq N - m$. Therefore, similar to the pure OFDM-I/Q-IM, all $2^4 = 16$ SAPs in Table.7.3 have a chance to be selected. At the receiver, since $U_f(\zeta), U_f(\zeta + 1)$ are pre-known, the selector only needs to choose patterns that the last two bits are $U_f(\zeta)$ and $U_f(\zeta + 1)$ as possible answers. For example, based on Table.7.3 and pre-known frozen bits (for example: $U_f(\zeta) = 0, U_f(\zeta+1) = 0$), the estimated SAP can be only selected from $\mathrm{P}_1, \mathrm{P}_5, \mathrm{P}_9, \mathrm{P}_{13}$.

By using the random frozen bits, the available SAPs are extended. This proposed method is equivalent to a random interleaver, which may provide potential benefit to the proposed system. Here, we briefly analyze the advantage of the appending method using random $\mathbf{U}_f$ compared with the scheme that uses fixed frozen bits (The conventional scheme without appending frozen bits is equivalent to that uses fixed bits.) based on distance. First, we introduce the following definitions. For a n-elements vector $\mathbf{V}_g = [V_{g,1}, V_{g,2}, ..., V_{g,n}]$, the distance between any two vectors $\mathbf{V}_m$ and $\mathbf{V}_q$ is given as: $D(m, q) = \sqrt{\sum_{j=1}^{n} |V_{m,j} - V_{q,j}|^2}$. For simplicity, we consider an all one BPSK OFDM-I/Q-IM system with $n = 4$, $k = 2$, and $p_1 = 1$. We assume that sub-carriers in the same sub-block have similar CFR H_g. In this case, based on Table.7.1, the average distance (AD) of the appending method using fixed frozen bits (0) in a single OFDM block is derived as:

$$AD_f = \frac{2\sqrt{2}}{G(G-1)} \sum_{g=1}^{G-1} \sum_{i=g+1}^{G} |H_g - H_i| \tag{7.8}$$

Then, using the same system above, we assume that the first sub-block utilizes a non-zero appending frozen bit, such as 1. Based on Table.7.1, the AD of the appending method using random frozen bits in a single OFDM block is derived as:

$$AD_r = \frac{2\sqrt{2}}{G(G-1)} (\sum_{g=2}^{G} \sqrt{|H_1|^2 - |H_g|^2} + \sum_{g=2}^{G-1} \sum_{i=g+1}^{G} |H_g - H_i|) \tag{7.9}$$

The difference between AD_r and AD_f, denoted by Δ, is expressed as

$$\begin{aligned} \Delta &= AD_r - AD_f \\ &= \frac{2\sqrt{2}}{G(G-1)} \sum_{g=2}^{G} (\sqrt{|H_1|^2 + |H_g|^2} - |H_1 - H_g|) \end{aligned} \tag{7.10}$$

The advantage of the proposed appending method using random frozen bits over the one using fixed frozen bits Δ is proved in the case of $\Delta \geq 0$, i.e.

$$(\sqrt{|H_1|^2 + |H_g|^2} - |H_1 - H_g|) \geq 0 \tag{7.11}$$

The inequality (7.11) can be shown to hold as follows:

$$\begin{aligned}
&(\sqrt{|H_1|^2 + |H_g|^2} - |H_1 - H_g|) \geq 0 \\
&\Rightarrow (|H_1|^2 + |H_g|^2) - |H_1 - H_g|^2 \geq 0 \\
&\Rightarrow 2|H_1||H_g| \geq 0
\end{aligned} \tag{7.12}$$

Simulation results in the following section also verified above assumption that compared with the appending method using fixed frozen bits, the proposed appending method is helpful to decrease the BER.

Table 7.2: A Look-Up Table Example For $k = 6$, $n = 8$, $b_1 = 2$

Pattern	Bits $\mathbf{i}$	Indices $\mathbf{I}$
P_1	[0, 0]	[2, 4, 5, 6, 7, 8]
P_2	[0, 1]	[1, 3, 5, 6, 7, 8]
P_3	[1, 0]	[1, 2, 3, 4, 6, 8]
P_4	[1, 1]	[1, 2, 3, 4, 5, 7]

The bits after appending $\mathbf{U}_f$ can be treated by an OFDM-I/Q-IM modulator given in Fig.7.1.(b). Then, after IFFT and CP insertion, an OFDM block is generated and transmitted. Also, as what we note before, an advantage of OFDM-I/Q-IM compared with OFDM-IM is that OFDM-I/Q-IM is more flexible for polar-coded systems when variant constellations are applied. After introducing the bits appending method, we show the advantage of OFDM-I/Q-IM for polar-coded systems in Table.7.4, where b_a is the number of random frozen bits appended after the original b_1 bits. Table.7.4 illustrates that with the restriction of polar codes, OFDM-I/Q-IM can be adopted in more scenarios, which is more flexible than OFDM-IM. For the proposed system, unlike pure OFDM-I/Q-IM, b_1, b_2, b_a need to be carefully selected under the restriction

Table 7.3: A Look-Up Table Example For $k = 6$, $n = 8$, $b_1 = 2$, $b_a = 2$

Pattern	Bits $[i(1), i(2), U_f(\zeta), U_f(\zeta+1)]$	Indices $\mathbf{I}$
P_1	[0, 0, 0, 0]	[2, 4, 5, 6, 7, 8]
P_2	[0, 0, 0, 1]	[2, 3, 5, 6, 7, 8]
P_3	[0, 0, 1, 0]	[2, 3, 4, 6, 7, 8]
P_4	[0, 0, 1, 1]	[2, 3, 4, 5, 7, 8]
P_5	[0, 1, 0, 0]	[1, 3, 5, 6, 7, 8]
P_6	[0, 1, 0, 1]	[1, 2, 5, 6, 7, 8]
P_7	[0, 1, 1, 0]	[1, 2, 3, 6, 7, 8]
P_8	[0, 1, 1, 1]	[1, 2, 3, 5, 7, 8]
P_9	[1, 0, 0, 0]	[1, 2, 3, 4, 6, 8]
P_{10}	[1, 0, 0, 1]	[1, 2, 3, 5, 6, 8]
P_{11}	[1, 0, 1, 0]	[1, 2, 3, 4, 5, 8]
P_{12}	[1, 0, 1, 1]	[1, 2, 3, 4, 5, 6]
P_{13}	[1, 1, 0, 0]	[1, 2, 3, 4, 5, 7]
P_{14}	[1, 1, 0, 1]	[1, 2, 3, 4, 7, 8]
P_{15}	[1, 1, 1, 0]	[1, 3, 4, 5, 6, 7]
P_{16}	[1, 1, 1, 1]	[1, 4, 5, 6, 7, 8]

of polar codes.

Table 7.4: The Bits Allocation Schemes For Polar-Coded OFDM-IM And Polar-Coded OFDM-I/Q-IM With $N_{fft} = 128$

<table>
<tr><th></th><th>Const.</th><th>k</th><th>n</th><th>b_1</th><th>b_2</th><th>b_a</th></tr>
<tr><td rowspan="7">Polar-OFDM-IM</td><td rowspan="2">BPSK</td><td>2</td><td>4</td><td>2</td><td>2</td><td>0</td></tr>
<tr><td>5</td><td>8</td><td>3</td><td>5</td><td>2</td></tr>
<tr><td rowspan="2">4-QAM</td><td>2</td><td>4</td><td colspan="3">Not Available</td></tr>
<tr><td>5</td><td>8</td><td colspan="3">Not Available</td></tr>
<tr><td rowspan="3">16QAM</td><td>2</td><td>4</td><td colspan="3">Not Available</td></tr>
<tr><td>5</td><td>8</td><td colspan="3">Not Available</td></tr>
<tr><td>6</td><td>8</td><td colspan="3">Not Available</td></tr>
<tr><td rowspan="7">Polar-OFDM-I/Q-IM</td><td rowspan="2">BPSK</td><td>2</td><td>4</td><td>2</td><td>2</td><td>0</td></tr>
<tr><td>5</td><td>8</td><td>5</td><td>5</td><td>2</td></tr>
<tr><td rowspan="2">4-QAM</td><td>2</td><td>4</td><td>2</td><td>2</td><td>0</td></tr>
<tr><td>5</td><td>8</td><td>5</td><td>5</td><td>2</td></tr>
<tr><td rowspan="3">16-QAM</td><td>2</td><td>4</td><td colspan="3">Not Available</td></tr>
<tr><td>5</td><td>8</td><td colspan="3">Not Available</td></tr>
<tr><td>6</td><td>8</td><td>4</td><td>12</td><td>0</td></tr>
</table>

7.2.2 The receiver design

After removing CP and invoking the FFT, unlike the conventional polar-coded OFDM system, the proposed polar-coded OFDM-I/Q-IM system needs to detect the indices of active sub-carriers and the corresponding information bits according to the received vector $y(\beta)$ with $\beta = 1, 2, ..., N_{fft}$. In this section, the channel detector in [69] is applied to obtain the active indices patterns $\mathbf{I}_g^I$ and $\mathbf{I}_g^Q$. We note that the indices detection for the in-phase and quadrature parts are same and implemented simultaneously. Hence, in the following section, we only take the in-phase sub-blocks as an example, and the superscript I is omitted for simplicity.

The channel detector of OFDM-I/Q-IM gives the *a posteriori* probabilities of frequency domain signals by considering the case that the values are either non-zero or zero [69]. For the g^{th} sub-block, channel detectors provide the probability of the active status of the corresponding index η with $\eta = 1, 2, ..., n$, given by:

$$\lambda_g(\eta) = \ln \frac{\sum_{\chi=1}^{M} P(S_g(\eta) = Q_\chi | y_g(\eta))}{P(S_g(\eta) = 0 | y_g(\eta))} \tag{7.13}$$

where Q_χ is the element of a M-array PAM constellation, and $y_g(\eta)$ is the received vector for the g^{th} sub-block after FFT operation, which can be written as:

$$y_g(\eta) = H_g(\eta) S_g(\eta) + w_g(\eta), \text{ for } \eta = 1, ..., n \tag{7.14}$$

where $w_g(\eta)$ denotes the zero-mean complex additive white Gaussian noise (AWGN) with variance σ_k^2 on the η^{th} sub-carrier of the g^{th} sub-block. It is assumed that the noise variance in the time domain is σ^2, which is related with the noise variance in the frequency domain via $\sigma_k^2 = (k/n)\sigma^2$ due to the normalization factor $\sqrt{(k/n)}$ of the FFT at the receiver [133].

The lager the value of $\lambda(\eta)$, the higher the probability that the corresponding η

is an active sub-carrier. Using Bayes formula, (7.13) can be expressed as:

$$\lambda(\eta) = \ln(k) - \ln(n-k) + \frac{|y_g(\eta)|^2}{\sigma_k^2} + \ln((\sum_{\chi=1}^{M} \exp(-\frac{1}{\sigma_k^2}|y_g(\eta) - H_g(\eta)Q_\chi|^2)) \quad (7.15)$$

The complexity of a channel detector is $O(M)$ per sub-carrier and dimension. Also, like conventional OFDM-IM, the Jacobian logarithm [150] can be applied in (7.15). For example, the identity $\ln(e^{a_1}+e^{a_2},...+e^{a_M}) = \int_{max}(\int_{max}(\int_{max}(a_1,a_2),a_3,...),a_M)$, where $\int_{max}(a,b) = \ln(e^{a_1}+e^{a_2}) = \max(a_1,a_2)+\ln(1+e^{-|a_1-a_2|})$ can be utilized to simplify (7.15). Then, the channel detector can do conjunction based on a look-up table. Let denote the set of possible active indices of the g^{th} sub-block by $\mathbb{I} = \{\mathbf{I}_g^1, \mathbf{I}_g^2, ..., \mathbf{I}_g^V\}$ for which $\mathbf{I}_g^\omega \in \mathbb{I}$, where $\mathbf{I}_g^\omega = [I_g^\omega(1), I_g^\omega(2), ..., I_g^\omega(k)]$ with $\omega = 1,..,V$ and $V = \lfloor \log_2 \mathbb{C}_n^k \rfloor$. For example, for Table.7.1, we have $\mathbf{I}_g^1 = [1,3]$, $\mathbf{I}_g^2 = [2,4]$, $\mathbf{I}_g^3 = [1,4]$, $\mathbf{I}_g^4 = [2,3]$. After obtaining all *a posteriori* probabilities based on (7.15), for each sub-block, the receiver can calculate the following V summations for all possible set of active indices using the corresponding look-up table as [69]:

$$d_g^\omega = \sum_{\gamma=1}^{k} \lambda(n(g-1) + I_g^\omega(\gamma)) \quad (7.16)$$

for $\omega = 1,2,...,V$. Let take Table.7.1 as an example, for sub-block g, we have $d_g^1 = \lambda(1)+\lambda(3)$, $d_g^2 = \lambda(2)+\lambda(4)$, $d_g^3 = \lambda(1)+\lambda(4)$, $d_g^4 = \lambda(2)+\lambda(3)$. Then, the receiver makes decision on the set of active sub-carriers based on the maximum sum among all V probability sums: $\hat{\omega} = \underset{\omega}{\operatorname{argmax}} d_g^\omega$. Then, the estimated $\mathbf{I}_g$ can be mapped to the index bits $\mathbf{i}_g$ according to the corresponding look-up tables.

The block diagram of the proposed polar-coded OFDM-I/Q-IM receiver is given in Fig.7.3.(a). For each in-phase or quadrature sub-block g, after obtaining the estimated $\mathbf{I}_g$ from channel detectors, the initial LLRs for polar decoding need to be calculated. The initial LLRs of the index bits for decoding rely on the *a posteriori* information provided by the index detector, and the corresponding information can be calculated from the hard valued detected index bits or the soft information obtained from the *a posteriori* probabilities $\lambda(\eta)$ of channel detectors and look-up tables. These initial LLRs for polar decoding are more reliable than the LLRs used in polar-coded OFDM because the index error rate (IER) for OFDM-I/Q-IM is lower than the BER of M-QAM demodulation. The corresponding proof is given in appendix. Therefore, by utilizing these reliable initial LLRs, we expect that the proposed system can achieve better performance than that of polar-coded OFDM.

For each in-phase or quadrature sub-block g, after obtaining the estimated $\mathbf{I}_g$, these index indicators are de-mapped to the indices bits $\mathbf{i}_g = [X_g(1), X_g(2), ..., X_g(k)]$ based on look-up tables. After de-mapping all $\mathbf{i}_g$, the detected indices are combined to have a $2Gb_1$ length sequence $\mathbf{X}_{id}$. The initial LLRs for polar decoding can be obtained through $\mathbf{X}_{id}$, denoted as:

$$\mathbf{X}_{id} = [X_{id}(1), X_{id}(2)..., X_{id}(2Gp_1)] \tag{7.17}$$

The LLRs obtaining method using hard information is given in the lower part of Fig.7.3.(b), where $\sqrt{E_b}$ is the energy per bit. This sequence (7.17) can be seen as a bit stream that is perfectly transmitted without affected by noise.

Nevertheless, intuitively, for a sub-block g with index bits $\mathbf{i}_g = [i(1), i(2), ..., i(b_1)]$, the initial LLR of index bit $i(j)$ in $\mathbf{i}_g$ can be obtained by fully utilizing the probability related to $\lambda(\eta)$. However, (7.15) only reflects the probability that the corresponding position η is zero or not. Therefore, by combining the look-up tables for mapping, we can indirectly obtain the LLR of $i(j)$ for polar decoding, where $1 \leq j \leq b_1$. Here, we define a mapping according to the look-up tables:

$$i(j) = b \Leftrightarrow \mathbb{P}_{i(j)=b} \tag{7.18}$$

where $\mathbb{P}_{i(j)=b} = [\mathrm{P}_{b,1}, ...\mathrm{P}_{b,\omega}..., \mathrm{P}_{b,V}]$ is the pattern corresponding to $i(j) = b$, where $b \in \{0, 1\}$. Pattern $\mathrm{P}_{b,\omega}$ is a length n sequence where the active position is denoted as $\times$ and the null position is denoted as 0. For example, according to Table.7.1, $\mathrm{P}_{0,1}$ and $\mathrm{P}_{0,2}$ can be written as: $[\times, 0, \times, 0]$ and $[0, \times, 0, \times]$, respectively. The probability that the η^{th} element in pattern $\mathrm{P}_{b,\omega}$ is zero or $\times$ can be written as:

$$\begin{aligned} P(\mathrm{P}_{b,\omega}(\eta) \text{ is } 0) =& \frac{1}{1+\exp(\lambda(\eta))} \\ P(\mathrm{P}_{b,\omega}(\eta) \text{ is } \times) =& \frac{\exp(\lambda(\eta))}{1+\exp(\lambda(\eta))} \end{aligned} \tag{7.19}$$

Then, the corresponding LLR of bit $i(j)$ can be written as:

$$LLR_{i(j)} = \ln \frac{P(i(j)=1|\mathbf{y})}{P(i(j)=0|\mathbf{y})} = \ln \frac{\sum\limits_{\omega=1}^{V} \prod\limits_{\eta=1}^{n} P(\mathrm{P}_{1,\omega}(\eta) \text{is } \mho_{i(j)=1})}{\sum\limits_{\omega=1}^{V} \prod\limits_{\eta=1}^{n} P(\mathrm{P}_{0,\omega}(\eta) \text{is } \mho_{i(j)=0})} \tag{7.20}$$

where $\mho \in \{\times, 0\}$, and $\mho_{i(j)=b}$ represents the active status of $\mathrm{P}_{b,\omega}$ corresponding to $i(j) = b$. The initial LLR calculation method using soft information is given in the upper part of Fig.7.3.(b).

For example, considering a sub-block with $n = 4$, $k = 2$, and Table.7.1, according to (7.19), the probability that $\mathrm{P}_{b,\omega}(\eta)$ with $b = \{0,\ 1\}$ equals to zero or not can be written as: $P(\mathrm{P}_{b,\omega}(\eta) \text{ is } 0) = \frac{1}{1+\exp(\lambda(\eta))}$ and $P(\mathrm{P}_{b,\omega}(\eta) \text{ is } \times) = \frac{\exp(\lambda(\eta))}{1+\exp(\lambda(\eta))}$ with $\eta = 1, 2, 3, 4$. Then, based on the mapping between $i(j)$ and $\mathbb{P}_{i(j)}$ with $1 \le j \le 2$. The probability that $i(1)$ equals to 0 or 1 can be written as ($i(2)$ can be obtained in a similar way):

$$\begin{aligned} P(i(1)=0|\mathbf{y}) =& P(\mathrm{P}_{0,1}(1) \text{ is } \times) \cdot P(\mathrm{P}_{0,1}(2) \text{ is } 0) \cdot P(\mathrm{P}_{0,1}(3) \text{ is } \times) \cdot P(\mathrm{P}_{0,1}(4) \text{ is } 0) + \\ & P(\mathrm{P}_{0,2}(1) \text{ is } 0) \cdot P(\mathrm{P}_{0,2}(2) \text{ is } \times) \cdot P(\mathrm{P}_{0,2}(3) \text{ is } 0) \cdot P(\mathrm{P}_{0,2}(4) \text{ is } \times) \end{aligned}$$

$$P(i(1)=1|\mathbf{y}) = P(\mathrm{P}_{1,1}(1) \text{ is } 0)\cdot P(\mathrm{P}_{1,1}(2) \text{ is } \times)\cdot P(\mathrm{P}_{1,1}(3) \text{ is } \times)\cdot P(\mathrm{P}_{1,1}(4) \text{ is } 0)+$$
$$P(\mathrm{P}_{1,2}(1) \text{ is } \times)\cdot P(\mathrm{P}_{1,2}(2) \text{ is } 0)\cdot P(\mathrm{P}_{1,2}(3) \text{ is } 0)\cdot P(\mathrm{P}_{1,2}(4) \text{ is } \times)$$

Then, according to (7.20), the corresponding LLR value of $i(1)$ can be obtained.

Compared with the LLR calculation method that using hard values, method that using soft information from $\lambda(\eta)$ fully takes advantage of the probabilities provided by channel detectors, which should bring benefit in terms of BER performance. However, this method owns higher complexity, especially when $\mathbb{C}_n^k$ is large. The computational complexity of the soft information based method can be roughly generalized to $O(2^{\lfloor \log_2 \mathbb{C}_n^k \rfloor})$ per sub-carrier and dimension. The simulation result shows that although using (7.19) and (7.20) to generate initial LLRs can achieve better performance, using (7.17) can still obtain a good performance with lower complexity.

After obtaining the LLRs of index bits, which are denoted as $\mathbf{LLR}_{id}$, LLRs of the rest transmitted codewords need to be confirmed. First, for the g^{th} sub-block, we write the symbols after idle sub-carriers removal as:

$$\{S_g(\eta)\}_{\eta=1}^{k} = [S_g(1), S_g(2), ..., S_g(k)] \tag{7.21}$$

Each symbol $S_g(\eta)$ consists $\log_2 M$ bits. Denote $Q_{c,i}$ as the sub-constellation of Q corresponding to bit c among $\log_2 M$ bits when bit c is $i \in \{0,1\}$. Then, for a given $S_g(\eta)$, the LLR of bit c is given by:

$$\begin{aligned} LLR_{g,c}(\eta) &= \ln \frac{P(y_g(\eta)|\left\langle S_g(\eta)\right\rangle_c = 0)}{P(y_g(\eta)|\left\langle S_g(\eta)\right\rangle_c = 1)} \\ &= \ln \frac{\sum_{S\in Q_{c,0}} \exp(-\frac{|y_g(\eta)-H_g(\eta)S|^2}{\sigma_k^2})}{\sum_{S\in Q_{c,1}} \exp(-\frac{|y_g(\eta)-H_g(\eta)S|^2}{\sigma_k^2})} \end{aligned} \tag{7.22}$$

where $\langle S(\eta)\rangle_c$ denotes the c^{th} bit of the symbol S. Then, combining with the $\mathbf{LLR}_{id}$, the N length LLRs becomes the initial input of the polar decoding part to obtain the estimated information bits $\hat{U}_1^m$. In this section, a widely used BP decoding scheme [91], which is a type of soft input and SISO decoding, is applied in both the proposed system and the polar-coded OFDM system for fair comparison. Also, we note that SC based decoding can be used in the proposed system.

7.3 Simulation results

In this section, methods proposed in above sections are verified, and the BER performance of the proposed polar-coded OFDM-I/Q-IM system is investigated. To make fair comparisons, both the proposed polar-coded OFDM-I/Q-IM and polar-coded OFDM are compared with the same transmission rate R, where $R = m/N_{fft}$. Perfect channel estimation was assumed. The parameters used in simulations are given in Table.7.5.

Table 7.5: Simulation Parameters

Number of available subcarriers (N_{fft})	64
Modulation	4-QAM
Length of cyclic prefix	8
Length of polar code (N)	128
Number of information bits (m)	$\{64, 84\}$
Number of indices bits (b_1)	$\{2, 4\}$
Number of sub-blocks (G)	$\{8, 16\}$

Fig.7.4 gives the BER performance between the polar-coded OFDM-I/Q-IM systems using different bits appending methods. The number of sub-block G is 8. When $b_1 = 2$, each sub-block has $n = 8$ available sub-carriers, and $k = 6$ sub-carriers are activated. Hence, $p_1 - b_1 = 2$ extra bits are appended. By appending random frozen bits, the corresponding BER performance can be improved. Therefore, we note that in the following simulations, the proposed appending method is applied whenever $p_1 > b_1$.

Then, BER performances of the proposed systems utilizing different LLRs calculation methods in Fig.7.3.(b). are investigated. Fig.7.5 illustrates that compared with

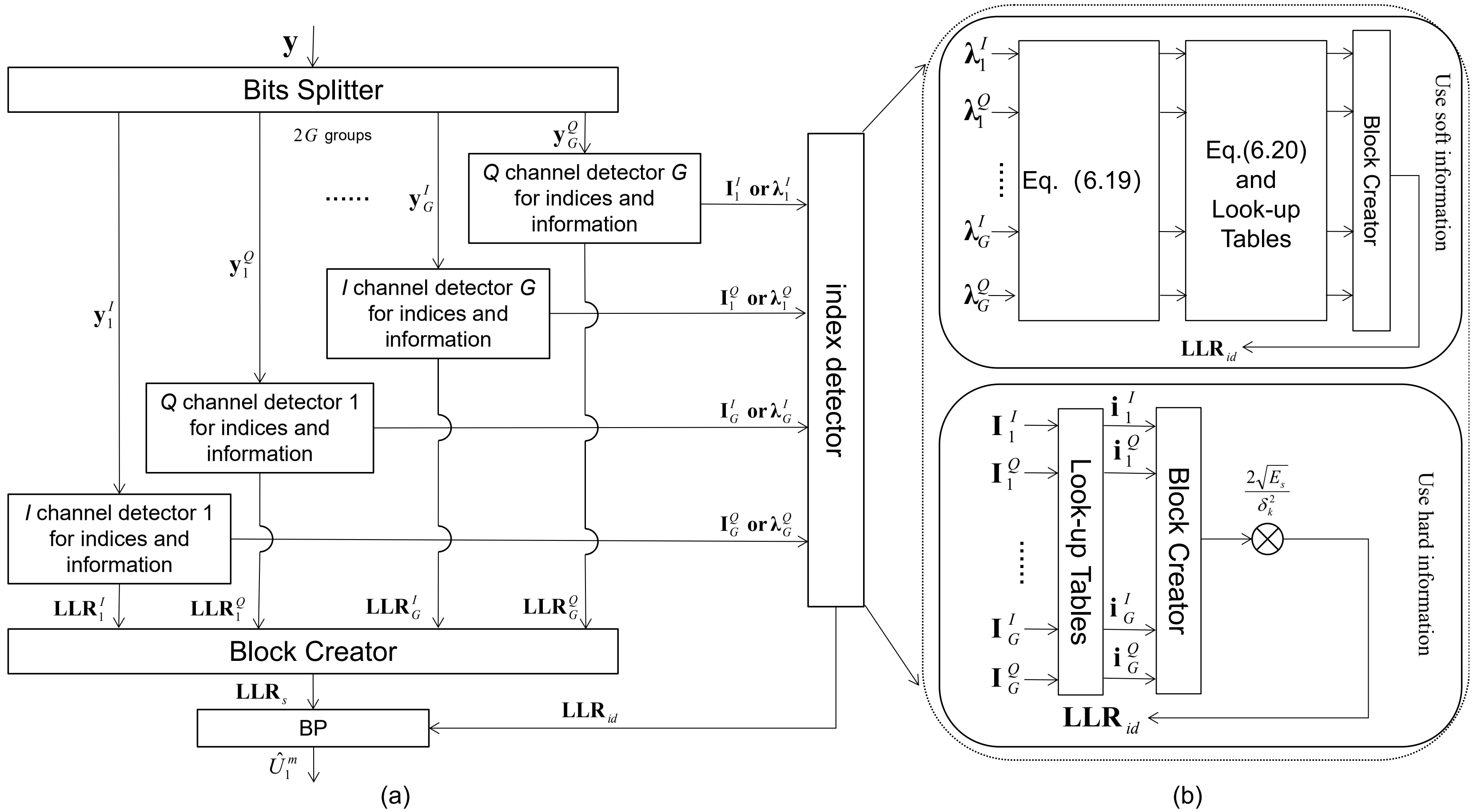

Fig. 7.3: Block diagram of (a). a polar-coded OFDM-I/Q-IM receiver (b). an example of the initial LLR generation process of the indices bits using hard or soft information

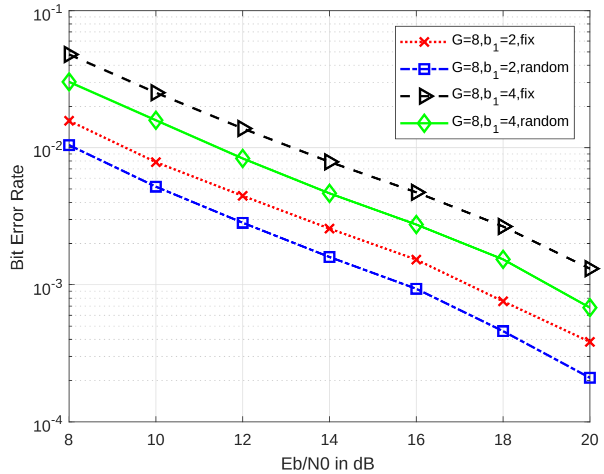

Fig. 7.4: BER performance between the polar-coded OFDM-I/Q-IM systems using different appending methods.

the initial LLRs obtained from (7.20), using the initial LLRs obtained through hard information caused BER degradation. In low-mid SNR, the gap is negligible. Nevertheless, the gap becomes larger in high SNR scenarios. At probability 1.6×10^{-4}, the black line which soft information are applied has around 2 dB performance gain compared with the red line that hard values are utilized. However, in terms of computational complexity, using hard valued sequence is an effective way to implement the decoding procedure. Therefore, in the following simulations, the LLRs calculation method using hard-valued sequences is utilized for simplicity.

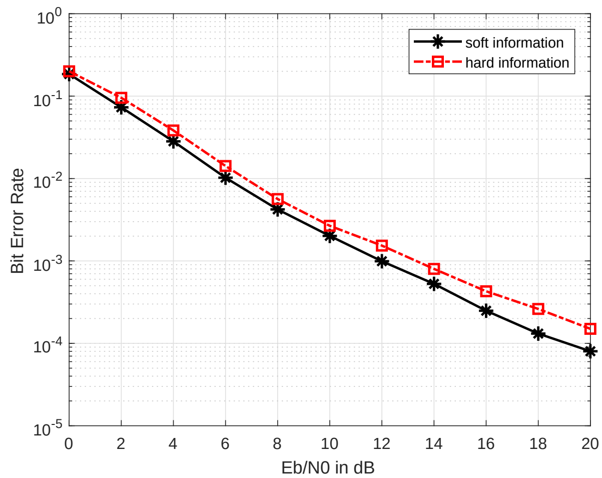

Fig. 7.5: BER performance between different LLR generation methods.

The BER comparison between the proposed polar-coded OFDM-I/Q-IM system (denoted as "proposed") and the conventional polar-coded OFDM system (denoted as "P-OFDM") with different transmission rate R is given in Fig.7.6. As a reference, the performance of a pure OFDM-I/Q-IM [133] and a polar-coded OFDM in slow Rayleigh fading channel (denoted as "O-PC-Frequency non selective") [142] are also included. In the simulation, $G = 16$, $b_1 = 4$. It was illustrated that compared with the OFDM-I/Q-IM, adding polar codes was helpful in terms of BER performance. Then, the proposed system can achieve significant BER enhancement compared with the conventional polar-coded OFDM. For example, when $R = 1$, at probability 10^{-3}, the proposed system obtained around 6 dB gains than that of the conventional polar-coded OFDM system.

Then, BER performance of the proposed polar-coded OFDM-I/Q-IM system by utilizing different number of sub-block G and index bits b_1 is investigated. Fig.7.7 indicates that various G and b_1 can cause different BER performances. When $G = 8$, and $b_1 = 4$, no matter what transmission rate R is, the corresponding BER performance is the worst compared with other allocation ways due to its large SAPs [151]. Intuitively, it was expected that when b_1 is same, larger G would bring better per-

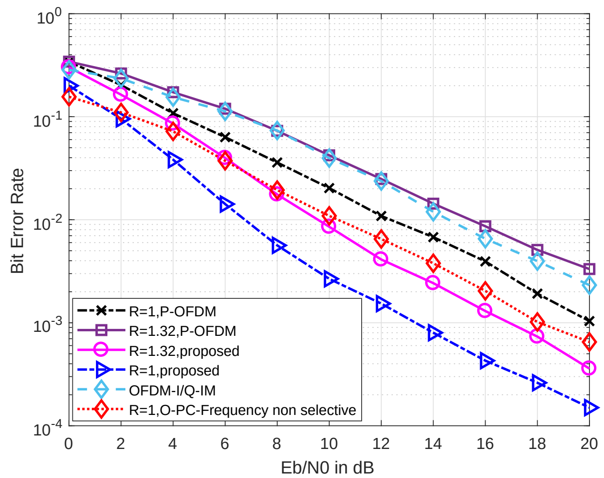

Fig. 7.6: BER performance between the proposed system and polar-coded OFDM.

formance because more index bits can be used for decoding. However, it is shown that in some cases, the allocation method using $G = 8$, $b_1 = 2$ achieves better BER performance than that of the method using $G = 16$, $b_1 = 2$ (The red and blue solid lines when $R = 1.32$). It can be explained by the index error rate (IER). We provide the corresponding IER result among different index allocations in Fig.7.8. It is illustrated that although the scheme using $G = 16$, $b_1 = 2$ has more index bits sent to the BP decoder, it also causes higher IER. Therefore, it is possible for the scheme using $G = 8$, $b_1 = 2$ to achieve better overall BER performance.

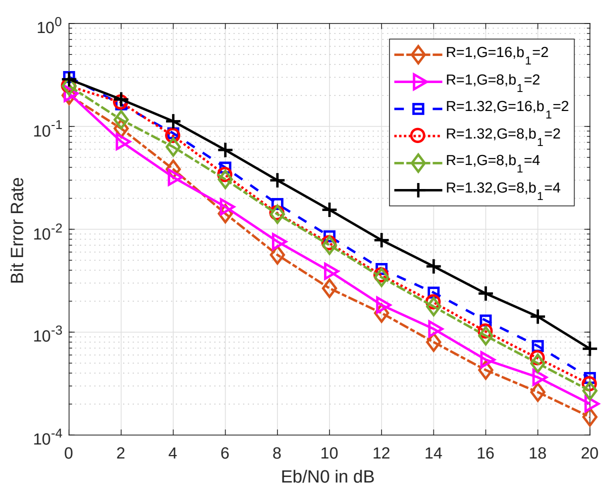

Fig. 7.7: BER performance of the proposed systems with various G and b_1

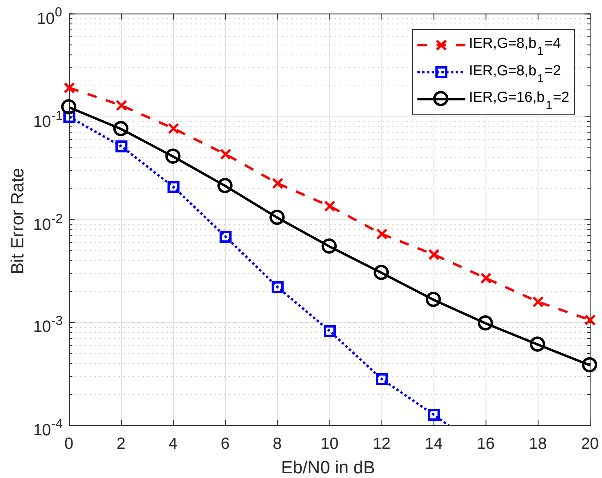

Fig. 7.8: IER performance of the proposed systems with different index bits allocations

7.4 Summary

In this chapter, a polar-coded OFDM-IM system was proposed. By introducing the concept of index modulation, the polar codeword can be transmitted not only by OFDM blocks, but also indices of active sub-carriers. For the proposed system, a part of polar codewords are transmitted implicitly through index modulation. Unlike the polar-coded OFDM, using polar codes in OFDM-IM systems has difficulties in terms of bits allocations due to the length and constellation restrictions of polar codes. Therefore, OFDM-I/Q-IM and random frozen bits appending method are introduced and proposed to make polar codes more compatible for OFDM-IM based systems. At the receiver, the index detector and a BP decoder are utilized for data recovery. For the proposed system, the detected index bits are regarded as reliable and the corresponding initial LLRs for decoding can be obtained through soft or hard information provided by such index detector. These initial LLRs are helpful to achieve better decoding performance. Simulation results show that the proposed polar-coded OFDM-I/Q-IM system can achieve significantly better BER performance than that of the conventional polar-coded OFDM system with different transmission rate. Nevertheless, how to obtain the initial LLRs of index bits with low complexity is still open for future research.

In next chapter, the author will summarize the main contributions of this thesis as the conclusion and propose some works that are valuable for future research.

8 CONCLUSION AND FUTURE WORKS

In this chapter, first, main contributions of this thesis are summarized. Then, potential works that can be investigated in future are presented.

8.1 Conclusion

In Chapter 1, the author reviewed the history of channel coding and show that polar coding has opened a door for reliable transmission because of its low en/decoding complexity and provable channel capacity achievement. Then, the preliminary knowledge, including the theory of polarization, polar encoding and decoding have been introduced in Chapter 2.

In Chapter 3, several modified polar decoding schemes were presented. These novel methods are based on SC, BP and SD, respectively. Moreover, for BP decoding, we also developed a stopping criterion that can reduce the latency of BP. Compared with existing works, the proposed modified schemes can achieve better error performance or complexity reduction.

In Chapter 4, the background knowledge of OFDM based techniques were introduced. The fundamentals of OFDM were reviewed in the first part of Chapter 4. Then, as a modified version of OFDM, OFDM-IM, which has unique advantages which are different from OFDM, was introduced. OFDM-IM provides interesting trade-off between spectral efficiency and error performance, which offers perfect properties of network slicing required by next generation wireless communication networks. A comparison between OFDM-IM and OFDM has been given in this chapter.

In Chapter 5, two modified polar-coded OFDM systems that introduce existing techniques were proposed. These schemes can improve the performance of polar-coded OFDM. OFDM transforms frequency selective fading to flat fading. However, it is very common that channel estimation is inaccurate. Hence, in the first part of Chapter 5, we developed a channel compensator that corrects initial LLRs of BP decoders with noisy channel estimation. Moreover, a turbo receiver for polar-coded OFDM systems was proposed to enhance the BP decoding performance with unknown CSI by utilizing the soft information provided by the EM detector and BP polar decoder. These two methods have been proven useful through mathematical proof and simulation results, and they can be easily applied in any OFDM based system.

In Chapter 6, a SI free SLM based on polar-coded OFDM-IM systems was proposed, which can reduce the high PAPR in OFDM-IM systems by utilizing the properties of polar en/decoding without compromising the error-correcting capability of polar codes.

In Chapter 7, a design guideline for polar-coded OFDM-I/Q-IM was proposed. OFDM-I/Q-IM is a modified OFDM-IM, which implements index modulation on in-phase and quadrature parts separately. OFDM-I/Q-IM achieves better spectral efficiency and error performance than that of the conventional OFDM-IM. By introducing polar codes to OFDM-I/Q-IM, a polar-coded OFDM-I/Q-IM system can be built. Moreover, by utilizing reliable index bits generated by the index detector, compared with the conventional polar-coded OFDM systems, the overall decoding performance of the proposed system can be significantly improved.

8.2 Suggestions for future studies

The research on polar-coded OFDM-I/Q-IM systems and related techniques in this thesis leads to some suggestions for the following future research.

- For the proposed hybrid SD in Chapter 3, compared with existing SD schemes, the proposed method can achieve significant complexity reduction without compromising the ML optimality. However, compared with existing polar decoding schemes, such as SC and BP, the hybrid SD is still with high complexity. Keeping ML performance while decreasing the complexity is still an important work in the future.

- In Chapter 7, the author proposed a guideline of polar-coded OFDM-IM systems. The proposed scheme takes advantages of the bits that are utilized for index modulation. Therefore, the proposed polar-coded OFDM-IM achieves better error performance than that of the conventional polar-coded OFDM. Also, it has been indicated that utilizing the soft information provided by the index detector can achieve better performance than that of using hard information. However, it was also shown that the corresponding complexity is high. Therefore, how to reduce the complexity of such soft-message-based method is the issue that needs to be solved.

- In this thesis, the author investigated polar decoding schemes rather than polar encoding schemes. However, a strong polar code construction scheme can significantly improve its performance. However, polar codes need to utilize the channel statistics when selecting message bit positions. Therefore, when the channel status is unknown or cannot be accurately acquired, it may fail to select the best split channels to transmit message bits, resulting in performance loss. The author notes that all polar construction methods utilized in this thesis are based on AWGN channels, which indicate that the decoding performance provided such encoding methods are sub-optimal in other channels. In order to solve this problem, it is necessary to introduce a method to estimate and predict the channel, and analyze the impact of inaccurate channel statistics on the performance of polar codes. A channel estimation methods utilizing polar decoding was proposed in [152], and some polar construction schemes have been proposed in [153, 66, 154, 155]. These methods make polar codes stronger in block or frequency selective channels. Based on these works, using the properties of polar codes, more polar codes construction and channel estimation schemes might be developed in the future.

- We know that in pure OFDM-IM systems, the available bits are decided by the length of FFT and SAPs. However, for polar-coded OFDM-IM based systems, the length of polar code is usually fixed. Thus, the number of bits that can be transmitted in OFDM-IM systems cannot always match the length polar codes, especially when the modulation order is high. In our proposed polar-coded OFDM-I/Q-IM system, common constellation mapping (i.e. BPSK, QPSK, 16QAM) can be applied. However, for higher order constellations, such as 64QAM, the availability of our proposed system is limited. Therefore, it is necessary to develop a novel OFDM-IM based scheme that can be perfectly combined with polar codes. These novel OFDM-IM schemes are expected to have higher spectral efficiency without compromising the error performance.

APPENDICES

A. Appendix for section.3.1

The average error probability of each bit over an AWGN channel can be obtained by GA [75]. If an all zero BPSK polar codeword is transmitted over the AWGN channel, the i^{th} bit's average error probability can be estimated as

$$\bar{P}_e(u_i) = 0.5\text{erfc}(0.5\sqrt{\gamma_i}) \tag{8.1}$$

where γ_i is the mean LLR of bit u_i, which can be obtained by using the method in [75], and $\text{erfc}(x) = (\frac{2}{\sqrt{\pi}}) \int_x^\infty e^{-\eta^2} d\eta$. For an all-zero polar codeword, the probability of the incorrect estimating $\hat{u}_i$ is equivalent to $P_e(\hat{u}_i) = P(\hat{u}_i = 1 | y_1^N, \hat{u}_1^{i-1})$, which is the bit error probability based on the observed estimation $\hat{u}_1^{i-1}$. The corresponding $P_e(\hat{u}_i)$ can be denoted as $P_e(\hat{u}_i) = 0.5\text{erfc}(0.5\sqrt{\alpha_i})$. Let the average estimated error probability for bit i denote as $\bar{P}_e(u_i)$, which is obtained from (8.1). Intuitively, if $\bar{P}_e(u_i)$ is lower than $P_e(\hat{u}_i)$, the corresponding bit is unreliable. Hence, in terms of LLR values, we have:

$$\alpha_i - \ln\frac{1 - \bar{P}_e(u_i)}{\bar{P}_e(u_i)} > 0 \tag{8.2}$$

Similarly, if the correct decision is $u_i = 1$, we have:

$$\alpha_i + \ln\frac{1 - \bar{P}_e(u_i)}{\bar{P}_e(u_i)} < 0 \tag{8.3}$$

Hence, assume $\bar{P}_e(u_i)$ is low, if the bit obtained from SC is reliable, the absolute value of the LLRs should be greater than $\ln\frac{1-\bar{P}_e(u_i)}{\bar{P}_e(u_i)}$.

B. Appendix for section.3.4

When the transmitted symbols are taken from $\{\sqrt{E_s}, -\sqrt{E_s}\}$ with equal probability 1/2. A low complex SD scheme with novel PM was proposed in [54] to maximize the likelihood probability:

$$2^{-i}P(\mathbf{y}|s_i^{N-1}s_0^{i-1}), \text{for } i=0,...,N-1 \tag{8.4}$$

where $s_i^{N-1}=[s[i],s[i+1],...,s[N-1]]$ and $s_0^{i-1}=[s[0],s[1],...,s[i-1]]$. It is assumed that the partial symbol s_i^{N-1} vector is correctly decoded. After the mathematical derivation, this novel PM can be expressed as:

$$\begin{aligned} M_0(u_i^{N-1}) &= \sum_{j=i}^{N-1}\frac{2\sqrt{E_s}y[j]s[j]}{N_0} - h_1(y_i^{N-1}) \\ &= \sum_{j=i}^{N-1}\frac{2\sqrt{E_s}}{N_0}y[j](1-2\sum_{k=j}^{N-1}u[k]g[k+1,j+1]) - h_1(y_i^{N-1}) \end{aligned} \tag{8.5}$$

where $0 \le i \le N-1$, $y_i^{N-1}=[y[i],y[i+1],...,y[N-1]]$, and

$$h_1(y_i^{N-1}) = \sum_{j=i}^{N-1}\text{lncosh}(\frac{2\sqrt{E_s}y[j]}{N_0}) + (N-i)\text{ln2} \tag{8.6}$$

This novel metric M_0 introduces the knowledge of the estimated s_i^{N-1} provided by the received sequence $\mathbf{y}$. The first term of the (8.5) adopts the correlation between the received partial vector y_i^{N-1} and the estimated symbols s_i^{N-1}. The second term covers some correction parts [54].

The (8.5) can be simplified as [156]:

$$M_1(u_i^{N-1}) = \sum_{j=i}^{N-1}(y[j]s[j]-|y[j]|) \tag{8.7}$$

which is the optimum PM in (3.35).

C. Appendix for Chapter.7

Here, we prove the conclusion claimed in the previous section that the IER of OFDM-I/Q-IM is lower than the BER of M-QAM demodulation. Let take an OFDM-I/Q-IM scheme with parameters n and k as an example. On the one hand, it is known that the estimation procedure of the activity of a single sub-carrier is similar to coherent binary ASK detection which probability of error over Rayleigh fading channels can be given as [157]:

$$P_{BASK} = 0.5(1 - \sqrt{\frac{\gamma_b}{1+\gamma_b}}) \tag{8.8}$$

where $\gamma_b = \alpha^2 \frac{E_b}{N_0}$ is the average SNR per bit, α is the average fading amplitude and E_b is the average bit energy. To have d errors, for a given n and k, the number of different sub-carrier states between a transmitted SAP_i and incorrectly received SAP_j is given as [151]:

$$d_{i,j} = \sum_{\mu=1}^{n} (\mathrm{SAP}_{i,\mu} \oplus \mathrm{SAP}_{j,\mu}) \tag{8.9}$$

where $1 \leq i \leq 2^{p_1}$, $1 \leq j \neq i \leq \mathbb{C}_n^k$, μ is denoted as an inactivated sub-carrier index and $\oplus$ is an exclusive NOR operator. Hence, the probability of incorrectly detecting an SAP with $d_{i,j}$ sub-carrier detection errors is:

$$P_{ICi,j} = P_{BASK}^{d_{i,j}} \tag{8.10}$$

The average probability of incorrectly detecting SAPs can be written as:

$$P_{IC} = \frac{1}{2^{p_1}(\mathbb{C}_k^n - 1)} \sum_{i=1}^{2^{p_1}} \sum_{j=1, j\neq i}^{\mathbb{C}_k^n} P_{ICi,j} \tag{8.11}$$

Considering an incorrect SAP, it is shown in [158] that an incorrect detected SAP causes an average error of about $0.5p_1$ in the de-mapped p_1 bits. Hence, the IER contribution of an incorrect detected SAP is:

$$B_{IC} = P_{IC}(\frac{0.5p_1}{p_1}) = 0.5P_{IC} \tag{8.12}$$

On the other hand, the approximate BER P_b of M-QAM demodulation over

Rayleigh fading channels can be written as [159]:

$$P_b = \frac{2}{\log_2 M}(\frac{\sqrt{M}-1}{\sqrt{M}}) \times (1 - \sqrt{\frac{1.5\gamma_s}{M-1+1.5\gamma_s}}) - (\frac{\sqrt{M}-1}{\sqrt{M}})^2$$
$$\times \frac{1}{\log_2 M}[1 - \sqrt{\frac{1.5\gamma_s}{M-1+1.5\gamma_s}}) \times (\frac{4}{\pi}\tan^{-1}\sqrt{\frac{1.5\gamma_s}{M-1+1.5\gamma_s}})] \tag{8.13}$$

where $\gamma_s = \gamma_b \log_2 M$ is the average SNR per symbol.

To prove the IER for the OFDM-I/Q-IM scheme is lower than the BER of the conventional M-QAM demodulation ($B_{IC} < P_b$), let assume $M = 4$, $n = 4$, and $k = 2$ (using Table.7.1). It is illustrated that when using Table.7.1, the errors d in a received SAP is larger than 2, given as:

$$d_{i,j} = \sum_{\mu=1}^{n} (\mathrm{SAP}_{i,\mu} \oplus \mathrm{SAP}_{j,\mu}) \geqslant 2$$

Thus $P_{IC,i,j} \leq P_{BASK}^2$. Then, the B_{IC} in (8.12) can be rewritten as:

$$\begin{aligned} B_{IC} &= 0.5 P_{IC} \\ &= \frac{0.5}{2^{p_1}(\mathbb{C}_k^n - 1)} \sum_{i=1}^{2^{p_1}} \sum_{j=1, j\neq i}^{\mathbb{C}_k^n} P_{ICi,j} \\ &\leq 0.5 \times 1 \times P_{BASK}^2 \\ &\leq 0.5 P_{BASK}^2 \end{aligned} \tag{8.14}$$

Then, for the conventional 4-QAM demodulation, the corresponding P_b can be denoted as:

$$\begin{aligned} P_b &\geq \frac{1}{2}(1 - \sqrt{\frac{\gamma_b}{1+\gamma_b}}) - \frac{1}{8}(1 - \sqrt{\frac{\gamma_b}{1+\gamma_b}} \times \frac{4}{\pi} \times \frac{\pi}{4}) \\ &\geq P_{BASK} - \frac{1}{4} P_{BASK} \\ &\geq \frac{3}{4} P_{BASK} \end{aligned} \tag{8.15}$$

Therefore: $B_{IC} - P_b \leq \frac{1}{2}P_{BASK}^2 - \frac{3}{4}P_{BASK} < 0$. Thus the bits detected by indices detector is more reliable and may benefit the decoding procedure.

REFERENCES

[1] S.-y. Zhang and B. Shahrrava, "Stopping criterion for belief propagation polar code decoders based on bits difference ratio," in *2019 IEEE 10th Annual Information Technology, Electronics and Mobile Communication Conference (IEMCON).* IEEE, 2019, pp. 0285–0289.

[2] ——, "Enhanced bp decoding schemes of polar codes," *IET Communications*, 2021.

[3] S.-Y. Zhang and B. Shahrrava, "Turbo receiver for polar-coded ofdm systems with unknown csi," in *2020 IEEE Canadian Conference on Electrical and Computer Engineering (CCECE).* IEEE, pp. 1–4.

[4] ——, "A slm scheme for papr reduction in polar coded ofdm-im systems without using side information," *IEEE Transactions on Broadcasting*, 2020.

[5] ——, "Polar-coded ofdm with index modulation," *IEEE Access*, 2020.

[6] C. E. Shannon, "A mathematical theory of communication," *Bell system technical journal*, vol. 27, no. 3, pp. 379–423, 1948.

[7] R. W. Hamming, "Error detecting and error correcting codes," *The Bell system technical journal*, vol. 29, no. 2, pp. 147–160, 1950.

[8] M. J. Golay, "Notes on digital coding," *Proc. IEEE*, vol. 37, p. 657, 1949.

[9] I. S. Reed, "A class of multiple-error-correcting codes and the decoding scheme," MASSACHUSETTS INST OF TECH LEXINGTON LINCOLN LAB, Tech. Rep., 1953.

[10] R. C. Bose and D. K. Ray-Chaudhuri, "On a class of error correcting binary group codes," *Information and control*, vol. 3, no. 1, pp. 68–79, 1960.

[11] I. S. Reed and G. Solomon, "Polynomial codes over certain finite fields," *Journal of the society for industrial and applied mathematics*, vol. 8, no. 2, pp. 300–304, 1960.

[12] V. D. Goppa, "Codes associated with divisors," *Problemy Peredachi Informatsii*, vol. 13, no. 1, pp. 33–39, 1977.

[13] P. Elias, "Coding for noisy channels," *IRE Conv. Rec.*, vol. 3, pp. 37–46, 1955.

[14] J. M. Wozencraft and B. Reiffen, *Sequential decoding.* The MIT Press, 1961, vol. 10.

[15] A. Viterbi, "Error bounds for convolutional codes and an asymptotically optimum decoding algorithm," *IEEE transactions on Information Theory*, vol. 13, no. 2, pp. 260–269, 1967.

[16] J. Omura, "On the viterbi decoding algorithm," *IEEE Transactions on Information Theory*, vol. 15, no. 1, pp. 177–179, 1969.

[17] L. Bahl, J. Cocke, F. Jelinek, and J. Raviv, "Optimal decoding of linear codes for minimizing symbol error rate (corresp.)," *IEEE Transactions on information theory*, vol. 20, no. 2, pp. 284–287, 1974.

[18] G. D. J. Forney, *Concatenated codes.* Cambridge, MA: MIT Press, 1966.

[19] H. Imai and S. Hirakawa, "A new multilevel coding method using error-correcting codes," *IEEE Transactions on Information Theory*, vol. 23, no. 3, pp. 371–377, 1977.

[20] C. Berrou and A. Glavieux, "Near optimum error correcting coding and decoding: Turbo-codes," *IEEE Transactions on communications*, vol. 44, no. 10, pp. 1261–1271, 1996.

[21] C. B. Schlegel and L. C. Perez, *Trellis and turbo coding: iterative and graph-based error control coding.* John Wiley & Sons, 2015.

[22] R. Gallager, "Low-density parity-check codes," *IRE Transactions on information theory*, vol. 8, no. 1, pp. 21–28, 1962.

[23] R. Tanner, "A recursive approach to low complexity codes," *IEEE Transactions on information theory*, vol. 27, no. 5, pp. 533–547, 1981.

[24] D. Divsalar, H. Jin, and R. J. McEliece, "Coding theorems for" turbo-like" codes," in *Proceedings of the annual Allerton Conference on Communication control and Computing*, vol. 36. UNIVERSITY OF ILLINOIS, 1998, pp. 201–210.

[25] A. Abbasfar, D. Divsalar, and K. Yao, "Accumulate-repeat-accumulate codes," *IEEE Transactions on Communications*, vol. 55, no. 4, pp. 692–702, 2007.

[26] J. Pearl, *Probabilistic reasoning in intelligent systems: networks of plausible inference.* Elsevier, 2014.

[27] D. J. Costello and G. D. Forney, "Channel coding: The road to channel capacity," *Proceedings of the IEEE*, vol. 95, no. 6, pp. 1150–1177, 2007.

[28] E. Arikan, "Channel polarization: A method for constructing capacity-achieving codes for symmetric binary-input memoryless channels," *IEEE Transactions on Information Theory*, vol. 55, no. 7, pp. 3051–3073, 2009.

[29] Z. Liang, "On the investigation and application of decoding algorithms of polar codes," Ph.D. dissertation, Zhejiang University, 2016.

[30] I. Tal and A. Vardy, "How to construct polar codes," *IEEE Transactions on Information Theory*, vol. 59, no. 10, pp. 6562–6582, 2013.

[31] N. Presman, O. Shapira, S. Litsyn, T. Etzion, and A. Vardy, "Binary polarization kernels from code decompositions," *IEEE Transactions on Information Theory*, vol. 61, no. 5, pp. 2227–2239, 2015.

[32] S. H. Hassani and R. Urbanke, "On the scaling of polar codes: I. the behavior of polarized channels," in *2010 IEEE International Symposium on Information Theory*. IEEE, 2010, pp. 874–878.

[33] G. Sarkis, P. Giard, A. Vardy, C. Thibeault, and W. J. Gross, "Fast polar decoders: Algorithm and implementation," *IEEE Journal on Selected Areas in Communications*, vol. 32, no. 5, pp. 946–957, 2014.

[34] G. Sarkis and W. J. Gross, "Increasing the throughput of polar decoders," *IEEE Communications Letters*, vol. 17, no. 4, pp. 725–728, 2013.

[35] C. Leroux, A. J. Raymond, G. Sarkis, and W. J. Gross, "A semi-parallel successive-cancellation decoder for polar codes," *IEEE Transactions on Signal Processing*, vol. 61, no. 2, pp. 289–299, 2012.

[36] S. J. Johnson, "Introducing low-density parity-check codes," *University of Newcastle, Australia*, p. V1, 2006.

[37] N. Hussami, S. B. Korada, and R. Urbanke, "Performance of polar codes for channel and source coding," in *2009 IEEE International Symposium on Information Theory*. IEEE, 2009, pp. 1488–1492.

[38] E. Arıkan, "Polar codes: A pipelined implementation," in *Proc. 4th Int. Symp. on Broad. Commun. ISBC 2010*, 2010, pp. 11–14.

[39] T. Rajaie, "Belief propagation decoding of finite-length polar codes," Ph.D. dissertation, 2012.

[40] A. Elkelesh, M. Ebada, S. Cammerer, and S. ten Brink, "Belief propagation list decoding of polar codes," *IEEE Communications Letters*, 2018.

[41] S. Sun, S.-G. Cho, and Z. Zhang, "Post-processing methods for improving coding gain in belief propagation decoding of polar codes," in *GLOBECOM 2017-2017 IEEE Global Communications Conference*. IEEE, 2017, pp. 1–6.

[42] A. C. Arlı and O. Gazi, "Noise-aided belief propagation list decoding of polar codes," *IEEE Communications Letters*, 2019.

[43] J. Guo, M. Qin, A. G. i Fabregas, and P. H. Siegel, "Enhanced belief propagation decoding of polar codes through concatenation," in *Information Theory (ISIT), 2014 IEEE International Symposium on*. IEEE, 2014, pp. 2987–2991.

[44] M. Qin, J. Guo, A. Bhatia, A. G. i Fàbregas, and P. H. Siegel, "Polar code constructions based on llr evolution," *IEEE Communications Letters*, vol. 21, no. 6, pp. 1221–1224, 2017.

[45] I. Tal and A. Vardy, "List decoding of polar codes," *IEEE Transactions on Information Theory*, vol. 61, no. 5, pp. 2213–2226, 2015.

[46] K. Chen, K. Niu, and J. Lin, "Improved successive cancellation decoding of polar codes," *IEEE Transactions on Communications*, vol. 61, no. 8, pp. 3100–3107, 2013.

[47] B. Li, H. Shen, and D. Tse, "An adaptive successive cancellation list decoder for polar codes with cyclic redundancy check," *IEEE Communications Letters*, vol. 16, no. 12, pp. 2044–2047, 2012.

[48] H. Jin and R. Liu, "List estimation-aided successive-cancellation list decoding of polar codes," in *2018 IEEE/CIC International Conference on Communications in China (ICCC)*. IEEE, 2018, pp. 242–246.

[49] X. Liu, S. Wu, X. Xu, J. Jiao, and Q. Zhang, "Improved polar scl decoding by exploiting the error correction capability of crc," *IEEE Access*, vol. 7, pp. 7032–7040, 2019.

[50] K. Niu and K. Chen, "Crc-aided decoding of polar codes," *IEEE Communications Letters*, vol. 16, no. 10, pp. 1668–1671, 2012.

[51] S. Kahraman and M. E. Çelebi, "Code based efficient maximum-likelihood decoding of short polar codes," in *Information Theory Proceedings (ISIT), 2012 IEEE International Symposium on*. IEEE, 2012, pp. 1967–1971.

[52] C. C. M. Husmann, P. C. Nikolaou, and K. Nikitopoulos, "Reduced latency ml polar decoding via multiple sphere-decoding tree searches," *IEEE Transactions on Vehicular Technology*, 2017.

[53] J. Guo and A. G. i Fabregas, "Efficient sphere decoding of polar codes," in *Information Theory (ISIT), 2015 IEEE International Symposium on*. IEEE, 2015, pp. 236–240.

[54] K. Niu, K. Chen, and J. Lin, "Low-complexity sphere decoding of polar codes based on optimum path metric," *IEEE Communications Letters*, vol. 18, no. 2, pp. 332–335, 2014.

[55] V. Bioglio, C. Condo, and I. Land, "Design of polar codes in 5g new radio," *IEEE Communications Surveys & Tutorials*, 2020.

[56] T. S. Rappaport, *Wireless communications principles and practice*, 2nd ed. Prentice Hall PTR, 2002.

[57] P. B. C. A. Bruce Carlson, *Communication Systems: An Introduction to Signals and Noise in Electrical Communication, Fifth Edition*, 5th ed. McGraw-Hill Higher Education, 2009.

[58] R. G. R. Chang, "A theoretical study of performance of orthogonal multiplexing data transmission scheme," *IEEE Transactions on Communication Technology*, vol. 16, no. 4, pp. 529–540, 1968.

[59] P. M. E. S. B. Weinstein, "Data Transmission by Frequency-Division Multiplexing Using the Discrete Fourier Transform," *IEEE Transactions on Communication*, vol. 19, no. 5, pp. 628–634, 1971.

[60] A. Peled and A. Ruiz, "Frequency domain data transmission using reduced computational complexity algorithms," in *Acoustics, Speech, and Signal Processing, IEEE International Conference on ICASSP'80.*, vol. 5. IEEE, 1980, pp. 964–967.

[61] S.-Y. Zhang and B. Shahrrava, "A hybrid papr reduction scheme for ofdm systems using perfect sequences," *IEEE Transactions on Broadcasting*, 2019.

[62] S. Zhang, "Low complex papr reduction schemes for ofdm systems," 2016.

[63] A. Zaidi and R. Baldemair, "In the race to 5g, cp-ofdm triumphs," *ericsson.com, para*, vol. 5, p. 29, 2017.

[64] A. Bhatia, V. Taranalli, P. H. Siegel, S. Dahandeh, A. R. Krishnan, P. Lee, D. Qin, M. Sharma, and T. Yeo, "Polar codes for magnetic recording channels," in *2015 IEEE Information Theory Workshop (ITW)*. IEEE, 2015, pp. 1–5.

[65] U. U. Fayyaz and J. R. Barry, "Polar code design for intersymbol interference channels," in *Global Communications Conference (GLOBECOM), 2014 IEEE*. IEEE, 2014, pp. 2357–2362.

[66] M. Oda and T. Saba, "Polar coding with enhanced channel polarization under frequency selective fading channels," in *2018 IEEE International Conference on Communications (ICC)*. IEEE, 2018, pp. 1–6.

[67] Y. Xiao, S. Wang, L. Dan, X. Lei, P. Yang, and W. Xiang, "Ofdm with interleaved subcarrier-index modulation," *IEEE Communications Letters*, vol. 18, no. 8, pp. 1447–1450, 2014.

[68] E. Başar, "Ofdm with index modulation using coordinate interleaving," *IEEE Wireless Communications Letters*, vol. 4, no. 4, pp. 381–384, 2015.

[69] E. Başar, Ü. Aygölü, E. Panayırcı, and H. V. Poor, "Orthogonal frequency division multiplexing with index modulation," *IEEE Transactions on Signal Processing*, vol. 61, no. 22, pp. 5536–5549, 2013.

[70] E. Basar, "Index modulation techniques for 5g wireless networks," *IEEE Communications Magazine*, vol. 54, no. 7, pp. 168–175, 2016.

[71] B. Yuan and K. K. Parhi, "Early stopping criteria for energy-efficient low-latency belief-propagation polar code decoders," *IEEE Transactions on Signal Processing*, vol. 62, no. 24, pp. 6496–6506, 2014.

[72] C. Simsek and K. Turk, "Simplified early stopping criterion for belief-propagation polar code decoders," *IEEE Communications Letters*, vol. 20, no. 8, pp. 1515–1518, 2016.

[73] Q. Zhang, A. Liu, and X. Tong, "Early stopping criterion for belief propagation polar decoder based on frozen bits," *Electronics Letters*, vol. 53, no. 24, pp. 1576–1578, 2017.

[74] J. Cui, J. Li, Y. Dong, X. Zhang, and Q. Zeng, "Simplified early stopping criterion for polar codes," in *2018 IEEE International Conference on Signal Processing, Communications and Computing (ICSPCC)*. IEEE, 2018, pp. 1–4.

[75] D. Wu, Y. Li, and Y. Sun, "Construction and block error rate analysis of polar codes over awgn channel based on gaussian approximation," *IEEE Communications Letters*, vol. 18, no. 7, pp. 1099–1102, 2014.

[76] P. Trifonov, "Efficient design and decoding of polar codes," *IEEE Transactions on Communications*, vol. 60, no. 11, pp. 3221–3227, 2012.

[77] G. He, J.-C. Belfiore, I. Land, G. Yang, X. Liu, Y. Chen, R. Li, J. Wang, Y. Ge, R. Zhang *et al.*, "Beta-expansion: A theoretical framework for fast and recursive construction of polar codes," in *GLOBECOM 2017-2017 IEEE Global Communications Conference*. IEEE, 2017, pp. 1–6.

[78] J. Guo, "Polar codes for reliable transmission," Ph.D. dissertation, University of Cambridge, 2015.

[79] O. Afisiadis, A. Balatsoukas-Stimming, and A. Burg, "A low-complexity improved successive cancellation decoder for polar codes," *arXiv preprint arXiv:1412.5501*, 2014.

[80] J. Guo, Z. Shi, Z. Liu, Z. Zhang, and Q. Liu, "Multi-crc polar codes and their applications," *IEEE Communications Letters*, vol. 20, no. 2, pp. 212–215, 2016.

[81] T. Richardson and R. Urbanke, *Modern coding theory*. Cambridge university press, 2008.

[82] R. Mori and T. Tanaka, "Performance of polar codes with the construction using density evolution," *IEEE Communications Letters*, vol. 13, no. 7, pp. 519–521, 2009.

[83] L. Chandesris, V. Savin, and D. Declercq, "Dynamic-scflip decoding of polar codes," *IEEE Transactions on Communications*, vol. 66, no. 6, pp. 2333–2345, 2018.

[84] F. Ercan, C. Condo, S. A. Hashemi, and W. J. Gross, "Partitioned successive-cancellation flip decoding of polar codes," in *2018 IEEE International Conference on Communications (ICC)*. IEEE, 2018, pp. 1–6.

[85] A. Alamdar-Yazdi and F. R. Kschischang, "A simplified successive-cancellation decoder for polar codes," *IEEE communications letters*, vol. 15, no. 12, pp. 1378–1380, 2011.

[86] Z. Zhang, K. Qin, L. Zhang, H. Zhang, and G. T. Chen, "Progressive bit-flipping decoding of polar codes over layered critical sets," in *GLOBECOM 2017-2017 IEEE Global Communications Conference*. IEEE, 2017, pp. 1–6.

[87] K. Niu, K. Chen, J. Lin, and Q. Zhang, "Polar codes: Primary concepts and practical decoding algorithms," *IEEE Communications magazine*, vol. 52, no. 7, pp. 192–203, 2014.

[88] V. Miloslavskaya and P. Trifonov, "Sequential decoding of polar codes," *IEEE Communications Letters*, vol. 18, no. 7, pp. 1127–1130, 2014.

[89] K. Niu and K. Chen, "Stack decoding of polar codes," *Electronics letters*, vol. 48, no. 12, pp. 695–697, 2012.

[90] L. Chandesris, V. Savin, and D. Declercq, "An improved scflip decoder for polar codes," in *Global Communications Conference (GLOBECOM), 2016 IEEE*. IEEE, 2016, pp. 1–6.

[91] B. Yuan and K. K. Parhi, "Architecture optimizations for bp polar decoders," in *Acoustics, Speech and Signal Processing (ICASSP), 2013 IEEE International Conference on*. IEEE, 2013, pp. 2654–2658.

[92] S. Sun, S.-G. Cho, and Z. Zhang, "Error patterns in belief propagation decoding of polar codes and their mitigation methods," in *2016 50th Asilomar Conference on Signals, Systems and Computers.* IEEE, 2016, pp. 1199–1203.

[93] S.-y. Zhang and B. Shahrrava, "A selected mapping technique using interleavers for papr reduction in ofdm systems," *Wireless Personal Communications*, vol. 99, no. 1, pp. 329–338, 2018.

[94] P. Giard, G. Sarkis, A. Balatsoukas-Stimming, Y. Fan, C.-y. Tsui, A. Burg, C. Thibeault, and W. J. Gross, "Hardware decoders for polar codes: An overview," in *Circuits and Systems (ISCAS), 2016 IEEE International Symposium on.* Ieee, 2016, pp. 149–152.

[95] S. A. Hashemi, C. Condo, and W. J. Gross, "Fast simplified successive-cancellation list decoding of polar codes," in *2017 IEEE Wireless Communications and Networking Conference Workshops (WCNCW).* IEEE, 2017, pp. 1–6.

[96] N. Doan, S. A. Hashemi, M. Mondelli, and W. J. Gross, "On the decoding of polar codes on permuted factor graphs," in *2018 IEEE Global Communications Conference (GLOBECOM).* IEEE, 2018, pp. 1–6.

[97] I. Tal and A. Vardy, "List decoding of polar codes." in *ISIT*, 2011, pp. 1–5.

[98] L. He, S. Ma, Y.-C. Wu, and T.-S. Ng, "Semiblind iterative data detection for ofdm systems with cfo and doubly selective channels," *IEEE Transactions on Communications*, vol. 58, no. 12, pp. 3491–3499, 2010.

[99] Y. S. Cho, J. Kim, W. Y. Yang, and C. G. Kang, *MIMO-OFDM wireless communications with MATLAB.* John Wiley & Sons, 2010.

[100] J. Xu, T. Che, and G. Choi, "Xj-bp: Express journey belief propagation decoding for polar codes," in *Global Communications Conference (GLOBECOM), 2015 IEEE*. IEEE, 2015, pp. 1–6.

[101] J. Piao, J. Dai, and K. Niu, "Crc-aided sphere decoding for short polar codes," *IEEE Communications Letters*, vol. 23, no. 2, pp. 210–213, 2019.

[102] K. Z. W. B. Wang, *Wideband Wireless Communication OFDM Technologies*, 1st ed. Posts and Telecom Press, 2003.

[103] R. W. S. A. V. Oppenheim and J. R. Buck, *Discrete-Time Signal Processing*. Upper Saddle River, NJ: Prentice-Hall, 1998.

[104] "Digital Vedio Broadcasting (DVB); Framing Structure, Channel Coding and Modulation for Digital Terrestrial Television," *ETSI EN 300 744 V1.4.1 ETSI*, Jan 2001.

[105] J. M. C. J. S. Chow, J. C. Tu, "A Discrete Multitone Transceiver System for HDSL Applications," *IEEE Journal on Selected Areas in Communications*, vol. 9, no. 6, pp. 895–908, 1991.

[106] J. M. C. P. S. Chow, J. C. Tu, "Performance Evaluation of a Multichannel Transceiver System for ADSL and VHDSL Services," *IEEE Journal on Selected Areas in Communications*, vol. 9, no. 6, pp. 909–919, 1991.

[107] "IEEE Standard for Local and Metropolitan Area Networks-Part 11: Wireless LAN Medium Access Control(MAC) and Physical Layer (PHY) Specifications," *IEEE Std 802.11 IEEE*, Aug 1999.

[108] "IEEE Standard for Local and Metropolitan Area Networks-Part 16: Air Interface for Fixed Broadband Wireless Access Systems," *IEEE Std 802.16-2004 IEEE*, Oct 2004.

[109] "IEEE Standard for Local and Metropolitan Area Networks-Part 16: Air Interface for Fixed Broadband Wireless Access Systems-Amendment 2:Physical and Medium Access Control Layer for Combined Fixed and Mobile Operation in Licensed Bands," *IEEE Std 802.16e-2005 IEEE*, Feb 2006.

[110] E. Basar, M. Wen, R. Mesleh, M. Di Renzo, Y. Xiao, and H. Haas, "Index modulation techniques for next-generation wireless networks," *IEEE Access*, vol. 5, pp. 16 693–16 746, 2017.

[111] X. Cheng, M. Wen, L. Yang, and Y. Li, "Index modulated ofdm with interleaved grouping for v2x communications," in *17th International IEEE Conference on Intelligent Transportation Systems (ITSC)*. IEEE, 2014, pp. 1097–1104.

[112] B. Zheng, F. Chen, M. Wen, F. Ji, H. Yu, and Y. Liu, "Low-complexity ml detector and performance analysis for ofdm with in-phase/quadrature index modulation," *IEEE Communications Letters*, vol. 19, no. 11, pp. 1893–1896, 2015.

[113] N. Michailow, M. Matthé, I. S. Gaspar, A. N. Caldevilla, L. L. Mendes, A. Festag, and G. Fettweis, "Generalized frequency division multiplexing for 5th generation cellular networks," *IEEE Transactions on Communications*, vol. 62, no. 9, pp. 3045–3061, 2014.

[114] B. Farhang-Boroujeny, "Ofdm versus filter bank multicarrier," *IEEE signal processing magazine*, vol. 28, no. 3, pp. 92–112, 2011.

[115] V. Vakilian, T. Wild, F. Schaich, S. ten Brink, and J.-F. Frigon, "Universal-filtered multi-carrier technique for wireless systems beyond lte," in *2013 IEEE Globecom Workshops (GC Wkshps)*. IEEE, 2013, pp. 223–228.

[116] E. K. Hall and S. G. Wilson, "Design and analysis of turbo codes on rayleigh fading channels," *IEEE journal on selected areas in communications*, vol. 16, no. 2, pp. 160–174, 1998.

[117] A. Worm, P. Hoeher, and N. Wehn, "Turbo-decoding without snr estimation," *IEEE Communications Letters*, vol. 4, no. 6, pp. 193–195, 2000.

[118] V. Tarokh, N. Seshadri, and A. R. Calderbank, "Space-time codes for high data rate wireless communication: Performance criterion and code construction," *IEEE transactions on information theory*, vol. 44, no. 2, pp. 744–765, 1998.

[119] Q. Zhang, A. Liu, and Y. Zhang, "Signal-to-noise ratio mismatch in polar codes," *Electronics Letters*, vol. 52, no. 5, pp. 365–367, 2016.

[120] P. Frenger, "Turbo decoding for wireless systems with imperfect channel estimates," *IEEE Transactions on Communications*, vol. 48, no. 9, pp. 1437–1440, 2000.

[121] P. Banelli, S. Buzzi, G. Colavolpe, A. Modenini, F. Rusek, and A. Ugolini, "Modulation formats and waveforms for 5g networks: Who will be the heir of ofdm?: An overview of alternative modulation schemes for improved spectral efficiency," *IEEE Signal Processing Magazine*, vol. 31, no. 6, pp. 80–93, 2014.

[122] X. Wang and H. V. Poor, *Wireless communication systems: Advanced techniques for signal reception.* Prentice Hall Professional, 2004.

[123] R. W. Bauml, R. F. Fischer, and J. B. Huber, "Reducing the peak-to-average power ratio of multicarrier modulation by selected mapping," *Electronics letters*, vol. 32, no. 22, pp. 2056–2057, 1996.

[124] S. H. Muller and J. B. Huber, “Ofdm with reduced peak-to-average power ratio by optimum combination of partial transmit sequences,” *Electronics letters*, vol. 33, no. 5, pp. 368–369, 1997.

[125] J. A. Davis and J. Jedwab, “Peak-to-mean power control in ofdm, golay complementary sequences, and reed-muller codes,” *IEEE Transactions on information theory*, vol. 45, no. 7, pp. 2397–2417, 1999.

[126] Y.-C. Tsai, S.-K. Deng, K.-C. Chen, and M.-C. Lin, “Turbo coded ofdm for reducing papr and error rates,” *IEEE Transactions on Wireless Communications*, vol. 7, no. 1, pp. 84–89, 2008.

[127] A. A. Abouda, “Papr reduction of ofdm signal using turbo coding and selective mapping,” in *Proceedings of the 6th Nordic Signal Processing Symposium, 2004. NORSIG 2004.* Citeseer, 2004, pp. 248–251.

[128] M. Sabbaghian, Y. Kwak, B. Smida, and V. Tarokh, “Near shannon limit and low peak to average power ratio turbo block coded ofdm,” *IEEE transactions on communications*, vol. 59, no. 8, pp. 2042–2045, 2011.

[129] T. Matsumine and H. Ochiai, “A novel papr reduction scheme for polar-coded ofdm systems,” *IEEE Communications Letters*, vol. 23, no. 12, pp. 2372–2375, 2019.

[130] H. Breiling, S. H. Muller-Weinfurtner, and J. B. Huber, “Slm peak-power reduction without explicit side information,” *IEEE Communications letters*, vol. 5, no. 6, pp. 239–241, 2001.

[131] N. Carson and T. A. Gulliver, “Papr reduction of ofdm using selected mapping, modified ra codes and clipping,” in *Proceedings IEEE 56th Vehicular Technology Conference*, vol. 2. IEEE, 2002, pp. 1070–1073.

[132] A. D. S. Jayalath and C. Tellambura, "Slm and pts peak-power reduction of ofdm signals without side information," *IEEE transactions on Wireless communications*, vol. 4, no. 5, pp. 2006–2013, 2005.

[133] R. Fan, Y. J. Yu, and Y. L. Guan, "Generalization of orthogonal frequency division multiplexing with index modulation," *IEEE transactions on wireless communications*, vol. 14, no. 10, pp. 5350–5359, 2015.

[134] H. Vangala, E. Viterbo, and Y. Hong, "A comparative study of polar code constructions for the awgn channel," *arXiv preprint arXiv:1501.02473*, 2015.

[135] N. Chen and G. T. Zhou, "Peak-to-average power ratio reduction in ofdm with blind selected pilot tone modulation," *IEEE Transactions on Wireless Communications*, vol. 5, no. 8, pp. 2210–2216, 2006.

[136] S. O'Hara, B. Chen, and J. Periard, "A bandwidth efficient peak power reduction scheme for multicarrier modulation using selected mapping," in *Proc. Conference on Information Sciences and Systems*, 2003.

[137] H.-B. Jeon, J.-S. No, and D.-J. Shin, "A low-complexity slm scheme using additive mapping sequences for papr reduction of ofdm signals," *IEEE Transactions on Broadcasting*, vol. 57, no. 4, pp. 866–875, 2011.

[138] A. V. Oppenheim, *Discrete-time signal processing.* Pearson Education India, 1999.

[139] J. Zakaria and M. Salleh, "On the papr reduction technique: Wp-pts scheme with embedding the side information data," in *2013 IEEE 11th Malaysia International Conference on Communications (MICC).* IEEE, 2013, pp. 351–356.

[140] M. Wen, B. Zheng, K. J. Kim, M. Di Renzo, T. A. Tsiftsis, K.-C. Chen, and N. Al-Dhahir, "A survey on spatial modulation in emerging wireless systems:

Research progresses and applications," *IEEE Journal on Selected Areas in Communications*, vol. 37, no. 9, pp. 1949–1972, 2019.

[141] J. Choi, "Coded ofdm-im with transmit diversity," *IEEE Transactions on Communications*, vol. 65, no. 7, pp. 3164–3171, 2017.

[142] R. Umar, F. Yang, S. Mughal, and H. Xu, "Distributed polar-coded ofdm based on plotkin's construction for half duplex wireless communication," *International Journal of Electronics*, vol. 105, no. 7, pp. 1097–1116, 2018.

[143] D. R. Wasserman, A. U. Ahmed, and D. W. Chi, "Ber performance of polar coded ofdm in multipath fading," *arXiv preprint arXiv:1610.00057*, 2016.

[144] M. Wen, Q. Li, E. Basar, and W. Zhang, "Generalized multiple-mode ofdm with index modulation," *IEEE Transactions on Wireless Communications*, vol. 17, no. 10, pp. 6531–6543, 2018.

[145] M. Wen, B. Ye, E. Basar, Q. Li, and F. Ji, "Enhanced orthogonal frequency division multiplexing with index modulation," *IEEE Transactions on Wireless Communications*, vol. 16, no. 7, pp. 4786–4801, 2017.

[146] J. Li, S. Dang, M. Wen, X.-Q. Jiang, Y. Peng, and H. Hai, "Layered orthogonal frequency division multiplexing with index modulation," *IEEE Systems Journal*, vol. 13, no. 4, pp. 3793–3802, 2019.

[147] N. Ishikawa, S. Sugiura, and L. Hanzo, "Subcarrier-index modulation aided ofdm-will it work?" *IEEE Access*, vol. 4, pp. 2580–2593, 2016.

[148] V. Miloslavskaya, "Shortened polar codes," *IEEE Transactions on Information Theory*, vol. 61, no. 9, pp. 4852–4865, 2015.

[149] R. Wang and R. Liu, "A novel puncturing scheme for polar codes," *IEEE Communications Letters*, vol. 18, no. 12, pp. 2081–2084, 2014.

[150] P. Robertson, E. Villebrun, and P. Hoeher, "A comparison of optimal and sub-optimal map decoding algorithms operating in the log domain," in *Proceedings IEEE International Conference on Communications ICC'95*, vol. 2. IEEE, 1995, pp. 1009–1013.

[151] A. I. Siddiq, "Effect of subcarrier activation ratio on the performance of ofdm-im over rayleigh fading channel," *IEEE Communications Letters*, vol. 21, no. 6, pp. 1293–1296, 2017.

[152] L. Li, Z. Xu, and Y. Hu, "Channel estimation with systematic polar codes," *IEEE Transactions on vehicular technology*, vol. 67, no. 6, pp. 4880–4889, 2018.

[153] D. Zhou, K. Niu, and C. Dong, "Construction of polar codes in rayleigh fading channel," *IEEE Communications Letters*, vol. 23, no. 3, pp. 402–405, 2019.

[154] H. Si, O. O. Koyluoglu, and S. Vishwanath, "Polar coding for fading channels: Binary and exponential channel cases," *IEEE Transactions on Communications*, vol. 62, no. 8, pp. 2638–2650, 2014.

[155] S. Liu, Y. Hong, and E. Viterbo, "Polar codes for block fading channels," in *2017 IEEE Wireless Communications and Networking Conference Workshops (WCNCW)*. IEEE, 2017, pp. 1–6.

[156] J. Massey, "Optimum frame synchronization," *IEEE transactions on communications*, vol. 20, no. 2, pp. 115–119, 1972.

[157] M.-S. Alouini and A. J. Goldsmith, "A unified approach for calculating error rates of linearly modulated signals over generalized fading channels," *IEEE Transactions on Communications*, vol. 47, no. 9, pp. 1324–1334, 1999.

[158] A. I. Siddiq, "Low complexity ofdm-im detector by encoding all possible subcarrier activation patterns," *IEEE Communications Letters*, vol. 20, no. 3, pp. 446–449, 2016.

[159] R. Abu-Alhiga and H. Haas, "Subcarrier-index modulation ofdm," in *2009 IEEE 20th International Symposium on Personal, Indoor and Mobile Radio Communications*. IEEE, 2009, pp. 177–181.

VITA AUCTORIS

NAME:	Siyu Zhang
PLACE OF BIRTH:	Beijing, China
YEAR OF BIRTH:	1992
EDUCATION:	Jilin University, Changchun, Jilin, China Bachelor of Electrical Engineering, Communication Engineering 2010-2014
	University of Windsor, Windsor ON, Canada Master of Applied Science, Electrical and Computer Engineering 2014-2016